Electrocatalytic carbon dioxide reduction - A mechanistic study

Schouten, K.J.P.

ELECTROCATALYTIC CARBON DIOXIDE REDUCTION

A mechanistic study

PROEFSCHRIFT

ter verkrijging van
de graad van Doctor aan de Universiteit Leiden,
op gezag van de Rector Magnificus prof. mr. C. J. J. M. Stolker,
volgens besluit van het College voor Promoties
te verdedigen op dinsdag 8 oktober 2013
klokke 16.15 uur

door

Klaas Jan Pieter Schouten

geboren te Gouda in 1986

Promotiecommissie

Promotor: Prof. dr. M. T. M. Koper

Co-promotor: Dr. L. B. F. Juurlink

Overige leden: Prof. dr. J. Brouwer
Prof. dr. I. Chorkendorff (Technical University of Denmark)
Dr. P. J. Kooyman (Technische Universiteit Delft)
Prof. dr. G. Mul (Universiteit Twente)
Prof. dr. B. E. Nieuwenhuys
Prof. dr. M. Robert (Université Paris Diderot)

The research described in this thesis has been supported financially by the Dutch National Research School Combination - Catalysis (NRSC-C).

ISBN 978-94-6182-332-8

Printed by Off Page

Voor Margreet

De hemelen vertellen Gods eer,
en het uitspansel verkondigt Zijner handen werk.
De dag aan den dag stort overvloediglijk spraak uit,
en de nacht aan den nacht toont wetenschap.
Psalm 19

Contents

1 | Introduction

1.1 Motivation

Carbon dioxide is the main product of the oxidation of hydrocarbons. Since hydrocarbon-based fuels are the world's most important energy source, the use of fossil fuels has lead to significant increases of atmospheric CO_2 levels, and they are not expected to level down in the coming decades unless drastic measures are taken.[1] The increasing presence of CO_2 in the atmosphere is causing a widespread concern about its possible consequences. On the other hand, from a more positive perspective, CO_2 is a vast and sustainable carbon feedstock, that could partly replace the widespread use of petroleum-based hydrocarbons as chemical building blocks. Therefore, converting carbon dioxide into hydrocarbons would not only limit the emission of carbon dioxide, but also supply us with a sustainable carbon feedstock, provided the conversion is performed using renewable energy, and without much additional CO_2 production. In this way, the re-usage of the carbon dioxide caused by human emissions would enable a sustainable carbon cycle. If the produced hydrocarbons can be used as fuels, a carbon energy cycle is created. Such a carbon-based energy cycle has two main advantages compared to other proposed energy cycles that are, for example, based on storing energy in hydrogen or batteries. First, hydrocarbons have a higher energy density, and second, storage is easier and there will be no need to change the existing fuel infrastructure, provided the generated fuel is a liquid.

In the Earth's natural carbon cycle, photosynthesis is one of the most important processes through which CO_2 is recycled. CO_2 is inserted in carbon

chains using the energy from sunlight to create carbohydrates, which are used in nature as chemical building blocks and energy carriers. Although these fuels used by nature are oxygen-rich, in contrast to fossil fuels that are oxygen poor and therefore more energy rich, mimicking photosynthesis would still be an attractive way to close our carbon-based energy loop, and to create a sustainable carbon energy cycle.

One of the promising ways to convert carbon dioxide into hydrocarbons is to do this electrochemically, and to ultimately integrate such a process in a photo-electrochemical device. An auspicious discovery in this area was made by Hori in 1985, who showed that CO_2 can be directly converted to hydrocarbons on copper electrodes.[2] Only copper electrodes catalyze this reaction to a significant extent, and the main carbon products are methane and ethylene.[3] Ample research has been performed to understand the electrochemical reduction on the molecular level, but in spite of the extensive literature, the molecular mechanism is still a matter of debate.[4,5] With the renewed interest in solar fuels and CO_2 reduction and recycling, the mechanistic details of the electrochemical CO_2 reduction have become a topical subject of interest again in recent years. Understanding the mechanism of this reaction is important as it would open up routes to the production of high energy fuels by the (photo-)electrochemical reduction of CO_2.

1.2 Outline of this thesis

The focus of this thesis is on the electrochemical reduction of CO_2 on copper electrodes, and in particular on the mechanistic aspects of this reaction. We start in Chapter 2 by comparing the reaction mechanisms of the electrochemical reduction of CO_2 to the reaction mechanisms of the metal-catalyzed hydrogenation and reduction of CO_2, both heterogeneously in the gas phase and homogeneously in solution, to obtain more insights in the key intermediates that determine the selectivity of CO_2 reduction to the various products.

In Chapter 3, we identify key intermediates that determine if CO_2 is reduced to methane or ethylene. Identification of intermediates could lead to new ways in which the reaction rate can be increased, or the selectivity of the reaction can be tuned towards desired products. We describe how we have identified new intermediates by reducing small organic species, to

investigate whether or not they can be reduced to either methane or ethylene on copper electrodes.

The formation and stabilization of these intermediates also depends on the atomic configuration of the electrode surface. Therefore, we have studied the reduction of CO, a well known intermediate of CO_2 reduction on copper electrodes, by using copper single crystals. The use of Cu single crystal electrodes requires a method to carefully characterize the surface structure. Therefore, we have developed a characterization method using blank voltammetry in alkaline media, which is presented in Chapter 4.

In Chapter 5 we have investigated the reduction of CO on two different Cu(*hkl*) basal planes, *viz.* Cu(100) and Cu(111). We have observed two different reaction mechanisms for ethylene formation: a first pathway that has a common intermediate with the formation of methane and that takes place preferentially at (111) facets or steps, and a second pathway at (100) facets in which CO is selectively reduced to ethylene at relatively low overpotentials.

Since the (100) orientation turned out to be very important for selective ethylene formation we have studied stepped Cu single crystals to compare the reactivity of a surface with (100) terraces to a surface with (100) steps, the results of which are presented in Chapter 6.

The pH is another important parameter in the reaction mechanism. In Chapter 7 we have investigated the influence of the pH by reducing carbon dioxide and carbon monoxide on Cu(111) and Cu(100) single crystal electrodes at different pH values.

2 | Key intermediates in the hydrogenation and electrochemical reduction of CO_2

Abstract

Mimicking photosynthesis by (re)using carbon dioxide as a carbon feedstock for the production of hydrocarbons would enable a sustainable carbon cycle. Electrochemically, CO_2 can be reduced on copper electrodes to hydrocarbons, mainly methane and ethylene, and the integration of this process in a photo-electrochemical device could be a promising way to close the carbon cycle. Understanding the mechanism of this reaction is one of the keys to open up new, sustainable routes to carbon based fuels. In this chapter we aim to obtain more insights in the key intermediates that determine the selectivity of CO_2 reduction to various products, by comparing the electrochemical reduction of CO_2 to the metal-catalyzed hydrogenation and reduction of CO_2 both homogeneously in solution and heterogeneously in the gas phase. We distinguish four main pathways: (1) methane is formed via carboxyl (COOH) and carbon monoxide (CO), (2) methanol is formed via formate (HCOO) and formaldehyde, (3) ethylene is formed via the coupling of CO, leading to surface enolates, and (4) CO_2 is inserted into existing carbon chains, close to the way CO_2 is fixed in nature.

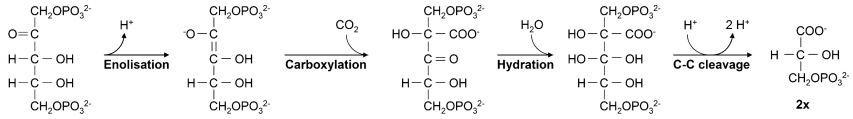

Figure 2.1 Carbon dioxide fixation in the Calvin cycle.

2.1 Introduction

To further our understanding of the mechanistic aspects of the electrochemical conversion of CO_2, it is worthwhile to compare this mechanism with other hydrogenation reactions of CO_2. Both homogeneous and heterogeneous catalysis have been used to convert CO_2 to various hydrocarbons, *i.a.* carbon monoxide, methanol, methane, and formic acid.[6]

This chapter will focus on the reaction mechanisms of CO_2 reduction on a molecular level using metal catalysts. We will compare the electrochemical reduction of CO_2, using copper and other metal electrodes in solution, with the metal-catalyzed hydrogenation and reduction of CO_2, both homogeneously with metal complexes in solution, and heterogeneously in the gas phase, to obtain more insights into the key intermediates that determine the selectivity of CO_2 reduction to the various products. We will not discuss the technical and economical feasibility studies of the various ways in which CO_2 can be converted, for such discussions we refer to other recent literature.[7–10]

We will start with a brief mechanistic overview of CO_2 fixation as it takes place in nature. Next we will give an overview of the reaction mechanisms for the various processes that are based on the hydrogenation of CO_2 including (I) the synthesis of carbon monoxide via the reverse water-gas shift (RWGS) reaction, (II) the methanation of CO_2, (III) methanol synthesis, (IV) hydrocarbon synthesis, and (V) the hydrogenation of CO_2 to formic acid using homogeneous catalysis. We will discuss the latest insights into the mechanisms of the electrochemical CO_2 reduction using metal electrodes and metal complexes, and will finally compare the various mechanisms in a concluding section.

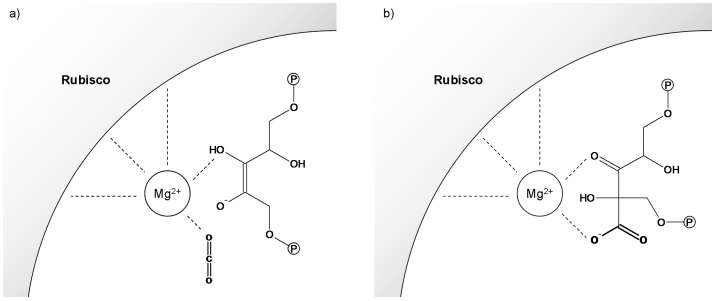

Figure 2.2 Carboxylation in the active site of Rubisco.

2.2 CO_2 fixation in the Calvin cycle

The conversion of CO_2 to carbohydrates in plants is called the Calvin cycle, named after Melvin Calvin who discovered the cycle in the 1950's (and who was awarded the Nobel Prize for Chemistry in 1961). In this cycle the energy of sunlight is used to fix CO_2 and convert it into triose phosphates.[11] The carbon fixation in the Calvin cycle can be broken down in four steps, as shown in Fig. 2.1. First, a proton is removed from ribulose-1,5-biphosphate, resulting in the formation of an enediolate intermediate. CO_2 binds to this enediolate to form a C_6 intermediate through a carboxylation reaction. This intermediate is hydrated in the next step, after which it breaks into two 3-phosphoglycerates.

After the carboxylation, the two 3-phosphoglycerates are converted into glyceraldehyde 3-phosphates, a three-carbon sugar phosphate. Five of these glyceraldehyde 3-phosphates are regenerated by converting them into three ribulose-1,5-biphosphates. So overall, three turns of the Calvin cycle yield one C_3 product, the glyceraldehyde 3-phosphate. These triose phosphates are used to synthesize hexose phosphates, which can be converted to (I) sucrose for transport, (II) starch for energy storage, (III) cellulose for cell wall synthesis, and (IV) pentose phosphates for metabolic intermediates.

The enzyme that catalyzes the carboxylation reaction is Ribulose-1,5-biphosphate carboxylase oxygenase (Rubisco). The active site of this enzyme contains an Mg^{2+} ion, that brings together and orients the reactants, as shown in Fig. 2.2.[12] Deprotonation of ribulose-1,5-biphosphate results in

the formation of the enediolate, shown in Fig. 2.2a. CO_2, polarized by the Mg^{2+} ion, is then added to the double C-C bond of the enediolate, resulting in the formation of a carboxylate, as shown in Fig. 2.2b.[11]

2.3 The mechanisms of CO_2 reduction using heterogeneous catalysis

2.3.1 Carbon monoxide synthesis via the reverse water-gas shift reaction

The formation of carbon monoxide from CO_2 via the reverse water-gas shift (RWGS) reaction,

$$CO_2 + H_2 \longrightarrow CO + H_2O \tag{2.1}$$

is one of the most promising ways to convert CO_2, for several reasons.[13] First, since the RWGS is an endothermic reaction, the reaction product CO is a way to store energy, *i.e.* the conversion of CO_2 to CO can be used to store hydrogen energy. Next, this reaction can be used to change the ratio of H_2/CO in syngas, allowing for selective hydrocarbon formation. Furthermore, the RWGS occurs as a side reaction in many processes where CO_2 and H_2 are present, for example in methanol synthesis. Finally, CO can be converted to various useful chemicals such as formic acid, methanol, formaldehyde, and long hydrocarbon chains.

Since the RWGS is a reversible reaction, catalysts active in the water-gas shift (WGS) reaction are often also active in the reverse reaction.[9]

$$CO + H_2O \rightleftharpoons CO_2 + H_2 \tag{2.2}$$

Since Cu-based catalysts are the most studied for the WGS reaction, they are also applied for the RWGS reaction.[6] Examples of catalysts used for the RWGS are Cu-Ni/γ-Al_2O_3 and Cu-ZnO/Al_2O_3, the latter is used for methanol synthesis as well.[6] Cerium-based catalysts are also active in the (R)WGS reaction.[6,9]

The mechanism of the RWGS reaction is still controversial. According to two recent review articles, two main reaction mechanisms have been proposed: the redox-mechanism and the associative formate-mechanism.[6,9] In the redox-mechanism, the CO_2 dissociates directly to CO and O, followed

by the reduction of the oxide by hydrogen, resulting in the formation of water. On a Cu-based catalyst, this reaction can by modeled by:

$$CO_2 + 2\,Cu^0 \longrightarrow Cu_2O + CO \tag{2.3}$$

$$H_2 + Cu_2O \longrightarrow 2\,Cu^0 + H_2O \tag{2.4}$$

Both reaction 2.3 and 2.4 have been suggested as the rate determining step (RDS) for the (R)WGS.[14–17] Since it is a continuous process, the reduction of the oxidized Cu has to be faster than the oxidation process, and the RDS is probably the dissociation of CO_2.[6,16,18]

In the formate-mechanism, formate is formed by the association of hydrogen with CO_2. CO is subsequently formed by the decomposition of formate into CO and OH.

$$CO_2 \longrightarrow CO_{2,ads} \tag{2.5}$$

$$H_2 \longrightarrow 2\,H_{ads} \tag{2.6}$$

$$CO_{2,ads} + H_{ads} \longrightarrow HCO_{2,ads} \tag{2.7}$$

$$HCO_{2,ads} \longrightarrow CO + OH_{ads} \tag{2.8}$$

$$OH_{ads} + H_{ads} \longrightarrow H_2O \tag{2.9}$$

The dissociation of formate is assumed to be the RDS.[18] However, considering the mechanistic studies of the WGS reaction,[19,20] and taking into account the microscopic reversibility of the models used, it cannot be excluded that also in the RWGS carboxyl, COOH, is the intermediate to CO instead of formate. One indication why formate is unlikely as an intermediate to CO formation, is that formate binds bidentate with two O atoms to the surface, whereas CO binds with its C atom, which makes the reaction step from HCOO to CO + OH (reaction 2.8) very difficult.[19] Although adsorbed formate has been observed during the (R)WGS with several techniques, it could be only a spectator species.[19] Next to formate and carboxyl, carbonate has also been proposed as an intermediate for the RWGS reaction.[21]

2.3.2 Methanation of carbon dioxide

The hydrogenation of CO_2 to methane is an important process. This reaction, called the Sabatier reaction, can be used for the production of syngas

(via steam reforming), and is a way to store hydrogen energy and use this in the existing natural gas network.

$$CO_2 + 4H_2 \longrightarrow CH_4 + 2H_2O \tag{2.10}$$

Supported Ni is the most studied catalyst material; other catalytic systems that are used for the Sabatier reaction are mainly based on Ru.[6,22]

Although differences in the rate and the selectivity for the methanation of CO_2 and CO are observed,[23] the general proposed mechanism of CO_2 hydrogenation is that CO_2 reacts to CO first, and subsequently follows the reaction mechanism of CO methanation.[6,22,24] For the first step, the formation of CO, it is proposed that, similar to the RWGS reaction and methanol synthesis, CO is formed via the decomposition of formate[6,22,25] or carboxyl.[24] Interestingly, it was proposed recently that the hydrogenation of CO_2 to formate (HCOO) is a dead-end in the reaction, and that only carboxyl (COOH) is leading to the formation of CO.[26]

The mechanism of CO methanation was proposed in the seventies to occur via an CH_xO intermediate,[27,28] but the generally accepted mechanism nowadays assumes the formation of surface carbon by CO dissociation via the Boudouard reaction, with subsequent hydrogenation.[6,22,24]

2.3.3 Methanol synthesis

The synthesis of methanol is an important industrial process, since methanol is an alternative fuel and an important building block for synthesis in the chemical industry; over 40 million tons of methanol are produced per year. Most methanol plants are fed by natural gas which is converted to syngas by steam reforming, and the syngas subsequently is converted to methanol using copper-based catalysts. It is a promising process since CO_2 and H_2 can be used as a starting material using the same catalysts.

$$CO_2 + 3H_2 \longrightarrow CH_3OH + H_2O \tag{2.11}$$

The mechanistic details of the reaction of CO_2 to methanol are still a matter of debate. Two possible reaction pathways have been proposed for methanol synthesis from CO_2 and H_2 over Cu-based catalysts.[6,15,30] One pathway is the formate-pathway, in which the reaction to methanol proceeds through the formation of formate (HCOO), dioxomethylene (H_2COO), formaldehyde

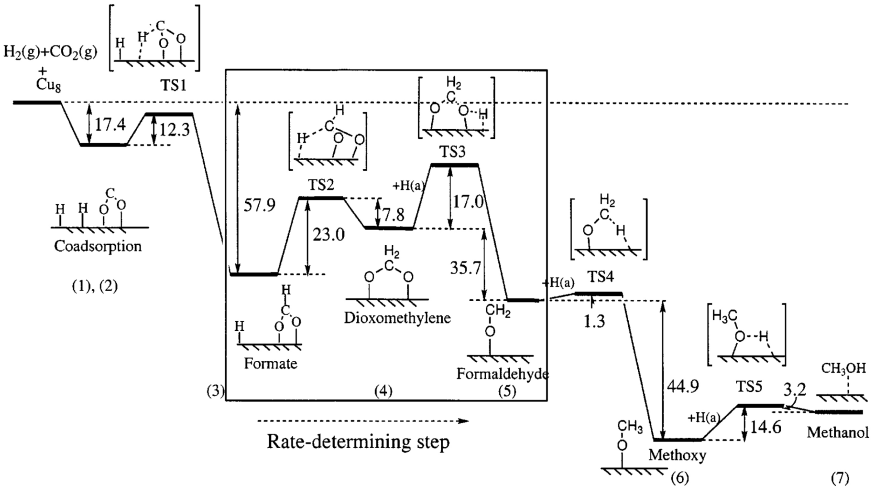

Figure 2.3 Hydrogenation of CO_2 to methanol via the formate-pathway on Cu(100). Reprinted with permission from Ref. 29. Copyright 2000 John Wiley & Sons, Inc.

(CH_2O), and methoxy (CH_3O). On Cu, this is usually considered as the predominant pathway.[15] An example of this pathway, calculated by Nakatsuji and Hu on Cu(100),[29] is shown in Fig. 2.3. There is no agreement in the literature on the RDS for this particular pathway. Usually the hydrogenation of adsorbed formate, as shown in Fig. 2.3, is considered to be the RDS,[29,31–34] but also the hydrogenation of dioxomethylene[15,35] or methoxy[36] have been proposed as the RDS.

The other pathway involves the RWGS reaction (2.1), where CO_2 is first converted to CO, which is then hydrogenated to form methanol.

$$CO + 2\,H_2 \longrightarrow CH_3OH \tag{2.12}$$

This RWGS-pathway can explain the formation of CO as the major byproduct during methanol synthesis from CO_2.[6,15,37] In this pathway, the CO will be hydrogenated to formyl (HCO) and formaldehyde (H_2CO) after which it will follow the same path as shown in Fig. 2.3. The overall RDS for the RWGS-pathway is the recombination of water from H and OH on the sur-

face.[15] Concerning the reduction of CO to methanol only, the hydrogenation of methoxy has the highest activation energy.[15,30,36]

To avoid undesired by-products, a highly selective catalyst is needed. Although many kinds of metal-based catalysts have been examined for the synthesis of methanol, modified Cu, in particular Cu/ZnO, remains the main active catalyst. Although this Cu/ZnO system has been studied extensively, there is no consensus in literature on the promotional role of ZnO, and on the active site of the catalyst. One proposition is that the active site is metallic Cu,[32,35] and that the ZnO improves the dispersion and stabilization of metallic copper.[6,15] On the other hand it has been proposed that the active site in methanol synthesis is a Cu^+ species, stabilized by the ZnO phase.[38–40] Recent work by Behrens *et al.* suggests that the active sites are steps at the Cu surface, alloyed with Zn.[41] The $Zn^{\delta+}$ at the steps increases the binding strength of oxygenated intermediates, which decreases the energy barriers in the reaction.

Other catalysts that have been used for methanol synthesis are Pd/β-Ga_2O_3, Cu/ZrO_2, and molybdenum sulfide.[6]

2.3.4 Synthesis of hydrocarbons

Hydrogenation of CO_2 to hydrocarbon chains would be the ultimate goal of CO_2 utilization. Investigations into this subject can be divided into two categories: methanol-mediated and non-methanol mediated.[6,42]

The hydrogenation of CO_2 via methanol is performed on a composite catalyst, a combination of the standard Cu-Zn catalyst used for methanol synthesis, with a zeolite used for the methanol-to-gasoline (MTG) process.[43,44] However, this method usually gives light alkanes as major hydrocarbon products because the methanol synthesis catalyst further hydrogenates the intermediate alkenes formed in the zeolites.[43,45]

The non-methanol mediated hydrogenation of CO_2 is usually performed using Fischer-Tropsch (FT) catalysts.[42] The most common metals in the FT process are cobalt and iron. Cobalt is the catalyst of choice in FT when long carbon chains are needed. However, when switching the feed gas from syngas to a gas mixture containing CO_2 and H_2, the product distribution changes significantly. In the presence of CO_2, cobalt acts as a methanation catalyst. Iron has a higher catalytic activity for the WGS reaction than cobalt, which means that under FT conditions CO_2 is formed from syngas,

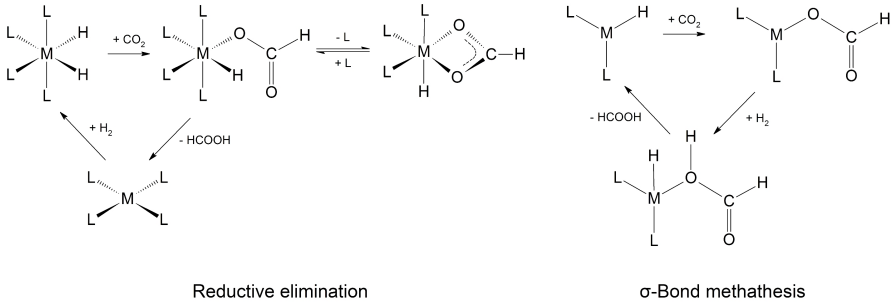

Figure 2.4 Reaction mechanisms of the hydrogenation of CO_2 to formic acid. 'M' represents a metal atom and 'L' a ligand group, which could also be the solvent.

making it often a less attractive FT catalyst. However, for the hydrogenation of CO_2 this is an advantage, since iron also catalyzes the RWGS reaction. CO_2 hydrogenation on Fe has been shown to occur in two steps: first CO_2 is converted to CO via the RWGS reaction, followed by chain propagation via the FT mechanism resulting in alkenes in the range C_2–C_5.[42,45]

It would go beyond the scope of this chapter to discuss the controversial FT mechanism in detail. Several different mechanisms have been proposed since the discovery in the 1920's.[46] Currently, the proposed mechanisms can be divided into two classes: according to the first class, CO or CH_xOH species are inserted into the growing hydrocarbon chain, after which the C-O or C-OH bond is broken. In the other class, the C-O or C-OH bond is broken first, leading to the formation of CH_x species that are incorporated into the growing chain. The currently generally accepted mechanism is the latter, where CO is dissociated first resulting in the formation of C_1 (CH_2) species, followed by FT chain growth.[46,47] The breaking of the C-O bond can be activated by the assistance of hydrogen, through the formation of adsorbed CHO or COH. Calculations on single-crystal surfaces have shown that this so-called "hydrogen assisted CO activation", is the optimum pathway on flat surfaces whereas at defects on the surface the direct dissociation of CO is favored.[47]

2.4 The mechanisms of CO_2 reduction using homogeneous catalysis

2.4.1 Synthesis of formic acid

The main product of CO_2 hydrogenation using homogeneous catalysis is formic acid. Formic acid has a wide range of applications in, for example, the leather industry and food preservation, and is a starting material for the production of various chemicals. Formic acid has also been proposed as a way to store hydrogen,[6,48] and as a fuel for formic acid fuel cells.[49] Complexes of several transition-metals are used to catalyze this reaction, *i.a.* rhodium, ruthenium and iridium.[6,50,51] Ru complexes often show the best activity and selectivity.[6]

$$CO_2 + H_2 \longrightarrow HCOOH \tag{2.13}$$

The key step in the reduction of CO_2 with H_2 to formic acid is the formation of the C-H bond. For the formation of this bond, formate has always been detected as an intermediate.[50] Formate is formed by the insertion of CO_2 into the metal-hydride bond. The binding of formate to the active site can be bidentate, ionic, or monodentate.[52,53] Various reaction mechanisms for the different metal complexes have been proposed,[6,51,52] but two fundamental different reaction mechanisms for the formation of formic acid are distinguished, as shown in Fig. 2.4.[54] In the mechanism shown in the left-hand panel of Fig. 2.4, the formate is formed upon oxidative addition of the CO_2, followed by reductive elimination of the formate by a hydride in the complex. On Rh, a different pathway is observed, with a smaller energy barrier compared with the reductive elimination mechanism, where the formic acid is formed from the formate directly from a dihydrogen complex by σ-bond metathesis.[52,54,55]

The reaction is often performed in organic solvents, but the addition of small amounts of water or alcohols has been shown to improve the catalytic hydrogenation of CO_2 to formic acid.[6,51,56] A proposed explanation is that hydrogen-bonding to the oxygen atom of CO_2 enhances the electrophilicity of carbon, thereby facilitating its insertion into the metal-hydride bond of the metal complex.[6,56]

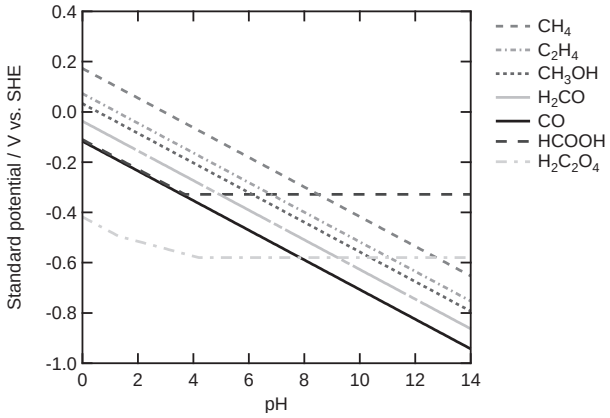

Figure 2.5 Standard potentials of various products of CO_2 reduction vs. pH.

2.4.2 Synthesis of other products

While active homogeneous catalysts for the production of formic acid have been discovered, there has only been a preliminary development of catalysts for the production of other products like methanol and CO.[51] The formation of CO is more thermodynamically favorable at elevated temperatures.[51] Using Ru complexes, the formation of CO, methanol and methane has been observed.[51,57] In this case, CO is observed as initial product, followed by the formation of methanol and methane, suggesting that methanol is formed from CO. For the formation of ethanol, a bimetallic catalyst of Ru and Co is used, where the Ru-complex is believed to be primarily responsible for the the reduction of CO_2 to CO and methanol, while the Co-complex is responsible for the formation of ethanol from methanol and CO.[51,57] Interestingly, the formation of ethanol was only observed in the presence of iodide.

2.5 Mechanisms of the electrochemical reduction of CO_2

The electrochemical reduction of carbon dioxide has attracted sustained attention in the past decades, for the synthesis of organic molecules as well as a possible means of energy storage, *e.g.* of high-energy electrons generated

by photo-excitation. The most common reaction products are those that require the transfer of 2 electrons,[58] *i.e.* formic acid, carbon monoxide, and oxalic acid, but examples of 6 and 8 electron conversions into *e.g.* methanol, ethylene and methane have also been reported:

$$CO_2 + 2H^+ + 2e^- \longrightarrow CO + H_2O \tag{2.14}$$

$$CO_2 + 2H^+ + 2e^- \longrightarrow HCO_2H \tag{2.15}$$

$$2CO_2 + 2H^+ + 2e^- \longrightarrow H_2C_2O_4 \tag{2.16}$$

$$CO_2 + 4H^+ + 4e^- \longrightarrow H_2CO + H_2O \tag{2.17}$$

$$CO_2 + 6H^+ + 6e^- \longrightarrow CH_3OH + H_2O \tag{2.18}$$

$$CO_2 + 8H^+ + 8e^- \longrightarrow CH_4 + 2H_2O \tag{2.19}$$

$$2CO_2 + 12H^+ + 12e^- \longrightarrow C_2H_4 + 4H_2O \tag{2.20}$$

Fig. 2.5 shows a Pourbaix diagram of the equilibrium potentials for the reduction of CO_2 to various products in water as a function of pH.[5,59,60] The formation of these products proceeds usually through proton-coupled multi-electron steps, that are generally more favorable than single electron reductions, since thermodynamically more stable molecules are formed.[59] The standard potential of the outer-sphere single electron reduction of CO_2 to $CO_2^{\cdot -}$ is -1.90 V vs. SHE in water, due to the large reorganizational energy needed for the formation of the bent radical anion.[59]

$$CO_2 + e^- \longrightarrow CO_2^{\cdot -} \tag{2.21}$$

Catalysts (partially) overcome the high overpotential for outer-sphere CO_2 reduction by binding and protonating the CO_2 species such that its stability is improved. Still, high overpotentials may lead to a broad product distribution, especially on heterogeneous catalysts. Therefore, considerable efforts have been made to find catalysts that not only lower the overpotential but also steer the selectivity of the reaction. Both homogeneous molecular catalysis and heterogeneous catalysis, mostly metals, have been investigated for these purposes.[61]

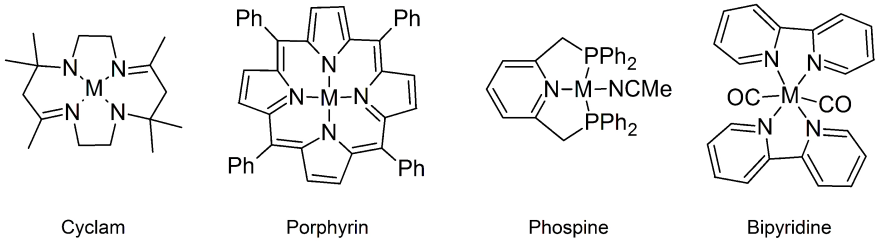

Figure 2.6 Examples of the types of metal complexes that are used to reduce CO_2.

2.5.1 Homogeneous electrocatalysis

The field of CO_2 (electro)reduction using transition metal complexes in non aqueous media started in the 1970's. In the homogeneously catalyzed reduction of CO_2, the reduced form of a reversible couple with an equilibrium potential negative to the reduction potential of CO_2 reacts with the CO_2 and generates the oxidized form. The reduction of the metal complex at the electrode starts a new catalytic cycle. With respect to homogeneous electrocatalysis, Savéant differentiates between redox catalysis and chemical catalysis.[60] In redox catalysis, the reduced form of the catalyst is only an outer-sphere electron donor, whereas in chemical catalysis the interactions between the catalyst and substrate are stronger, and involve the formation of an addition product between the catalyst and (a group of atoms initially belonging to) the substrate.[60]

Two families of transition metal complexes have been reported, namely Ag and Pd porphyrins, as well as some Ni macrocycles, that only form oxalate at potentials close to the $CO_2/CO_2^{\cdot -}$ couple, and therefore likely involve a redox or quasi-redox catalysis, in which electron transfer acts as a pre-equilibrium to the rate determining dimerization of $CO_2^{\cdot -}$. A quasi redox catalysis mechanism has also been reported for the reduction of CO_2 to oxalate by anion radicals of aromatic nitriles and esters.[60,62]

Electrocatalytic CO_2 reduction with metal complexes in solution typically proceeds through chemical catalysis.[60] The reported catalysts can be divided into different categories, as shown in Fig. 2.6: metal catalysts with macrocyclic ligands, which can be divided into cyclam-like and porphyrin-

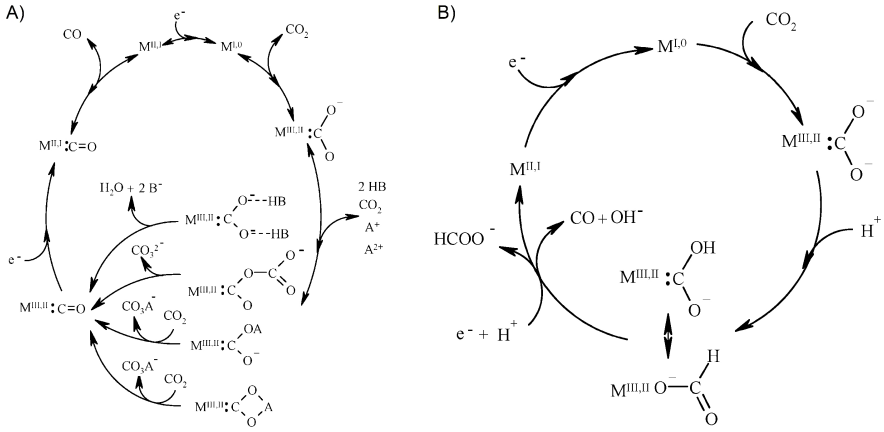

Figure 2.7 A) Various mechanisms for the reduction of CO_2 to CO in the presence of Lewis acids 'A' and weak Brønsted acids 'B'. B) Proposed mechanism for the reduction of CO_2 to CO and formate. Reprinted with permission from Ref. 60. Copyright 2008 American Chemical Society.

like complexes, metal catalysts with phosphine ligands, and metal catalysts with polypyridyl ligands.[59,60,63] The best efficiencies and/or selectivities are obtained with Ni (cyclams), Fe (porhyrins), Re and Ru (polypyridyls), and Pd (phosphines).

The most common reduction product using these catalysts is CO, at potentials much less negative than the $CO_2/CO_2^{\cdot -}$ couple, which clearly excludes a redox mechanism. Therefore, the first step in CO_2 reduction is most likely the coordination of CO_2 to the previously reduced metal complex.[60] On Ni cyclams this complexation has been shown to be stabilized by a strong back donation from Ni to CO_2. This causes an increase in negative charge at the O atoms of the CO_2, in a similar configuration to the $CO_2^{\cdot -}$ radical.[5,64] The presence of weak Brønsted acids and Lewis acids has been shown to stabilize the coordination of CO_2 and facilitate the breaking of the C-O bond to form CO, see Ref. 60 and references therein. Also water and CO_2 itself may have the same role as these acids. This has led to the proposed mechanisms for the formation of CO shown in Fig. 2.7A.[60,63,65,66]

The other common product obtained is formate. The suggested mechanism for the formation of formate, shown in Fig. 2.7B, is a proton-coupled electron transfer to the coordinated CO_2 that, depending on the catalyst, will lead to the formation of CO or formate.[60] Another mechanism, comparable to the reductive elimination reaction shown in Fig. 2.4, is via an internal hydride transfer to the coordinated CO_2.[63,67]

In some cases higher reduction products have been obtained with Ru complexes, *i.a.* formaldehyde, methanol, and even some C_2 species such as $CHOCO_2^-$ and $CH_2OHCO_2^-$.[68] These C_2 products, that are the result of 4 and 6 electron transfer reactions, are only possible if CO is a stable intermediate ligand that can be further reduced, and coupled with another CO_2. The nature of the catalyst is very important in this stabilization, and lower temperatures are used to stabilize the intermediates.[60,68] Interestingly, pyridinium has been shown to be able to reduce CO_2 to methanol through six sequential electron transfers.[69] This is probably the first case in which sequential one-electron transfers provide the low energy pathway for catalysis, in contrast to multi-electron transfer pathways. The mechanism of the reaction was studied on Pt electrodes with pyridinium in solution. Formic acid and formaldehyde were observed as intermediate products to the formation of methanol, and the reaction has been shown be first order in CO_2 and pyridinium.[69,70] The pyridinium radical is proposed as the actual catalyst[69,70] (although recent work by Keith and Carter suggests differently[71]). This radical can bind CO_2 and reduced intermediates through a coordinative interaction that stabilizes the intermediate species. The first step is the coordination of CO_2 to the pyridinium radical resulting in the formation of a carbamate species, suggesting a covalent N-C bond.[70] Subsequent electron transfer results in the formation of formic acid. Formic acid again is coordinated to a pyridinium radical and is, via the formyl-radical, reduced to formaldehyde. Coordination of formaldehyde results in hydroxymethyl, which is reduced to methanol. This mechanism suggests an inner-sphere-type electron transfer from the pyridinium radical to the intermediates for the various mechanistic steps, where the pyridinium radical is able to covalently bind the (radical) intermediate species and transfer the electron.

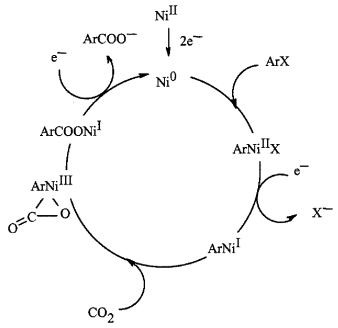

Figure 2.8 Mechanism of the carboxylation of aryl halides (ArX; X = Br, Cl, I). Reprinted with permission from Ref. 72. Copyright 2002 WILEY-VCH.

Electrochemical carboxylation

The application of CO_2 as a C_1 source in organic synthesis might be a way to CO_2 fixation, and could yield various useful carboxylic acids, including pharmaceuticals. In organic chemistry, low-valent Ni and Pd species are generated in situ from Ni^{II} or Pd^{II} precursors, and facilitate C-C coupling reactions.[72] Electrochemistry can provide an easy way to generate a desired oxidation state of a metal complex that becomes the active catalytic species for an organic reaction, at potentials that avoid the direct reduction of the organic compound. An example is the carboxylation of aryl halides.[72–74] The reaction was shown to proceed through Ni^0, Ni^I, Ni^{II} and Ni^{III} intermediates, as shown in Fig. 2.8. Another way of electrochemical carboxylation is the direct reduction of the organic compound, followed by the carboxylation.[74,75] An example is the carboxylation of α-chloroethylbenzene.[76] At the Pt cathode, the α-chloroethylbenzene is reduced, which effectively removes the chlorine. The reduced intermediate reacts with CO_2 to form the carboxylate. An Mg anode enhances the reaction, the created Mg^+ cations stabilize the carboxylate anions by producing an insoluble Mg salt that prevents oxidation or protonation.[76] Hindering the competing protonation reaction is also the reason why this direct carboxylation is usually performed in organic electrolytes or ionic liquids.

2.5.2 Heterogeneous electrocatalysis

The conversion of CO and CO_2 to hydrocarbons using heterogeneous catalysis is usually performed at elevated temperatures and pressures. The direct electrochemical conversion of CO_2 would allow a process that avoids high temperatures, and where the production rate can be controlled directly, depending on the availability of surplus electricity. Only a few metals are active in this process, and the product distribution is broad, depending heavily on the applied potential, the electrode material and electrolyte used.

Aqueous media

In aqueous media, metals can be divided roughly into 4 groups, based on the products formed during the electrochemical CO_2 reduction.[3,5] The first group includes the metals that evolve hydrogen at low potentials and with a high CO adsorption strength, such as Ni, Fe, Pt, and Ti. On these metals CO_2 is reduced to strongly bound CO that blocks further reduction. Therefore, the main product on these metals is hydrogen.

The second group of metals are those with a high hydrogen overvoltage and a very low CO adsorption strength, such as Sn, In, Tl, Pb, Hg, Bi, and Cd. Since the reduced intermediates are not, or very weakly adsorbed on the surface, these metals are not able to catalyze the breaking of the C-O bond in CO_2. These metals facilitate the conversion of CO_2 to formic acid with high current efficiencies. On Hg, formic acid is formed with 100% current efficiency. The first step in the formation of formic acid is the formation of $CO_2^{\cdot -}$. The formation of this radical is observed in aqueous and non aqueous solutions, and during its formation and subsequent reduction only a very small fraction of the electrode is covered by adsorbates (see Ref. 5 and references therein). The subsequent reduction and protonation of $CO_2^{\cdot -}$ to formate does not depend on pH, which shows that the proton donor is not H^+ but H_2O. This indicates a mechanism, in which CO_2 is reduced to $CO_2^{\cdot -}$ in solution, followed by the protonation by water to form $HCO_2^{\cdot}$ and its subsequent reduction to $HCOO^-$:

$$CO_2 + e^- \longrightarrow CO_2^{\cdot -} \tag{2.22}$$

$$CO_2^{\cdot -} + H_2O \longrightarrow HCO_2^{\cdot} + OH^- \tag{2.23}$$

$$HCO_2^{\cdot} + e^- \longrightarrow HCO_2^- \tag{2.24}$$

The third group of metals produces mainly CO. These include Au, Ag, Zn, and Ga, metals with a weak CO adsorption and a medium hydrogen overvoltage. The potentials at which CO is formed on these metals is less negative compared with the potentials where formic acid is formed, especially on Au.

Hori has shown that the heat of fusion of the various metal electrodes correlates well with the potentials of CO_2 reduction.[3] The heat of fusion is related to the *d*-electron contribution to the metallic bond, and may be taken as a measure of *d*-electron availability, which affects the strength of CO_2 adsorption. Therefore, metals with a higher heat of fusion adsorb CO_2 stronger, and reduce it at lower potentials. In this context, the CO and HCOOH forming metals are well separated; CO is formed at less negative potentials on metals with a higher heat of fusion. This suggests a different mechanism for the formation of CO, where the intermediate(s) are much more stabilized, *i.e.* adsorbed at the electrode.[5]

A similar relation between adsorption strength and overpotential has been suggested by Peterson and Nørskov, who investigated the correlation between the binding energies of the intermediates of CO_2 reduction vs. CO (for intermediates binding to the surface through carbon) and vs. OH (for intermediates binding to the surface through oxygen) for various transition metals.[77] From these binding energies, the limiting potential can be derived, at which each elementary step of a reaction becomes exergonic. The protonation of adsorbed CO is singled out as the most important step dictating the overpotential, with Cu having the lowest overpotential compared with other transition metals.

Hori suggested a mechanism for the formation of CO where the CO_2 is bound to the surface, coordinated in a similar way to the CO_2 shown in Fig. 2.7B,[5] as has has been calculated for the Ni cyclams discussed in section 2.5.1.[64] The negative charge on the O atoms then facilitates the protonation, and formation of adsorbed COOH. The next step is the breaking of the C-O bond, and the formation of CO and OH^-:

$$CO_2 + e^- \longrightarrow CO^-_{2,ads} \tag{2.25}$$

$$CO^-_{2,ads} + H_2O \longrightarrow COOH_{ads} + OH^- \tag{2.26}$$

$$COOH_{ads} + e^- \longrightarrow CO + OH^- \tag{2.27}$$

The fundamental possibility of the reversible conversion of CO_2 to CO and formate has been illustrated by Armstrong and Hirst.[78] They have discussed the immobilization of enzymes (carbon monoxide dehydrogenase (CODH) and formate dehydrogenase (FDH)) on electrodes and showed that the electrocatalytic conversion of CO_2 on these electrodes is reversible, *i.e.* they convert CO_2 to CO or formate and vice versa around the equilibrium potential of the corresponding redox couple. For the interconversion of CO_2 and CO by CODH, CO_2 binds at reducing potentials as a bridging ligand between the Ni and the dangling Fe atom in the [Ni4Fe-4S] active site. Then, CO migrates to Ni, and OH forms on Fe.[79] In contrast to metal surfaces, these highly efficient active sites can bind and stabilize the intermediate due to the precisely positioned functional groups and thereby lower the overpotential, or kinetically couple the formation and onward reaction of the intermediates. Moreover, enzymes seem to avoid the formation of poisons, such as CO, which frustrate the development of metallic formic acid oxidation catalysts.

Only a few metals can catalyze the conversion of CO_2 to hydrocarbons. The most interesting metal is Cu, with a moderate CO adsorption, where methane and even C_2 species such as ethylene are formed in significant amounts.[80] Some other metals such as Mo and Ru are able to convert CO_2 to methanol and methane, but with low efficiencies.[81,82]

Copper electrodes

In 1985, Hori discovered that on copper electrodes CO_2 can be reduced to hydrocarbons, mainly methane and ethylene.[2,80] Next to these hydrocarbons, also CO and formic acid are formed during CO_2 reduction. Also oxygenates such as ethanol and propanol are observed, although usually only in trace amounts.[4,5] Recently, up to 16 different reduction products have been observed.[83]

In spite of the extensive literature on carbon dioxide reduction on copper electrodes, the detailed mechanism of this reaction is still unclear.[4] It is known that ethylene and methane are formed through a different reaction mechanism and that carbon monoxide is a key intermediate in the formation of both ethylene and methane.[3,84,85] The exact reaction mechanism of carbon monoxide reduction to either ethylene or methane is still debated. Interestingly, methanol is not or produced only in very small amounts on a

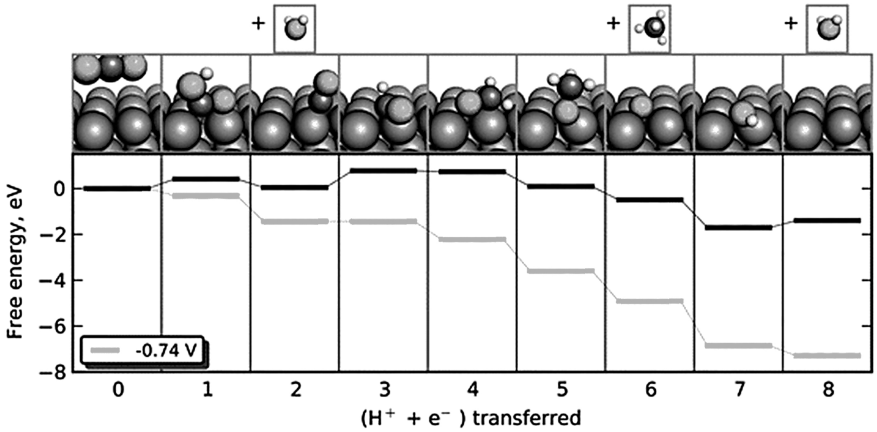

Figure 2.9 Free energy diagram for the lowest energy pathway to CH_4. The black pathway represents the free energy at 0 V vs. RHE and the gray pathway the free energy at the indicated potential. Reprinted with permission from ref. 86. Copyright 2010 Royal Society of Chemistry.

metallic Cu electrode, suggesting that the C-O bond is broken early in the reaction.[5]

The formation of methane from CO depends on pH, in such a way that the rate determining step must involve the transfer of a proton and an electron.[84] Recently, DFT calculations by Peterson *et al.* (see Fig. 2.9), as well as our own experiments presented in Chapter 3, suggested that the key intermediate to form methane is CHO_{ads}.[86] A similar path, but via adsorbed COH has been suggested by Hori.[84]

The formation of ethylene from CO, on the other hand, does not depend on pH.[84] Therefore, a dimer of carbon monoxide, whose formation does not involve the transfer of an hydrogen atom but does depend on potential (*i.e.* involves electron transfer), has been suggested as the key intermediate in the C-C coupling, see Chapter 3 for more details. A Fischer-Tropsch-like mechanism where CO is coupled to CH_x species cannot explain the observed selectivity to ethylene. We will show in Chapter 3 that the only C_2 species that can be reduced to ethylene is ethylene oxide, suggesting a shared oxametallacycle intermediate for the reduction reactions of CO_2 and ethylene

oxide. Enol-type species have also been proposed as key intermediates in the formation of C_2 species by Kuhl *et al.*[83]

Hori *et al.* showed that the extent of methane and ethylene formation sensitively depends on the surface orientation of the copper electrode.[87] On the (111) facet of the copper fcc crystal the formation of methane is favored, whereas on the (100) facet the formation of ethylene is dominant. Recent DFT calculations predicted that the limiting potential for the formation of the intermediates of the CO_2 reduction to CH_4 is lower on the Cu(211) surface compared with the Cu(111) and Cu(100) surface.[88]

Using Online Electrochemical Mass Spectrometry (OLEMS) we will show in Chapter 5 that on Cu(100), CO can be selectively reduced to ethylene at low overpotentials, whereas at higher potentials ethylene and methane are formed simultaneously both on Cu(100) and Cu(111), suggesting two different pathways for the formation of ethylene from CO.

Interestingly, methanol has been observed as a product of CO_2 reduction on intentionally oxidized Cu electrodes.[81,89] The electronic properties of Cu(I) in *p*-Cu_2O are thought to play an important role in the adsorption of CO_2, causing a stronger binding of CO_2 and CO on *p*-Cu_2O and other Cu(I) centers.[81] *p*-Cu_2O covered Cu has been shown to be able to absorb atomic O into the bulk Cu.[81] This might facilitate the dissociation of CO_2, but the exact mechanism leading to methanol is still unclear. Recently, Li and Kanan have shown that thick Cu_2O films catalyze the reduction of CO_2 to CO and HCOOH with high faradaic efficiencies at low overpotentials.[90]

Non aqueous media

The electrochemical reduction of CO_2 in non aqueous solutions, *e.g.* methanol, propylene carbonate or dimethyl sulfoxide, has several advantages compared with the reduction in water. The solubility of CO_2 is higher, and the hydrogen evolution is heavily suppressed. The main products are CO, HCOOH and $(COOH)_2$.[5] CO is the main product in non aqueous media on Cu, Ag, Au, Zn, In, Sn, Ni, and Pt. $(COOH)_2$ is formed on Cu, Sn, Ag, Zn, In and Au. Some metals form both CO and $(COOH)_2$, like Fe, Cr, Mo, Pd, and Cd. HCOOH is formed on Pt, Pb, Hg, Ag and Au. On Cu, hydrocarbons such as CH_4 and C_2H_4 have also been obtained.

The product selectivity is mainly determined by whether or not the reduced CO_2 is stabilized at the electrode surface. Metals like Hg and Pb

reduce CO_2 at potentials close to the potential of the $CO_2/CO_2^{\cdot-}$ couple (2.21).[5] The main product is oxalate or formate, depending on the concentration of water.[5,91] Therefore, Savéant *et al.* proposed that oxalate is formed by the dimerization of $CO_2^{\cdot-}$, similar to the oxalate formation in homogeneous catalysis.[91]

$$2\,CO_2^{\cdot-} \longrightarrow C_2O_4^{2-} \tag{2.28}$$

An alternative route to oxalate is the coupling of CO_2 to $CO_2^{\cdot-}$ resulting in the formation of $(CO_2)_2^{\cdot-}$, which is further reduced to oxalate.[5,92]

Formate is formed in a similar way as suggested for aqueous media and for homogeneous catalysis, where the small amount of water present reacts as a Lewis acid and protonate the $CO_2^{\cdot-}$ (2.23).[5,60,91] Increasing water concentrations in non-aqueous media lead to increasing formate, and decreasing oxalate formation.

On the metals that stabilize the reduced intermediates to a much greater extent, like Au, Zn and Ag, the main product is CO. In the absence of water, CO_2 reacts as a Lewis acid with adsorbed CO_2^- to form $OCOCO_2^-$, in a comparable way as occurs in homogeneous catalysis, depicted in Fig. 2.7A.[5,60] The breaking of the C-O bond then results in the formation of CO and CO_3^{2-}:

$$CO_2 + e^- \longrightarrow CO_{2,ads}^- \tag{2.29}$$

$$CO_{2,ads}^- + CO_2 \longrightarrow OCOCO_2^- \tag{2.30}$$

$$OCOCO_2^- + e^- \longrightarrow CO + CO_3^{2-} \tag{2.31}$$

2.5.3 Photoelectrochemical CO_2 reduction

The ultimate goal of CO_2 reduction would be to couple the CO_2 electrocatalyst to light harvesting by photo-excitation. This would yield a kind of artificial photosynthesis device to store the energy of sunlight in hydrocarbons. The basic steps always involve (I) the absorption of light to generate an excited state, (II) charge separation of the created electron-hole pair, (III) the energy of this charge separated state is used to reduce CO_2, (IV) catalyst regeneration.

The photoreduction of CO_2 can be divided into two general categories: the first category includes the homogeneous systems, which are entirely

molecule based.[93] The molecular light absorber and the catalyst could be the same molecule, or a molecular light absorber and a transition metal catalyst work in concert. In the second category, a semiconductor is used for the light absorption and charge separation steps, after which this energy is transfered to a homogeneous or heterogeneous catalyst.

The most frequently used photosensitizers in homogeneous systems are Ru(II) polypyridyl complexes, such as $[Ru(bpy)_3]^{2+}$. This photosensitizer (P) is irradiated by light and forms an excited state, P^*. This excited state is quenched by an electron donor (D), typically triethylamine, to P^-. The reduced photosensitizer in turn reduces the catalyst (cat), which then reduces the CO_2.[94]

$$P + h\nu \longrightarrow P^* \tag{2.32}$$

$$P^* + D \longrightarrow P^- + D^{\cdot+} \tag{2.33}$$

$$P^- + cat \longrightarrow P + cat^- \tag{2.34}$$

$$cat^- + CO_2 \longrightarrow cat + products \tag{2.35}$$

Cobalt and nickel macrocylic compounds are often used as catalysts. Sometimes the catalyst is linked to the photosensitizer in a supramolecular complex to increase the efficiency of the electron transfer to the catalyst.[94] Metalloporphyrins with Fe and Co can react both as a light absorber and a catalyst.[94] The obtained products are mainly CO and formate, in a similar way as described in section 2.5.1.[94,95]

Semiconductors have been shown to be efficient in the conversion of incident photon energy into electrical energy.[93] The semiconductor could be an electrode or a colloid. If the semiconductor surface is not electrocatalytically active, the separated charge has to be transfered to a catalytic species, which could be adsorbed on the surface or a species in solution. On these electrodes, not only the usual two-electron reduction products, formate and CO, are observed, but also formaldehyde and methanol.[95] A special case is *p*-GaAs. On the (111) facets of this electrode, the (photo)-electrochemical reduction of CO_2 to methanol with a current efficiency close to 100 % has been reported.[81,95] The mechanism for methanol formation is unclear. Even without applied potential and illumination, arsenic-rich surfaces of GaAs spontaneously produce CH_3OH, which is attributed to dissolution of the semiconductor in carbonic acid, resulting in the formation of Ga and As hydroxides and methanol.[96]

2.6 Discussion and conclusions

In this chapter, we have compared various mechanisms for the catalytic reduction of carbon dioxide, with particular emphasis on the low-temperature electrocatalytic reduction. The reduction of carbon dioxide may yield a variety of products, and most of these reactions tend to suffer from slow kinetics and/or poor selectivity. From the electrochemical point-of-view, only the conversion of carbon dioxide to carbon monoxide or to formic acid have been shown to be potentially reversible.[78] This is indeed expected for two-electron transfer reactions. In electrocatalysis, thus far this feat has only be accomplished with enzymes, whereas in heterogeneous catalysis the (reverse) water gas shift reaction is also known as a reversible catalytic reaction, though at higher temperature. No synthetic room-temperature electrocatalyst has yet been developed which can do the same. Such a catalyst would be extremely interesting for formic acid fuel cells, and its reversible counterpart, *i.e.* carbon dioxide and hydrogen storage in formic acid. Higher-energy fuels from carbon dioxide require the transfer of more than 2 electrons, and this invariably leads to overpotential losses.[58,77]

We believe that there are four main pathways for CO_2 reduction to high-energy fuels. The first pathway is methanation, which is the thermodynamically most favorable process. A key intermediate, not only in this pathway but also in the FT process and the electrochemical reduction of CO_2 on copper electrodes, is carbon monoxide. In all processes described in this chapter the intermediate leading to CO is carboxyl, COOH, with the only exception being the RWGS reaction for which a pathway via formate, HCOO, has been proposed. However, as argued in section 2.3.1, there is evidence that also in the RWGS carboxyl is the intermediate to CO, instead of formate. A next important step in the methanation is the breaking of the C-O bond in carbon monoxide. This dissociation can be either directly, forming surface carbon, or hydrogen assisted via the formation of CH_xO species. The latter has also been suggested for the electrochemical reduction of CO and CO_2, where CHO is considered to be the key intermediate in the formation of methane. It is not only the nature of the metal catalyst which determines whether or not CO can be dissociated. Cu and Ru are methanation catalysts, both under electrochemical and heterogeneous gas phase conditions. Under electrochemical conditions the methane formation rate is much higher on Cu, whereas under gas phase conditions Ru is far more active.[81] Frese has

attributed the higher activity of Ru in the gas phase to a higher hydrogen coverage compared with Cu, since the chemisorption of H_2 is more favorable on Ru, and to Ru being able to dissociate CO on defect sites whereas Cu binds CO normally in a non-dissociated form. The higher methanation rate on Cu under electrochemical conditions has been explained by the ability of Cu to allow large overpotentials without hydrogen evolution overwhelming the CO_2 reduction reaction. The high potential, in combination with the HCO formation, is here the driving force for the dissociation of CO.

The second pathway is the formation of methanol. It seems that methanol is always formed via the formate-formaldehyde route, as has been evidenced for methanol synthesis and for the (photo)-electrochemical reduction using pyridinium. Stabilization of the various intermediates, *e.g.* by adding ZnO to the Cu catalyst or as observed on the pyridinium by covalent bonding to the radical, seems to play an important role. Oxidized copper also seems to offer this (structural) stabilization, since on oxidized copper electrodes the formation of CO and HCOOH is enhanced,[90] and even the formation of methanol has been observed.[89] The formate-formaldehyde route also explains why methanol is not observed when CO_2 is reduced on metallic copper electrodes, as on copper formate cannot be further reduced.[4,5] On the other hand, C_2 oxygenates are, in low quantities, observed on copper electrodes. This is consistent with a reaction mechanism involving early breaking of the C-O bond, followed by C-C bond formation between CO or CO_2 and the reduced intermediate. Interestingly, heterogeneous gas phase catalysts which are effective for methanol synthesis are in general ineffective for C_2 oxygenate formation, and metals that are active in C_2 oxygenate formation are known to favor CO dissociation.[97]

The third pathway is the pathway that leads to ethylene, observed during the electrochemical reduction on copper electrodes. This reaction has been discovered and described in great detail by Hori, and is investigated further in this thesis. Ethylene is normally formed simultaneously with methane, although at lower overpotentials the formation of ethylene is favored, and formed via a carbon monoxide intermediate. In this thesis, its formation is suggested to involve reductive CO coupling and ene(di)ol(ate) intermediates. The dehydroxylation of enol-like surface species also explains the formation of C_2 and C_3 oxygenated species, such as ethanol. An enol is also the intermediate to the C-C bond formation in the Calvin cycle.

The fourth pathway is closest to the way CO_2 is fixated in nature through the Calvin cycle, namely through CO_2 insertion into an existing carbon chain, and subsequent carboxylate reduction. In electro-organic synthesis, this strategy is known as electrocarboxylation, but it has not gained much popularity yet as a sustainable solution for fuel production. It is interesting that the same Mg_2^+ ion that plays an important role in the active site of the carboxylation enzyme in the Calvin cycle, strongly enhances the electrocarboxylation reaction.[76]

In conclusion, the (electrochemical) reduction of CO_2 to interesting products, such as potential fuels, can take place through a variety of different pathways, and the pathway selected is highly sensitive to the catalyst material, electrode (over)potential, pH, electrolyte composition, solvent, etc. Although some common patterns can be observed, as discussed in some detail in this chapter, it appears that many pathways are similar in energy, involving intermediates with similar stability. This makes the search for or development of active and selective catalysts highly interesting but also highly challenging. Catalyst stability is an additional issue, that we have not touched upon in any detail, but that will clearly be crucial for any future deployment of this technology.

3 | A new mechanism for the selectivity to C_1 and C_2 species in the electrochemical reduction of carbon dioxide on copper electrodes

Abstract

We have investigated the reaction mechanism of the electrochemical reduction of carbon dioxide to hydrocarbons on copper electrodes. This reaction occurs via two pathways: a C_1 pathway leading to methane, and a C_2 pathway leading to ethylene. To identify possible intermediates in the reduction of carbon dioxide we have studied the reduction of small C_1 and C_2 organic molecules containing oxygen. We followed the formation and consumption of intermediates during the reaction as a function of potential, using online mass spectrometry. For the C_1 pathway we show that it is very likely that CHO_{ads} is the key intermediate towards the breaking of the C-O bond and, therefore, the formation of methane. For the C_2 pathway we suggest that the first step is the formation of a CO dimer, followed by the formation of a surface-bonded enediol or enediolate, or the formation of an oxametallacycle. Both the enediol(ate) and the oxametallacycle would explain the selectivity of the C_2 pathway towards ethylene. This new mechanism is significantly different from existing mechanisms but it is the most consistent with the available experimental data.

3.1 Introduction

The emission of carbon dioxide into the atmosphere due to our combustion of fossil fuels and the decreasing reserves of fossil fuels are forcing us to look for new energy sources and energy carriers. A possible solution would be to find a way to reduce carbon dioxide back to fuels. This would enable a carbon energy cycle, in which renewable energy sources are used to reduce carbon dioxide back to hydrocarbons.[98] The main advantage of such a carbon energy cycle compared to, for example, a hydrogen based economy would be that we can keep on using our existing fuel infrastructure, provided the generated fuel is a liquid. One of the most promising ways to reduce carbon dioxide is to do this electrochemically, and to ultimately integrate such a process in a photoelectrochemical device.

A landmark discovery in this area was made by Hori in 1985, who found that on copper electrodes carbon dioxide can be reduced to hydrocarbons, mainly ethylene and methane.[2] Since then ample research has been performed to characterize and understand this reaction, not in the least by Hori himself.[5,81,84,85,99] With the renewed interest in solar fuels, carbon dioxide reduction has become a topical subject of interest again in recent years. In spite of the extensive literature on carbon dioxide reduction on copper electrodes, many aspects of the molecular-level details of the mechanism of this reaction are still unclear.[99] It is known that ethylene and methane are formed through a different reaction mechanism and that carbon monoxide is a key intermediate in the formation of both ethylene and methane.[3,84,85] The exact reaction mechanism of carbon monoxide reduction to either ethylene or methane is still debated. One of the important remaining questions is what determines the selectivity of the reaction to form first ethylene at relatively low cathodic potentials and, at more negative potentials, methane. Also one would like to determine which intermediates are involved in the pathways to either C_1 or C_2 species.

To identify possible intermediates in the reduction of carbon dioxide we studied the reduction of small C_1 and C_2 organic molecules containing oxygen. Previous work using similar strategies has all been performed using long term electrolysis.[84,100] However, using online electrochemical mass spectrometry, one can measure the reduction of the various species online while changing the potential and, therefore, follow the formation and consumption of intermediates during the reaction.[101–104] The possible

intermediates we investigate are formaldehyde, methoxy (methanol at high pH), glyoxal, glycolaldehyde, ethylene glycol, and ethylene oxide. Based on our results, in combination with what is already known about the mechanism from experimental and computational results in the literature, we will propose a new model for the overall reaction mechanism. Especially our suggested pathway for C_2 formation is significantly different from previous proposals. Our mechanism will be compared to existing mechanisms and important remaining issues will be identified.

3.2 Experimental

All experiments were carried out in an electrochemical cell using a three-electrode assembly at room temperature. The cell and glassware were first cleaned by boiling in a mixture of 1:1 concentrated sulfuric and nitric acid and before each experiment by boiling in ultra clean water (Millipore MilliQ gradient A10 system, 18.2 $M\Omega \cdot cm$). A gold wire was used as counter electrode and a reversible hydrogen electrode (RHE) in the same electrolyte was used as reference electrode. All potentials in this paper are referred to this electrode.

The copper electrodes used were 99.999% copper cylinders with a diameter of 5 mm and cut from the same rod (Matek), embedded in Teflon or used in the hanging meniscus configuration. Prior to each experiment the electrode was polished mechanically using alumina pastes with subsequent decreasing particle diameter down to 0.3 µm, after which the electrode was sonicated in ultra pure water. After this mechanical polishing, the electrode was electropolished in a 10:5:2 mixture of H_3PO_4:H_2O:H_2SO_4 at 2.3 V for two times 2 seconds with an interval of 30 seconds at open circuit potential.[105,106] Blank cyclic voltammograms at a sweep rate of 50 mV s^{-1} were recorded after each surface preparation until a stable voltammogram was obtained, in order to reduce possible surface oxides created during electropolishing, and to verify a clean state of the surface. The potential was controlled using an Ivium A06075 potentiostat.

The experiments were carried out in 0.1 M K_2HPO_4 + 0.1 M KH_2PO_4 (pH 7) prepared from high purity reagents (Merck Suprapur, Sigma-Aldrich TraceSelect) and ultra clean water. Argon (Air Products, 5.0) bubbling was used to deaerate the electrolyte. The deactivation of the Cu electrode, as reported in literature during long term electrolysis measurements was not

observed, except in the case of CO_2 reduction, probably because we are using high purity reagents and are not working at constant negative potentials as is required for the long term electrolysis measurements.[107] The CO_2 used was of less purity (2.5) so probably contamination, most likely of iron carbonyls, causes the deactivation of the electrode.

Online Electrochemical Mass Spectrometry (OLEMS) was used to detect the gaseous products formed during the reaction. The reaction products at the electrode interface were collected with a small tip positioned close (~10 µm) to the electrode.[108] The tip is a 0.5 mm diameter porous Teflon cylinder with an average pore size of 10-14 µm in a Kel-F holder. This tip is connected to a mass spectrometer with a PEEK capillary. The tip configurations were cleaned in a solution of 0.2 M $K_2Cr_2O_7$ in 2 M H_2SO_4 and rinsed with ultra pure water before use. A SEM voltage of 2400 V was used, except for hydrogen ($m/z = 2$) where a SEM voltage of 1200 V was used. The products were measured while changing the potential of the electrode from 0.0 to -1.0 V and back with 1 mV s^{-1}. Because the equilibration of the pressure in the system after introduction of the tip in the electrolyte takes a very long time, all mass fragments show a small decay during the measurement. We corrected for this background by fitting a double exponential function to the data in the potential regions were no change in activity is observed and subtracted this fit from the data. All mass fragments shown in this paper are background corrected in this way.

Non-volatile reaction products were detected with high-performance liquid chromatography (HPLC). While changing the potential, samples of the electrolyte were collected with a similar tip as used for OLEMS, positioned close to the center of the electrode surface.[109] The main difference between this tip and the tip used for OLEMS is that this tip does not have the hydrophobic porous Teflon cylinder, but is instead open to allow electrolyte to pass through. Samples were collected with a rate of 60 µl min^{-1} and each sample had a volume of 60 µl. Since we changed the potential with 1 mV s^{-1}, each sample contained the average reaction products of a potential change of 60 mV. Collected samples during voltammetry were analyzed afterwards by HPLC (Prominence HPLC, Shimadzu; Aminex HPX 87-H column, Biorad).

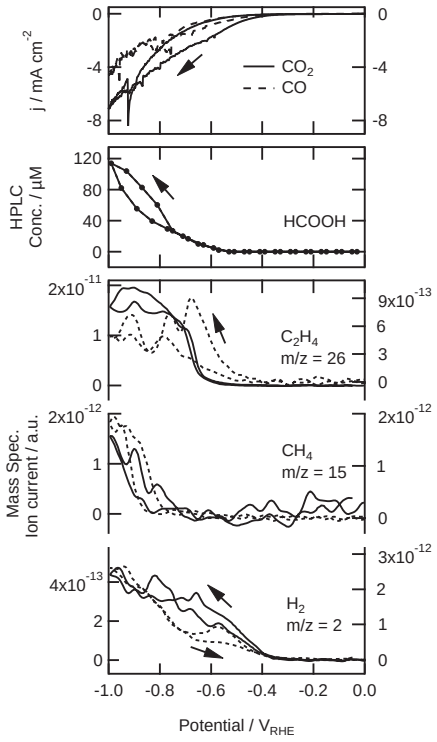

Figure 3.1 Top: cyclic voltammograms for the reduction of saturated CO_2 (~ 33 mM) and CO (~ 1 mM) on copper in a phosphate buffer (pH 7) at a scan rate of 1 mV s^{-1}. Middle: associated non-volatile products measured with HPLC. Bottom: associated mass fragments of volatile products measured with OLEMS. Data for CO_2 is shown with a solid line and plotted against the left axis, data for CO is shown with a dashed line and plotted against the right axis.

3.3 Results

The reaction products formed during the reduction of saturated CO_2 (~ 33 mM) and CO (~ 1 mM) on copper in a phosphate buffer are shown in Fig. 3.1, together with the measured current density. From 0.0 V till -0.4 V there is no reduction current for both reduction reactions, neither any product detected by HPLC and OLEMS. From -0.4 V the current increases due to the formation of H_2 as can be seen by the increase of $m/z = 2$ in the mass spectrometer. At lower potentials the H_2 formation continues to increase, resulting in the formation of hydrogen gas bubbles starting at -0.6 V which causes the fluctuations in the current below this potential. The amount of hydrogen gas formed is about 10 times lower in the case of CO reduction. At -0.5 and -0.6 V $m/z = 26$ appears in the mass spectrometer for respectively CO and CO_2. This is $C_2H_2^+$ and could be a fragment of ethane and ethylene. Since we did not observe a similar increase in $m/z = 29$ and 30 (fragments of ethane) we could relate this $C_2H_2^+$ fragment to the formation of ethylene. The absence of ethane formation is in agreement with the earlier results of Hori.[5] The amount of ethylene produced from CO_2 is about 20 times higher than from CO, mainly caused by the difference in solubility and hence solution concentration of CO and CO_2. At -0.8 V $m/z = 15$ is detected for both reactions. This CH_3^+ fragment represents the formation of methane. The only non-volatile reaction product measured by HPLC is formic acid, from the reduction of CO_2, which is observed at -0.6 V and increases at lower potentials.

In Fig. 3.2 the results are shown for the reduction of 0.05 M formaldehyde in the phosphate buffer. The current, shown in the top panel, is larger than the current observed during CO_2 reduction which cannot only be explained by the difference in concentration. At -0.3 V $m/z = 31$ is detected, followed by the formation of H_2 at -0.4 V ($m/z = 2$). Fragment $m/z = 31$ (CH_2OH^+) is very typical for alcohols. In this measurement this alcohol is methanol, since no fragments of bigger alcohols are observed. As methanol itself is not reduced on copper electrodes,[100,110] it is clear that methanol must be the end product of the reduction of formaldehyde. The formation of methanol shows a small plateau at -0.5 V, becomes stable at -0.7 V and is higher on the back scan. We also measured the other main fragments of methanol, $m/z = 15$, 29, and 30 as shown in Fig. 3.3. The signals in this figure are normalized to allow for a direct comparison, which is not possi-

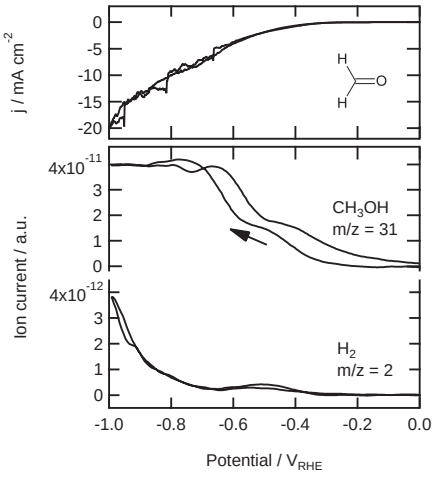

Figure 3.2 Top: cyclic voltammogram for the reduction of 0.05 M formaldehyde on copper in a phosphate buffer (pH 7) at a scan rate of 1 mV s^{-1}. Bottom: associated mass fragments measured with OLEMS.

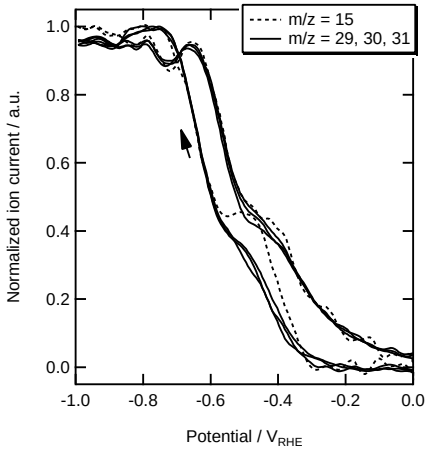

Figure 3.3 Normalized mass signals for the reduction of 0.05 M formaldehyde on copper in a phosphate buffer (pH 7).

ble on the real scale. The normalization was done by dividing each signal (after the background correction) by its highest value, thereby obtaining a signal that has its minimum at 0 and its maximum at 1. It can be seen that m/z = 29, 30, and 31 show the same trend after normalization, which clearly shows that they are fragments of the same molecule. To a large extent, m/z = 15 follows the same trend except at -0.5 V in the negative-going scan and, with a smaller deviation, at -0.4 V in the positive-going scan. This shows that at these potentials a product is formed, different from methanol, with CH_3^+ as one of its mass fragments. This peak is not found in any mass fragment higher than 15 (m/z = 16 we cannot measure because this is a fragment of water, that dominates the signal). Therefore, this peak must be related to the formation of methane.

Since DFT calculations suggest methoxy to be the precursor to methane, we tried to reduce methanol at high pH.[86] Methanol at high pH will be deprotonated, resulting in the formation of methoxide in solution. However, we did not observe any formation of methane nor any reduction activity.

The results of the reduction of glyoxal ($(HCO)_2$) and glycolaldehyde (OHCCOH) are shown in Fig. 3.4. The currents, shown in the top panel of this figure, are higher than the current for the reduction of CO_2 but lower than for the reduction of formaldehyde. The production of H_2 is severely delayed and becomes only significant at -0.7 V. The peak in H_2 production at -0.55 V observed during the reduction of CO and formaldehyde is much smaller for glyoxal reduction and not observed for the glycolaldehyde reduction. For both reactions, at -0.35 V the formation of a reduction product with one of its main fragments at m/z = 29 is observed. This mass fragment shows two reproducible peaks at -0.5 V and -0.7 V. These peaks are also observed in the back scan, but at less negative potentials. The intensity of the signal is also lower in the back scan. Mass fragments m/z = 41 en 44 (data not shown) showed the same trend as m/z = 29 and from the relative intensities it was clear that acetaldehyde is formed here. At -0.6 V the formation of an alcohol starts, as shown by the increase of m/z = 31. The formation of this alcohol is higher in the positive going scan. Mass fragment m/z = 46 ($C_2H_5OH^+$, data not shown) showed the same trend as m/z = 31, which means that the alcohol formed here is ethanol. This clearly shows that both glyoxal and glycolaldehyde are first reduced to acetaldehyde starting at -0.35 V, which is then further reduced to ethanol at -0.6 V. Only during

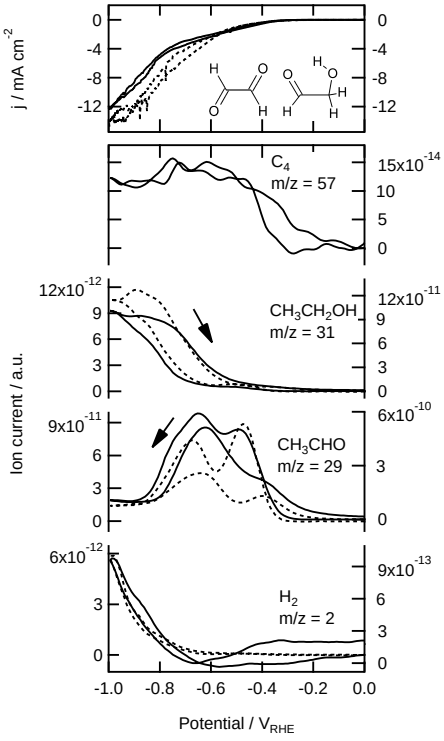

Figure 3.4 Top: cyclic voltammograms for the reduction of 0.05 M glyoxal and 0.05 M glycolaldehyde on copper in a phosphate buffer (pH 7) at a scan rate of 1 mV s^{-1}. Bottom: associated mass fragments measured with OLEMS. Data for glyoxal is shown with a dashed line and plotted against the left axis, data for glycolaldehyde is shown with a solid line and plotted against the right axis.

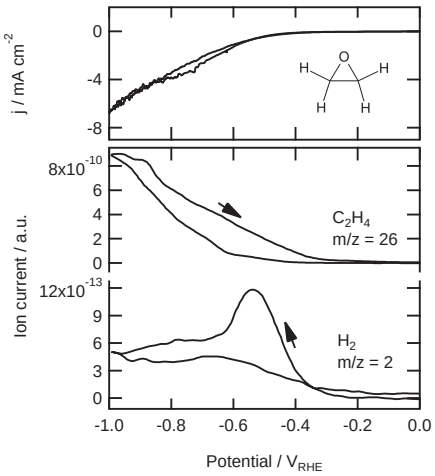

Figure 3.5 Top: cyclic voltammogram for the reduction of ethylene oxide on copper in a phosphate buffer (pH 7) at a scan rate of 1 mV s^{-1}. Bottom: associated mass fragments measured with OLEMS.

the reduction of glycolaldehyde we observe bigger mass fragments, m/z = 57, 62, and 70, which are indicative for C_4 species (only m/z = 57 is shown). These fragments are not observed during the reduction of glyoxal. The most likely candidates, if we assume that this C_4 species is formed by the combination of two reaction products or intermediates of glycolaldehyde, are 1,4-butanediol (m/z = 57, 62) and 1,4-butenediol (m/z = 57, 70).

Another interesting molecule to reduce, if we consider that glyoxal and glycolaldehyde both are reduced to ethanol, is ethylene glycol. We tried to reduce 0.05 M ethylene glycol in 0.1 M phosphate buffer but did not observe any reduction product. We also tried oxalic acid, but did not observe any reduction products either.

The possible formation of an epoxide as the intermediate in the formation of ethylene was investigated by the reduction of ethylene oxide, the results of which are shown in Fig. 3.5. The exact concentration was unknown since ethylene oxide is highly soluble in water but it was dosed as gas bubbles in the solution. We followed the increase of ethylene oxide concentra-

tion with OLEMS during dosing and after a significant increase we stopped bubbling and started the reduction. During the reduction, the formation of hydrogen (m/z = 2) was lower compared with the other measurements (10^{-13} vs. 10^{-12}) and showed a peak at -0.55 V as observed before in the other measurements. Around -0.5 V we observe an increase in m/z = 26. We only observed the same increase in m/z = 27 (not shown), indicating that the product formed here is ethylene. In the positive going scan the formation of m/z = 26 is higher than the negative going scan and disappears around -0.3 V. The other mass fragments measured (m/z = 15, 29-31, 43-45) also increased (data not shown) but with relative intensities that were exactly the same as observed during the dosing of ethylene oxide, which means that with the formation of (gas bubbles of) hydrogen and ethylene at the electrode also ethylene oxide from the solution enters the tip of the OLEMS.

3.4 Discussion

3.4.1 Hydrogen and hydrogenation

From Fig. 3.1 it is clear that, when lowering the potential at the copper electrode in a CO_2 or CO saturated solution at pH 7, first hydrogen gas is formed from water. Then, at -0.5 V and -0.6 V ethylene is formed from CO and CO_2 respectively, and finally at -0.8 V methane is formed. The currents are mainly determined by the water reduction and do not give any specific information about the reduction reactions. The currents observed during the reduction of the other organic molecules are all higher than the current observed during the CO and CO_2 reduction. The current of the CO reduction is most likely the lowest because the concentration of CO (~1 mM) is much lower than the concentrations of the other species (0.05 M). The concentration of ethylene oxide might be even higher, since the observed intensity of m/z = 26 is higher (10^{-10} vs. 10^{-11}) and the hydrogen production lower (10^{-13} vs. 10^{-12}) compared with the other measurements at 0.05 M. The current for the reduction of CO_2 is most likely lower because CO_2 is a very stable molecule and, therefore, hard to reduce as appears from the observations that the rate determining step in the overall CO_2 reduction is the first electron transfer.[99]

In almost all cases there is a peak in the hydrogen production around -0.55 V. It is also around this potential that, for all reductions performed

in this study, the first reduction products are measured. From this we can conclude that, as might be expected since we are hydrogenating small organic molecules, there is a relation between the hydrogen concentration or hydrogen coverage at the surface and the reduction reaction taking place. Previous research also showed the relation between the hydrogen and carbon monoxide adsorption at the electrode as a function of potential. It is known that the hydrogen evolution is suppressed by CO adsorption, *i.e.* the surface is blocked by CO.[99,111] This could also explain the lower currents observed during the reduction of CO and CO_2, since the current is mainly determined by the hydrogen evolution, which is partly blocked by the presence of CO. The adsorption of CO has also been suggested to be accompanied by hydrogen, resulting in the formation of a surface hydridocarbonyl complex.[3]

3.4.2 The C_1 pathway: route to methane

From Figs. 3.2 and 3.3 we can conclude that formaldehyde is not an intermediate in the reduction of carbon dioxide, since its main reduction product is methanol which is not a product observed during the reduction of carbon dioxide. We can exclude that the methanol is formed by a chemical, so-called Cannizzaro reaction.[112,113] In this reaction, aldehydes without an α-hydrogen, such as formaldehyde, are disproportionated into a carboxylic acid and an alcohol. Since we do not observe formic acid with HPLC during formaldehyde reduction, methanol must be formed by the electrochemical reduction of formaldehyde.

The observed peak in m/z = 15 around -0.5 V during the reduction of formaldehyde can only be explained by the formation of methane, since no larger mass fragments are observed. This is in agreement with the literature, in which the formation of small amounts of methane during the reduction of formaldehyde using long term electrolysis has been observed.[84,100,114] These and our results indicate the presence of an intermediate related to formaldehyde which can be reduced to methane. The most likely candidate for this intermediate is formyl (CHO_{ads}).

Formyl has been studied in detail because of its importance for the mechanism of the Fischer-Tropsch process. From these studies it is known that with formaldehyde in solution formyl is formed.[100,115] In addition, quantum chemical calculations have been performed on adsorbed CO and formyl

to elucidate the mechanism of the Fischer-Tropsch process. These calculations show that on Co and Ru, the most frequently used metals for this process, the dissociation of adsorbed carbon monoxide can be activated by the assistance of hydrogen, *i.e.* through the formation of formyl.[116–119] This, so-called "hydrogen assisted CO activation", is only the optimum pathway on flat surfaces whereas at defects on the surface the direct dissociation of CO is favored. Recently, density functional theory (DFT) calculations of CO on Cu(100) performed in our research group show that also on Cu(100) the C-O bond breaking in adsorbed carbon monoxide may be facilitated by the formation of formyl.[120]

These DFT calculations also suggest that there will be a relation between the surface structure of the copper electrodes and the mechanism of the CO reduction. This is in agreement with the work of Hori *et al.* on Cu single crystals, which showed that on the Cu(100) surface more ethylene is formed whereas the Cu(111) surface produces more methane.[87] Moreover, with the introduction of steps in Cu(111) and, to a lesser extent in Cu(100), ethylene becomes the major product. Therefore, one could speculate that the formation of methane through the indirect dissociation of CO is likely to happen on atomically flat (111) parts of the electrode or steps and defects in such a surface, whereas ethylene will be formed at (100) sites, and (100)-type defects in the (111) terraces. We have studied this issue in more detail using copper single crystals, see Chapter 5.

Using DFT, Peterson *et al.* suggested that the key "potential-determining" step in the formation of both methane and ethylene is the hydrogenation of adsorbed CO to form CHO_{ads}.[86] Although we do not have any experimental proof that CHO_{ads} is the precursor to ethylene, these calculations support our suggestion that CHO_{ads} is the intermediate in the formation of methane. These calculations, on the other hand, also suggest that the energetically favored route to methane is through adsorbed formaldehyde and methoxy. This appears in conflict with the experimental observations that the main reduction product of formaldehyde is methanol and that methoxy cannot be reduced to methane on copper electrodes.

Since the reduction of CO does not result in the formation of methanol whereas the reduction of formaldehyde does, there must be a precursor formed during the reduction of formaldehyde that is not formed during the reduction of CO, which can be further reduced to methanol. We sug-

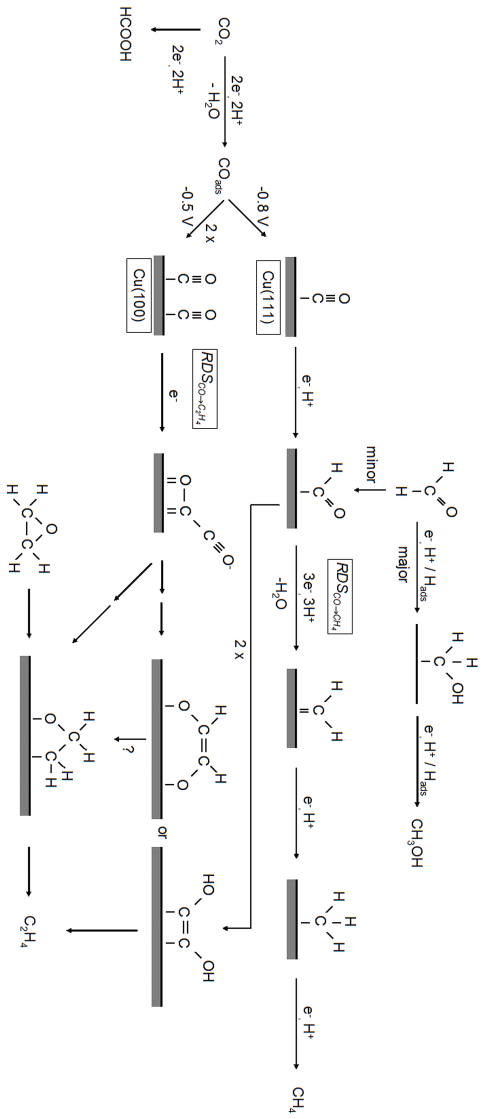

Figure 3.6 Proposed mechanism for the electrochemical reduction of carbon dioxide on copper

gest that the formation of CHO_{ads} lowers the energy needed to break the C-O bond and, therefore, facilitates the formation of methane. The pathway to methanol, in which the C-O bond is kept intact, will then probably occur via CH_2OH_{ads} because formaldehyde already has two hydrogen atoms bonded to the carbon and, therefore, CH_2OH_{ads} only needs to be protonated to form methanol.[114,121,122] These two pathways are shown in the top part of Fig. 3.6. In this figure, we suggest that CHO_{ads} is the intermediate that leads to methane, whereas CH_2OH_{ads} leads to the formation of methanol.

It is interesting to compare our mechanism for the electrochemical reduction of carbon dioxide to the mechanism proposed for the methanol synthesis process, since methanol is made from syngas using a copper based ($Cu/ZnO/Al_2O_3$) catalyst. Methanol, however, is not observed during the electrochemical reduction of CO_2. This indicates that the C-O bond is broken early in the electrochemical reaction mechanism. In the case of methanol synthesis, it is generally accepted that formate is the key intermediate to methanol.[29,31] This formate is further reduced to formaldehyde and finally to methanol. The latter reaction also takes place under electrochemical conditions, but the former does not. We speculate that the inactivity of formate to be further reduced in our experiments could be primarily due to the lower temperature, lower pressure, and different catalyst properties, compared with methanol synthesis, but clearly this subject would require further scrutiny.

If we compare our route to methane to the mechanism proposed by Hori, we observe that the routes to methane are quite similar. Hori *et al.* also proposed that, in agreement with our findings, CO is protonated before the C-O bond is broken.[84] However, they suggest the "hypothetical intermediate COH" to be the precursor to methane. We have shown that it is more likely that this intermediate is CHO.

3.4.3 The C_2 pathway: route to ethylene

To find intermediates in the reduction of carbon monoxide to ethylene we investigated the reduction of C_2 species containing one or two oxygen atoms. Comparing the reduction of C_2 species containing two oxygen atoms, namely glyoxal and glycolaldehyde (Fig. 3.4) and ethylene glycol (data not shown), we observe that glyoxal and glycolaldehyde are reduced to acetaldehyde. Ethylene glycol cannot be reduced at all. Acetaldehyde is reduced to ethanol,

which is in agreement with previous work.[84] From these measurements we can conclude that neither glyoxal or glycolaldehyde is an intermediate in the reduction of carbon monoxide, since their reduction products, acetaldehyde and ethanol, are not observed during CO_2 reduction.

The difference in reducibility between the various C_2 species can partly be explained by the various adsorption geometries. It is known that both glyoxal and glycolaldehyde are adsorbed on platinum with one or two carbons bonded to the surface, depending on the coverage.[123,124] Ethanol and acetaldehyde, on the other hand, are adsorbed with the oxygen towards the surface.[125–128]. This indicates that for the breaking of the C-O bond the carbon atom needs to be coordinated to the surface. However, this does not explain why ethylene glycol cannot be reduced since it is known to also adsorb with the carbon atoms to the surface.[129]

A more consistent explanation is that the breaking of a C-O or C-OH bond is only possible if the next (α) carbon is an aldehyde. If the α-carbon is an alcohol the bond remains intact. If the α-carbon is a methyl group (acetaldehyde, ethanol), the C-O bond cannot be broken but only reduced to an alcohol. The chemical environment of the C-O bond within the molecule, therefore, appears to be very important for the activation of the C-O bond.

Another important observation is that the C-O bonds for both the aldehyde in glyoxal and the alcohol in glycolaldehyde are broken at the same potential, which suggest that it is in fact the alcohol in which the C-O bond breaking occurs. One of the aldehydes of glyoxal is probably reduced to an alcohol first and this intermediate is directly further reduced to acetaldehyde by C-OH bond breaking.

Fig. 3.4 shows that only during the reduction of glycolaldehyde a very small amount of C_4 species is formed. The reason that only between glycolaldehyde molecules a C-C bond can be formed might be that it is mostly in the *cis*-configuration whereas both ethylene glycol and glyoxal are mostly in the *trans*-configuration. This *cis*-configuration could cause an adsorption configuration where two glycolaldehyde molecules can adsorb close to each other, which makes the formation of a C-C bond more feasible. For the *trans*-isomers the formation of the C-C bond would then be sterically hindered by the oxygen atoms.

The final possible intermediate in the reduction of carbon dioxide we studied was ethylene oxide (Fig. 3.5). The only product observed is ethy-

lene, no alcohols or aldehydes. The potential range in which ethylene is formed is in very good agreement with the potential range where ethylene is formed from CO, shown in Fig. 3.1. This suggests that an epoxide is a possible intermediate in the CO reduction to ethylene. However, ethylene oxide itself is never observed as a reduction product of CO or CO_2. Therefore, we propose adsorbed ethylene oxide to be a possible intermediate in the reduction of CO. A strongly adsorbed epoxide, in the form of an oxametallacycle, is a possible precursor to ethylene formation, and thereby a possible intermediate in the CO_2 reduction to ethylene. These oxametallacycles are known as key intermediates in the ethylene epoxidation.[130,131] We have attempted to 'trap' such oxametallacycle intermediates by quickly transferring a copper electrode from an ethylene oxide containing solution to a clean solution, but without success. Presumably, it is very unstable.

Although we now have a hint for a possible intermediate for the formation of ethylene from CO, we still do not know how the C-C bond is formed. Hori *et al.* suggested two routes to ethylene: the combination of two adsorbed CH_2 species, and a Fischer-Tropsch like combination of adsorbed CH_2 and CO ('CO insertion').[84] The latter route results in the formation of CH_xCO species. However, from the CH_xCO species we tried only ethylene oxide resulted in the formation of ethylene, suggesting that it is a different mechanism that leads to the formation of ethylene.

It is very likely that the C-C bond is formed very early in the reaction in a pathway separate from methane production. Two important indications for this are that (i) it is known that for the formation of ethylene from CO the rate determining step (RDS) is the first electron transfer (whereas the second electron transfer is RDS for methane formation), and (ii) the ethylene formation pathway is pH independent whereas the methane formation pathway involves a proton in or before the RDS.[84] Therefore, the pH-independent RDS for ethylene formation is probably the formation of the C-C bond. We suggest that the C-C bond is formed by the formation of a dimer of two CO molecules, and that this dimer is the first intermediate to the formation of ethylene. This CO dimer was also proposed as an intermediate to ethylene by Gattrell *et al.* [99]

Dimer formation is well known and accepted in the reduction of NO, a molecule similar though more reactive than CO. The involvement of NO dimer formation has been evidenced for NO reduction to N_2O in the gas-

phase heterogeneous catalysis literature [132,133] as well as in the electrochemical literature. [134,135] A potential link in mechanism between CO and N_2 reduction has also been suggested by Lee *et al.* [136]

The next important step in the reduction of the dimer, the breaking of the first C-O bond, may happen in analogy with the reduction of glyoxal and glycolaldehyde, where -OH is shown to be the leaving group if the α-carbon is an aldehyde. Since we show that ethylene oxide reduction only results in ethylene, we suggest that the remaining intermediate is an oxametallacycle. This leads to the pathway shown in Fig. 3.6.

Another possibility, shown in Fig. 3.6, is that the C-C double bond in ethylene is formed by so-called McMurry coupling. [137,138] In the McMurry reaction a reducing agent is used to make a bond between two carbonyl groups. This reducing agent, which would be the copper surface in our reaction, creates carbonyl radicals which react to form a C=C bond. The next step is the removal of the oxygen atoms by the reducing agent, with a double C-C bond as the end product. Since we have ethylene as the main C_2 product, a McMurry-like reaction would very well explain the observed selectivity towards ethylene. The distinguishing feature of the McMurry mechanism is that the C=C bond is formed before C-O bond breaking, leading to an enediol or enediolate intermediate. Such a McMurry mechanism has, for example, been observed during the coupling of carbon monoxide to acetylene and ethylene on $UO_2(111)$ surfaces as well as uranium complexes. [139,140] In these studies it has been shown that an enediolate is formed from CO and hydrogen, which reacts to form acetylene and ethylene. In addition, it is known that enediols can be formed by the reduction of α-dicarbonyl species, *e.g.* as happens in the reduction of quinone to catechol. [141,142] Therefore, we propose the enediol or enediolate as a possible intermediate to ethylene in Fig. 3.6.

3.4.4 General discussion

The mechanism proposed in Fig. 3.6 is based on our experimental results combined with the mechanisms suggested in literature. [84,99,100] The overall RDS in the reduction of CO_2 is the first electron transfer to form $CO^-_{2,ads}$. [99] This intermediate then reacts further to CO or formate, the latter being a dead-end in the reaction mechanism. [99,114] CO is further reduced to hydrocarbons via two pathways, a C_1 and a C_2 pathway, with the overall product

distribution being determined by the relative importance of the local RDS within each pathway.

The mechanism incorporates the important results by Hori *et al.* who showed that for the formation of ethylene from CO the first electron transfer is the RDS and is uncoupled from proton transfer, whereas for methane the RDS is after the first electron transfer and includes a proton transfer step.[84] In our mechanism the RDS to form ethylene would be the formation of the CO dimer accompanied by the first electron transfer, and the RDS to form methane is the breaking of the C-O bond in the formyl intermediate.

In many of the older mechanistic papers on CO_2 reduction, surface carbene ($CH_{2,ads}$) was considered as the key intermediate in the formation of both CH_4 and C_2H_4. Such a mechanism is in disagreement with the above-mentioned results of Hori *et al.*[84] and also does not easily explain why ethylene is the only multiple-carbon compound observed as a product. Hori *et al.* proposed a CO-insertion type mechanism (*i.e.* a coupling between CH_x and CO) as an alternative pathway, but again such a mechanism does not easily explain why ethylene is the only observed carbon-carbon coupling product. Peterson *et al.* suggest formyl as the intermediate to both methane and ethylene, though no explicit pathway was suggested for ethylene formation.[86] We believe that one of the very attractive features of the model suggested here is that it easily explains why C_2 products are the main coupling products (due to dimerization) and why ethylene is the only product (through an oxametallacycle or enediol-type intermediate). It appears to us that, at present, the mechanism suggested in Fig. 3.6 is the most consistent with the experimental data.

3.5 Conclusions

This chapter has introduced a new mechanism for the electrochemical reduction of carbon dioxide on copper electrodes. We have shown that it is very likely that CHO_{ads} is the key intermediate towards the breaking of the C-O bond and, therefore, the formation of methane. For the formation of ethylene we suggest that the first step is the formation of a CO dimer, followed by the formation of an enediol or enediolate, or the formation of an oxametallacycle as can be concluded from the reduction of ethylene oxide. In contrast to previous proposed Fischer-Tropsch like mechanisms, both the

enediol(ate) and the oxametallacycle would explain well the experimentally observed selectivity of the C_2 pathway towards ethylene.

4 | The electrochemical characterization of copper single crystal electrodes in alkaline media

Abstract

The use of single crystals in electrochemistry requires careful characterization of the surface structure. This paper addresses the characterization of Cu single crystals using blank cyclic voltammetry in alkaline media. The adsorption and desorption of OH species in the underpotential region of Cu_2O formation (-0.25 V - 0.2 V vs. RHE) in alkaline media occur at different potentials on Cu(111) and Cu(100), whereas OH adsorption on Cu(110) is not observed in this potential region. This allows for a direct distinction of the Cu(*hkl*) basal planes. The adsorption of OH on Cu(111) induces a reconstructed adlayer on the surface. On Cu(322), a stepped surface with 5 atom wide (111) terraces, OH adsorption is observed in the same potential range as on Cu(111), but on Cu(322) reconstruction does not seem to take place. This is explained by the fact that the unit cell of the reconstructed layer is much larger than the (111) terrace width of Cu(322) and, therefore, reconstruction cannot take place. Cu(911), having 5 atom wide (100) terraces, exhibits the same voltammetric features as Cu(100), but with a lower intensity. This is explained by the lower amount of (100) terraces present on this surface.

4.1 Introduction

Copper has some unique properties in electrocatalysis, such as a high activity for the electrochemical reduction of nitrate and carbon dioxide. For nitrate reduction, Cu is one of the most active electrode materials.[143] On Cu electrodes, carbon dioxide is converted to hydrocarbons with a relatively high selectivity.[4,5] Therefore, Cu single crystals have been the subject of several recent electrochemical investigations, with the aim to relate the catalytic activity to the atomic surface structure.[87,143–145]

The use of single crystals requires detailed characterization of the atomic surface structure, to allow for the relation between surface structure and (electro-)chemical activity. Single crystal electrodes are usually characterized using blank cyclic voltammetry (CV). For Cu single crystals, the knowledge about the electrochemical characterization of the Cu(*hkl*) surfaces using blank voltammetry is limited. Therefore, we present here a method using blank voltammetry in alkaline media that clearly distinguishes the Cu basal planes, which can also be used to indicate the presence of steps on the surface. Our method builds on previous procedures for the electrochemical characterization of Cu single crystals.

Using blank voltammetry in H_2SO_4, only Cu(111) terraces can be distinguished, since on these terraces sulphate adsorption and desorption can be observed in the potential region between hydrogen evolution and Cu oxidation (-0.3 V - 0.3 V vs. RHE).[146,147] However, on Cu(100) the CV is completely featureless in this potential region.[146,147] We have also measured Cu(110) in H_2SO_4, which gave a CV very similar to that of Cu(100) (data not shown).

In their work on CO_2 reduction, Hori *et al.* present CVs of the Cu basal planes and a number of stepped surfaces in carbon monoxide-saturated phosphate buffers at pH 7.[5,87,148] For Cu(100) and Cu(110) a pair of peaks is observed in the CV, whereas these peaks were not observed in the CV of Cu(111). These peaks, with the peaks observed on Cu(100) at lower potentials compared with Cu(110), have been attributed to charge displacement due to desorption of phosphate during CO adsorption, as was confirmed by IR spectroscopy.[149] For the CVs of several stepped Cu surfaces, with steps of (100) and (111) orientation, similar peaks have been observed. Hori *et al.* have found that the charge of the peaks corresponds to the step density.[87,149] Recently, using voltammetry combined with STM, phosphate ad-

sorption and desorption has been observed on Cu(111), accompanied with small peaks in the CV of Cu(111).[150] Overall, the characterization of Cu single crystals in CO saturated phosphate buffers can be used to distinguish the various Cu single crystals, but its main drawback is that it requires the use of carbon monoxide.

Another electrochemical characterization could make use of the differences in the CVs for the onset of Cu_2O formation in alkaline media. The formation of Cu_2O is preceded by the adsorption of oxygen species, which has been shown to be surface structure dependent.[151] Although it is possible to identify the Cu basal planes in this way, the differences are rather small, hence this method does not seem suitable for stepped surfaces.

For our characterization method we were inspired by the work of Jović and Jović, who have studied OH adsorption on Cu(111) and Cu(100) in alkaline media using cyclic voltammetry, a potentiostatic pulse technique and electrochemical impedance spectroscopy.[152,153] Their results showed very different CVs for Cu(111) and Cu(100) in the underpotential region of Cu_2O formation (-0.25 V - 0.2 V vs. RHE). It was shown that slow and irreversible reconstruction of Cu(111) occurs as a consequence of OH adsorption/desorption. In the same potential region we have investigated, next to Cu(111) and Cu(100), the CVs of Cu(110) and two stepped surfaces: Cu(911), with the [5(100)x(111)] orientation, and Cu(322), with the [5(111)x(100)] orientation. These CVs all exhibit clear differences, and can therefore be used to characterize Cu single crystals.

4.2 Experimental

All experiments were carried out in an electrochemical cell using a three-electrode assembly at room temperature. The cell and glassware were boiled in ultra clean water (Millipore MilliQ gradient A10 system, 18.2 $M\Omega \cdot cm$) before each experiment. A gold wire was used as counter electrode and a reversible hydrogen electrode (RHE) in the same electrolyte was used as reference electrode. All potentials in this paper are referred to this electrode. The potential was controlled using an Ivium A06075 potentiostat.

The single crystal copper electrodes used were bead-type electrodes cut and polished with an accuracy down to 0.5° (icryst). Prior to each experiment the electrode was electropolished in 66% H_3PO_4 at 3 V vs. a Cu counter electrode for 10 seconds.[154] After electropolishing, the electrode

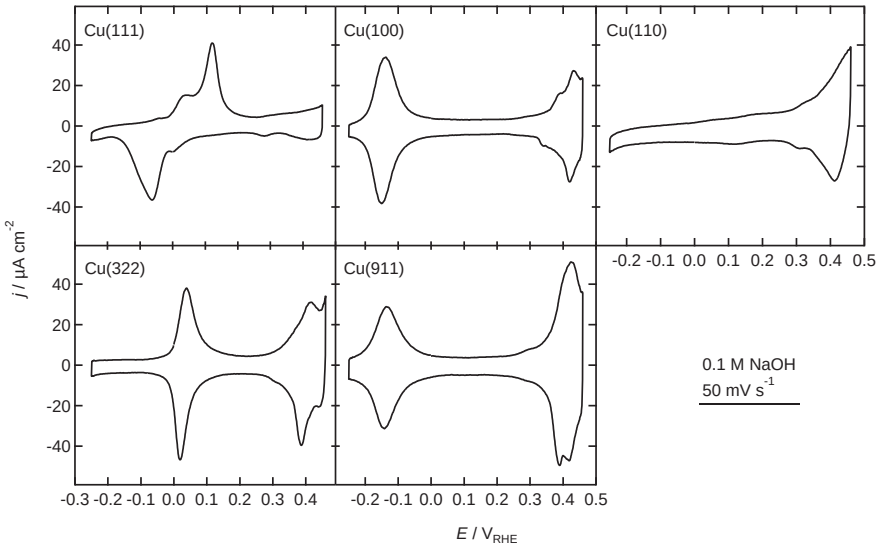

Figure 4.1 Cyclic voltammograms of five Cu single crystals in 0.1 M NaOH, recorded at 50 mV s^{-1}.

was rinsed with water and transferred to the electrochemical cell. The potential of the electrode was 0 V when immersed in the electrolyte. All cyclic voltammograms were recorded until a stable voltammogram was obtained, using a sweep rate of 50 mV s^{-1} .

The experiments were carried out in 0.1 M NaOH (pH 13) prepared from high purity reagents (Sigma-Aldrich TraceSelect) and ultra clean water. Argon (Air Products, 5.0) bubbling was used to deaerate the electrolyte.

4.3 Results

The CVs of the three Cu single crystal basal planes, Cu(111), Cu(100), and Cu(110) in 0.1 M NaOH are shown in Fig. 4.1. The CV of Cu(111) exhibits an anodic peak at 0.12 V, a cathodic peak at -0.06 V, and a pair of smaller peaks at 0.02 V. There is only a small oxidation/reduction current above 0.3 V. For Cu(100), a pair of peaks is observed at -0.15 V. The oxidation current

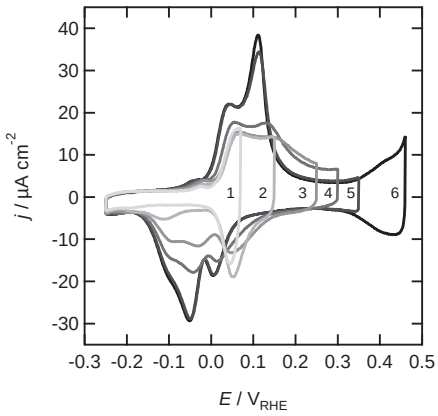

Figure 4.2 Cyclic voltammograms of Cu(111) in 0.1 M NaOH, scanned to increasing anodic potentials, recorded at 50 mV s^{-1}.

above 0.3 V is larger, with pair of peaks around 0.43 V. For Cu(110) the CV looks again different, no peaks are observed between -0.2 and 0.3 V. The oxidation current at high potentials is the largest of the three basal planes. For most CVs shown in Fig. 4.1, but in particular for Cu(111) and Cu(110), the current is not symmetrical around zero below 0 V, due to the presence of oxygen in the electrolyte which is reduced at the electrode. This oxygen is very hard to remove in alkaline media.

Fig. 4.1 also shows the CVs of the two stepped Cu single crystal surfaces investigated in this work. Cu(322), which has 5 atoms wide (111) terraces with a (100) step, shows a pair of peaks at 0.02 V, at a similar potential at which the small pair of peaks at Cu(111) is observed. The oxidation/reduction current above 0.3 V is significantly higher compared with Cu(111), has a peak at 0.41 V and a corresponding reduction peak at 0.38 V. Cu(911), with 5 atoms wide (100) terraces and a (111) step, exhibits a pair of peaks at the same potentials as observed on Cu(100), but the current density for the peak at -0.15 V is lower. At higher potentials we observe an anodic peak at 0.42 V, and two overlapping cathodic peaks at 0.39 V and 0.42 V.

To investigate the rather complicated CV of Cu(111) in more detail, we performed the measurement shown in Fig. 4.2. We kept the Cu(111) electrode at a standby potential of -0.25 V before and after recording the CV, which is different from the CVs shown in Fig. 4.1, where a standby potential of 0 V was used. Next, we performed a series of CVs in which we stepwise increased the maximum anodic potential. In the first scan (no. 1) a pair of peaks at 0.05 V is observed, which is at a slightly higher potential compared with the pair of peaks at 0.02 V in the CV of Cu(111). With increasing anodic potentials, the peaks at 0.12 V and -0.06 V start growing, until a CV is obtained that looks similar to the CV of Cu(111) shown in Fig. 4.1

4.4 Discussion

The underpotential region of Cu_2O formation (-0.25 V - 0.2 V) in alkaline media has not been extensively studied, only a few papers address the CV in this potential region.[152,153,155,156] By comparing surface-enhanced Raman spectra of H_2O and D_2O alkaline electrolytes, Härtinger *et al.* observed Raman bands corresponding to the formation of surface CuOH species on Cu(111).[155] The intensity of these bands was found to depend on potential, and on the time of holding the electrode at a given potential. The intensity of the bands increases when stepping from 0.5 V, a potential where the formation of Cu_2O starts, to a much more negative potential, -0.1 V.

Our CV of Cu(100), shown in Fig. 4.1, is very similar to the CV recorded by Jović and Jović,[153] and, based on the described literature, the pair of peaks observed at -0.15 V is assigned to OH adsorption/desorption. The charge corresponding to these peaks, measured between -0.25 V and 0 V, is $\sim$50 $\mu C\,cm^{-2}$. Since the charge corresponding to a full monolayer is 240 $\mu C\,cm^{-2}$, this charge corresponds to a coverage of 0.2 ML.

The same peaks are observed in the CV of Cu(911), although with a lower intensity: the calculated charge is $\sim$46 $\mu C\,cm^{-2}$. Since these peaks are observed at the same potential as for Cu(100), these peaks can be assigned to OH adsorption/desorption on/from the (100) terraces, and the lower charge corresponds well with the lower amount of (100) terraces present on this surface.

For Cu(111), we observe a more complicated voltammogram. The CV shown in Fig. 4.1 is similar, but not identical to the CV recorded by Jović and Jović.[153] However, as can be concluded from Fig. 4.2, the position and

intensity of the peaks strongly depends on the maximum anodic potential of the CV, and the CVs in Fig. 4.2 scanned to ∼0.3 V look much more like the CV shown in Ref. 153. From Fig. 4.2 it can also be concluded that the anodic peak at 0.12 V and the cathodic peak at -0.06 V are related, and in between those peaks there is a smaller pair of peaks at 0.02 V. Fig. 4.2 suggests that these peaks are developed only if the electrode is cycled to ∼0.2 V and higher. The total charge corresponding to these peaks, calculated between -0.25 V and 0.2 V, is ∼62 $\mu C\,cm^{-2}$. A full monolayer coverage on Cu(111) corresponds to a charge of 302 $\mu C\,cm^{-2}$,[157] so the charge of the CV corresponds to a coverage of 0.2 ML of OH species, in agreement with the work of Maurice *et al.* on Cu(111).[156]

Combining cyclic voltammetry with STM, Maurice *et al.* observed a reversible adsorption/desorption process in the underpotential region of Cu_2O formation on Cu(111) in NaOH, with a reversible potential of formation of 0.092 V.[156] Adsorption and desorption were observed to initiate at the step edges on the upper terrace side, causing a lateral growth of the terraces and the formation of Cu adislands having the $Cu_2O(111)$ structure, with a hexagonal lattice having a unit vector of 0.69 ±0.02 nm and two coincidence cells: $(\sqrt{21} \times \sqrt{21})$R.10° and $(\sqrt{49} \times \sqrt{49})$R.20°. Charge transfer measurements indicated adsorption of hydroxide or hydroxyl groups with one adsorbate per unit cell, *i.e.* a coverage of ca. 0.2 ML. In the presence of chlorine, no lateral growth of the terraces was observed, since the strongly adsorbing Cl^- blocks the step edges.[158] Jović and Jović suggested that irreversible surface reconstruction of Cu(111) occurs as a consequence of the adsorption/desorption of OH^- species, and that adsorption of OH^- species takes place in the potential range more negative than -0.17 V only on reconstructed surfaces. They related the large peaks in the CV at 0.12 V and -0.06 V to OH^- adsorption/desorption with a simultaneous lifting of the surface reconstruction. In Fig. 4.2 we observe a reversible CV up to ∼0.2 V, in agreement with the data of Maurice *et al.* When scanning to higher potentials (scan nos. 3-5) the CV becomes irreversible, which we attribute to OH adsorption/desorption on a irreversibly reconstructed surface induced by O or OH species.

Since the total charge in the CV of Cu(111) corresponds to a fifth of a monolayer, it is likely that the other, smaller pair of peaks at 0.02 V is also related to OH adsorption/desorption. These peaks at 0.02 V are also

observed on Cu(322), but with a higher intensity. The calculated charge of the peaks at 0.02 V in the CV of Cu(322) is ~48 $\mu C\,cm^{-2}$, similar to the charge measured on Cu(911), suggesting that the peaks are related to same phenomena: OH adsorption/desorption. Considering that the peaks at 0.02 V at Cu(322) occur at a similar potential on Cu(111), it is therefore likely that these peaks in both CVs are also related to OH adsorption/desorption from (111) terraces. We assign these peaks at 0.02 V, both on Cu(111) and Cu(322), to OH adsorption/desorption on/from unreconstructed (111) terraces. We propose this based on the fact that Cu(322) has only 5-atom wide (111) terraces, while the OH induced reconstruction has the $Cu_2O(111)$ structure, with a unit cell that is 29 or 44 times the unit cell of Cu(111),[156,159] which would not fit on the (111) terraces of Cu(322). Hence, the charge of the peaks at 0.02 V is much lower on Cu(111) than on Cu(322), since Cu(111) is mainly reconstructed. Since the adsorption of OH induces a lateral terrace growth,[156,158] this could mean that the average (111) terrace width on Cu(322) increases. However, from our CV we cannot deduce further information on the reconstruction/growth of the (111) terraces.

On Cu(100), OH induced reconstruction has also been reported, but the unit cell is much smaller than the $Cu_2O(111)$ reconstruction observed on Cu(111). Kunze *et al.* have reported on the OH induced structural modifications of Cu(100) in the underpotential range of Cu_2O formation.[160] Adsorption of OH induces the formation of dimers of superimposed Cu atoms, presumably in bridging positions. The dimers of superimposed Cu atoms form zig-zag chains, with long range ordering of the zig-zag chains in areas limited in width with $c(2\times6)$ and $c(6\times2)$ domains.

In the CV of Cu(110) no peaks are observed, suggesting that OH adsorption/desorption does not take place in this potential region. One possibility is that Cu(110) adsorbs OH stronger and, therefore, at more cathodic potentials. However, we did not observe a peak in the CV between the start of the hydrogen evolution (-0.35 V) and -0.2 V.

Comparing the CVs of the three Cu basal planes above 0.3 V, we observe the lowest oxidation/reduction current on Cu(111), a relatively high current on Cu(110), and a peak at 0.45 V on Cu(100). This is similar to the results obtained by Droog *et al.*[151] They observed the highest onset potential for Cu_2O formation on Cu(111) and a sharp peak at the onset of Cu_2O

formation on Cu(100). The stepped Cu single crystal surfaces investigated in this paper also have a high oxidation/reduction current in this potential region, and both the CVs of Cu(322) and Cu(911) exhibit a peak at 0.45 V. It seems that step sites, and more open surfaces like Cu(110), are more prone to Cu_2O formation. Our data suggest that the height of the current density in this potential region is at least indicative of the presence of steps on the surface.

4.5 Conclusions

We have shown that blank voltammetry in alkaline media is a good way to characterize Cu single crystals. The adsorption and desorption of OH species in alkaline media occur at different potentials on Cu(111) and Cu(100), whereas OH adsorption on Cu(110) is not observed in the same potential region. On Cu(111) this OH adsorption causes a reconstructed adlayer on the surface, leading to a rather complicated voltammetric response. On Cu(322), a stepped surface with 5 atom wide (111) terraces, OH adsorption is observed in the same potential range as on Cu(111), but here reconstruction does not seem to take place, leading to a corresponding simpler voltammetric response. This may be explained by the fact that the unit cell of the reconstructed adlayer is much bigger than the terrace width on Cu(322). The CV of Cu(911), which has 5 atom wide (100) terraces, shows the same voltammetric features as Cu(100) but with a lower intensity, which can be explained by the lower amount of (100) terraces present on this surface. The oxidation/reduction current above 0.3 V is higher on Cu(110) and the stepped surfaces, probably because on open surfaces sites and steps it is easier to form Cu_2O. Therefore, the CV in this potential range is indicative of steps on the surface.

5 | Two pathways for the formation of ethylene in CO reduction on single crystal copper electrodes

Abstract

Carbon monoxide is a key intermediate in the electrochemical reduction of carbon dioxide to methane and ethylene on copper electrodes. We investigated the electrochemical reduction of CO on two single crystal copper electrodes and observed two different reaction mechanisms for ethylene formation: a first pathway that has a common intermediate with the formation of methane and that takes place preferentially at (111) facets or steps, and a second pathway at (100) facets in which CO is selectively reduced to ethylene at relatively low overpotentials. The (100) facets seems to be the dominant crystal facet in polycrystalline copper, opening up new routes to an affordable (photo-)electrochemical production of hydrocarbons from CO_2.

5.1 Introduction

The low-temperature reduction of carbon dioxide to hydrocarbons could be a very important step in a future sustainable carbon energy cycle.[98] Since the discovery by Hori *et al.* in 1985 it has been known that carbon dioxide can be electrochemically reduced to methane and ethylene, using copper electrodes.[2] The formation of methane and especially ethylene is surprising, and only takes place to a significant extent on copper electrodes. In spite of the extensive literature, the molecular mechanism is still unclear, in particular in relation to the carbon-carbon coupling step leading to the formation of ethylene. Understanding this C-C bond formation is important as it would open up routes to the production of high-energy fuels by the (photo-)electrochemical reduction of CO_2.

It is known that carbon monoxide is a key intermediate in the carbon dioxide reduction, and that from carbon monoxide, methane and ethylene are formed following different mechanisms.[4,5,84,85] The central role of carbon monoxide as the intermediate in the formation of such highly non-trivial products as methane and ethylene follows from the fact that carbon monoxide is the only one-carbon molecule that gives the same product spectrum as carbon dioxide on a copper electrode, as documented in detail in the review by Hori.[5] The formation of methane from CO depends on pH, in such a way that the rate determining step must involve the transfer of a proton and an electron.[84] Our own experiments presented in Chapter 3, as well as DFT calculations by Peterson *et al.*[86] suggested that the key intermediate to form methane is CHO_{ads}. The formation of ethylene from CO, on the other hand, does not depend on pH.[84] Therefore, a dimer of carbon monoxide, whose formation does not involve the transfer of an hydrogen atom but does depend on potential (*i.e.* involves electron transfer), has been suggested as the key intermediate in the C-C coupling.[4,161]

Hori *et al.* showed that the extent of methane and ethylene formation sensitively depends on the surface orientation of the copper electrode.[87] On the (111) facet of the copper fcc crystal the formation of methane is favored, whereas on the (100) facet the formation of ethylene is dominant. Recent DFT calculations by Durand *et al.*[88] predicted that the limiting potential for the formation of the intermediates of the CO_2 reduction to CH_4 is lower on the Cu(211) surface compared with the Cu(111) and Cu(100) surface. No detailed DFT-based mechanism for the formation of ethylene

was suggested, although these authors also consider CHO_{ads} as the intermediate in the formation of ethylene. Since the experiments by Hori *et al.* were carried out as long-term electrolysis experiments at a constant current, detailed information on the pathways of the carbon-carbon bond formation and its potential dependence is missing. Therefore, we report here on the reduction of carbon monoxide on two basal planes, Cu(111) and Cu(100), using online electrochemical mass spectrometry, to investigate the pathway to ethylene. This tip-based sampling technique allows to follow the formation of volatile reaction intermediates and products while changing the potential at the electrode surface, and is similar to the DEMS (Differential Electrochemical Mass Spectrometry) technique.[108,162,163]

5.2 Experimental

All experiments were carried out in an electrochemical cell using a three-electrode assembly at room temperature. The cell and glassware were first cleaned by boiling in a mixture of 1:1 concentrated sulfuric and nitric acid and before each experiment by boiling in ultra clean water (Millipore MilliQ gradient A10 system, 18.2 $M\Omega \cdot cm$). A gold wire was used as counter electrode and a reversible hydrogen electrode (RHE) in the same electrolyte was used as reference electrode. All potentials in this paper are referred to this electrode. The potential was controlled using an Ivium A06075 potentiostat.

The experiments were carried out in 0.1 M K_2HPO_4 + 0.1 M KH_2PO_4 (pH 7) or 0.1 M NaOH (pH 13) prepared from high purity reagents (Merck Suprapur, Sigma-Aldrich TraceSelect) and ultra clean water. Argon (Air Products, 5.0) bubbling was used to deaerate the electrolyte before saturation of the electrolyte with carbon monoxide (Linde, 4.7). The carbon monoxide was used without further purification. Bubbling CO through a concentrated hydroxide solution before entering the working solution did not affect our measurements, suggesting that the CO used is uncontaminated.

The single crystal copper electrodes used were bead-type electrodes cut and polished with an accuracy down to 0.5° (icryst). Prior to each experiment the electrode was electropolished in 66% H_3PO_4 at 3 V vs. a Cu counter electrode for 10 seconds.[154] Blank cyclic voltammograms (CV) in 5 mM H_2SO_4 were taken regulary to verify that our electrode surfaces main-

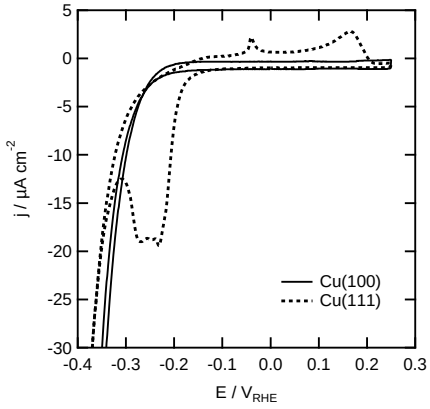

Figure 5.1 Cyclic voltammograms of Cu(100) and Cu(111) in 5 mM H_2SO_4 with a scan rate of 10 mV s^{-1}.

tain the right surface orientation. We used H_2SO_4 because the adsorption and desorption of sulphate on Cu(111) have characteristic features between the potentials of hydrogen evolution and copper dissolution, and therefore serve as a structural probe. On Cu(100), sulphate is not visible in the CV in this potential region. Examples of the CVs are shown in Fig. 5.1, and these voltamettric profiles agree well with the literature.[146]

Online Electrochemical Mass Spectrometry (OLEMS) was used to detect the gaseous products formed during the reaction.[108] The reaction products at the electrode interface were collected with a small tip positioned close ($\sim$ 50 µm) to the electrode. The tip is a 0.5 mm diameter porous Teflon cylinder with an average pore size of 10-14 µm in a Kel-F holder. This tip is connected to a mass spectrometer with a PEEK capillary. The tip configurations were cleaned in a solution of 0.2 M $K_2Cr_2O_7$ in 2 M H_2SO_4 and rinsed with ultra pure water before use. The products were measured while changing the potential of the electrode from 0.0 to -1.0 V and back with 1 mV s^{-1}. We only show m/z = 2 (H_2^+), 15 (CH_3^+) and 26 ($C_2H_2^+$) which correspond to respectively hydrogen, methane en ethylene, but also measured other mass fragments to distinguish, for example, ethylene from ethane. A secondary emission multiplier (SEM) voltage of 2400 V was used for all

mass fragments except hydrogen (m/z = 2) where a SEM voltage of 1200 V was used, because of the relatively high abundance of hydrogen gas caused by the reduction of water. We note that for most of the measurements to be described in this chapter, the Faradaic current is mainly determined by hydrogen evolution and does not give much specific information about the CO reduction.

Because the equilibration of the pressure in the system after introduction of the tip in the electrolyte takes a very long time, all mass fragments show a small decay during the measurement. We corrected for this background by fitting a double exponential function to the data in the potential regions were no change in activity is observed and subtracted this fit from the data. A mild smoothing function is applied to the data for the noise caused by gas bubble formation. All mass fragments shown in this chapter are background corrected in this way. Also note that between measurements, absolute values of the mass signals may vary as it is difficult to reproducibly place the OLEMS tip in relation to the single crystal electrode.

5.3 Results and discussion

Fig. 5.2 shows the reduction of carbon monoxide on Cu(111) in pH 7 (phosphate buffer, plotted with a dashed line with the current density and the mass signals on the left axis) and in pH 13 (NaOH, plotted with a solid line with the current density and the mass signals on the right axis). The potential is changed from 0 to -1 V and back with 1 mV per second. The recorded current is shown in the middle panel, and the volatile products measured during this potential scan are shown in the bottom panel. At -0.4 V the current increases due to the formation of hydrogen, both for pH 7 and 13 (although pH 13 appears to be more active for H_2 evolution). For all measurements performed, this current is mainly determined by hydrogen evolution and does not give any specific information about the CO reduction. The hydrogen evolution leads to the formation of gas bubbles trapped between the tip and the single crystal electrode and this explains the somewhat noisy character of the observed mass signals. At pH 13, hardly any hydrocarbons are observed, only very small amounts of methane (represented by m/z = 15, CH_3^+) and ethylene (represented by m/z = 26, $C_2H_2^+$) are formed at the most negative potentials, as well as a very small amount of ethylene but no methane) at -0.45 V. The latter is probably due to some (100) defects

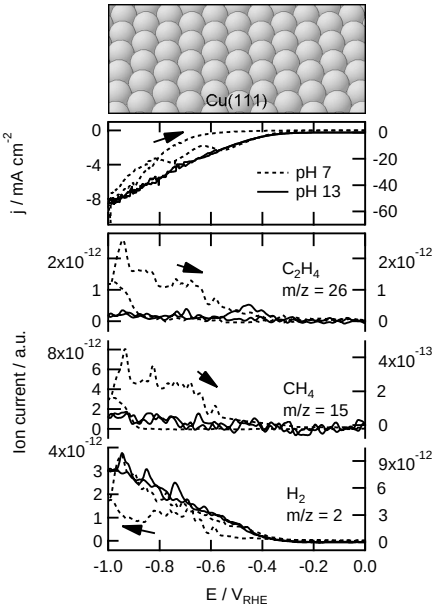

Figure 5.2 Top: (111) facet of the Cu fcc crystal. Middle: cyclic voltammograms on Cu(111) for the reduction CO saturated (∼ 1 mM) in a phosphate buffer (pH 7) and NaOH (pH 13). Bottom: associated mass fragments of volatile products measured with OLEMS. Data for pH 7 is shown with a dashed line and plotted against the left axis, data for pH 13 is shown with a solid line and plotted against the right axis.

in the crystal, as can be concluded by comparing this to the results obtained on Cu(100) to be presented in Fig. 5.4. At pH 7, both methane and ethylene are formed, starting at -0.8 V, and both continue being formed in the positive-going scan until -0.4 V. Note that the potential dependence of the m/z = 15 curve is very similar to that of the m/z = 26 curve. One possible explanation for this similarity is that both masses are fragments of the same molecule. However, besides the mass fragments of methane and ethylene we did not find other mass fragments with the same potential dependence, which shows that m/z = 15 and 26 are fragments of different molecules. Therefore, we conclude that there must be a common (surface-adsorbed) in-

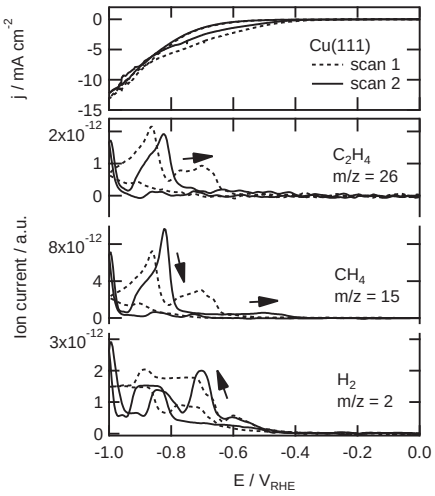

Figure 5.3 Hydrocarbon formation during consecutive scans of CO reduction on Cu(111). Top: cyclic voltammograms on Cu(111) for the reduction of a CO saturated (~ 1 mM) phosphate buffer (pH 7). Bottom: associated mass fragments of volatile products measured with OLEMS.

termediate in the reduction of CO (and hence CO_2) to CH_4 and C_2H_4, since methane and ethylene are formed with the same potential dependence on Cu(111). We suggest that the hydrogenation of CO, to form CHO_{ads}, is the key step in the formation of both methane and ethylene on Cu(111). This conclusion agrees well with the calculations by Peterson *et al.*, which indicated that for a stepped Cu(111) surface "the key step in the formation of the hydrocarbons CH_4 and C_2H_4 is the hydrogenation of the adsorbed CO to form CHO_{ads}".[86]

When performing our potential-scanning experiments we did not observe the fast and complete deactivation of the Cu electrode as is reported in literature during long term electrolysis measurements at a constant current.[107] An example of two consecutive scans of CO reduction on Cu(111) at pH 7 is shown in Fig. 5.3. Comparable to the data shown in Fig. 5.2, the methane and ethylene traces are very similar, and their formation only starts at ~0.9 V, continuing until ~0.6 V in the positive going scan. If we ob-

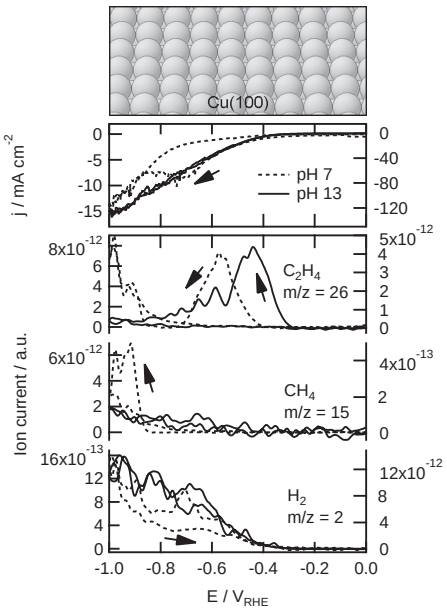

Figure 5.4 Top: (100) facet of the Cu fcc crystal. Middle: cyclic voltammograms on Cu(100) for the reduction CO saturated (∼ 1 mM) in a phosphate buffer (pH 7) and NaOH (pH 13). Bottom: associated mass fragments of volatile products measured with OLEMS. Data for pH 7 is shown with a dashed line and plotted against the left axis, data for pH 13 is shown with a solid line and plotted against the right axis.

serve a decrease in hydrocarbon formation, it occurs especially between the first and second scan, but the potentials at which hydrocarbon formation takes place do not change, for neither of the electrodes we measured.

The reduction of CO was also performed on a Cu(100) electrode, the results of which are shown in Fig. 5.4. The magnitude of the observed Faradaic current on Cu(100) is about twice as large as the current on Cu(111), which primarily reflects the enhanced ability of Cu(100) to catalyze hydrogen evolution.[147] The observed hydrocarbon formation differs remarkably from that on Cu(111). Ethylene is formed already at -0.4 V in pH 7 and -0.3 V in pH 13. Ethylene formation exhibits a maximum at -0.45 and -0.6 V, respectively,

after which it decreases and eventually stops. The current and charge corresponding to this peak of ethylene formation is too high to be explained by the reduction of a surface-adsorbed species. No methane is observed at these potentials. At -0.8 V in pH 7, the formation of ethylene is again observed, now accompanied by the formation of methane, similar to the simultaneous formation of CH_4 and C_2H_4 on Cu(111) at these potentials. This simultaneous formation of CH_4 and C_2H_4 below -0.8 V is not observed at pH 13 on Cu(100), in agreement with Cu(111) at this pH.

These results strongly suggest that there are two separate pathways to form ethylene: one that shares an intermediate with the pathway to methane, as we observe on Cu(111) and below -0.8 V on Cu(100) at pH 7, and a second pathway that only occurs on Cu(100). For this second pathway we suggest that the formation of a CO dimer is the key intermediate to form ethylene. Such a surface dimer could explain the unique selectivity to ethylene (for detailed arguments, see Chapter 3), and is in agreement with the suggestion of Gatrell *et. al*, who proposed that this CO dimer would be more stable on Cu(100) surfaces.[4]

As can be seen in Fig. 5.4, we only observe ethylene formation at low overpotentials in the negative going scan, as ethylene is not formed at potentials positive of -0.8 V in the positive going scan. However, the ethylene formation is not permanently blocked. An example of repeated scans of CO reduction on Cu(100) at pH 7 is shown in Fig. 5.5, for clarity only scan 1 and 3 are shown. The first scan is plotted with a dashed line to the left axis and the third scan is plotted with a solid line to the right axis. By comparing the left and right axis it can be seen that the hydrocarbon formation has decreased by a factor of four between the first and third scan. Because also both the current and the hydrogen evolution decreased by a factor of two, deactivation cannot be the only explanation for the decreased hydrocarbon formation, since hydrogen evolution is promoted on deactivated copper surfaces.[107] If we stop the potential-scan at a potential where the hydrocarbon formation is relatively high, an example of the evolution of ethylene and hydrogen on Cu(100) at -0.4 V is shown in Fig. 5.6, the ethylene formation shows a fast decrease over time. On a freshly polished electrode (solid lines) the hydrogen formation increases when the ethylene formation decreases. On an electrode that has been cycled to negative potentials several times already (dotted lines) the initial ethylene production is lower compared with

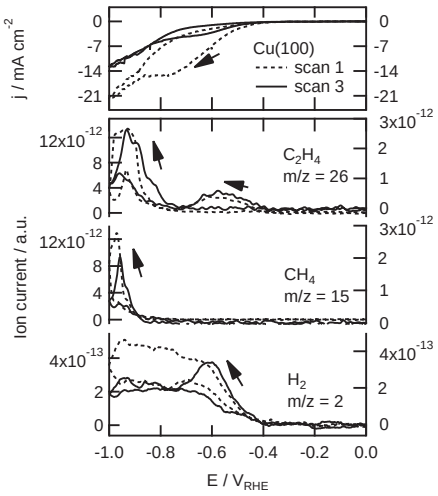

Figure 5.5 Hydrocarbon formation during multiple scans of CO reduction on Cu(100). Top: cyclic voltammograms on Cu(100) for the reduction of a CO saturated (~ 1 mM) phosphate buffer (pH 7). Bottom: associated mass fragments of volatile products measured with OLEMS. Data for scan 1 is shown with a dashed line and plotted against the left axis, data for scan 3 is shown with a solid line and plotted against the right axis.

the freshly polished electrode, which is in agreement with the results shown in Fig. 5.5, and the hydrogen evolution does not increase anymore.

To investigate why ethylene is only formed on Cu(100) in the negative going scan at less cathodic potentials, we performed consecutive scans of CO reduction at pH 13 on Cu(100) and increased the negative vertex potential with each scan, the results of which are shown in Fig. 5.7. In the first scan (lightest gray) the ethylene formation increases when the potential was reversed at -0.38 V. In the second scan to -0.4 V the ethylene formation is similar for the positive and negative going scan. In the third scan the ethylene formation starts to decrease below -0.42 V, and the ethylene formation in the positive going scan is much lower than that in the negative going scan, and in the fourth scan the ethylene formation is already lower in the negative-going scan. The hydrogen formation shows the op-

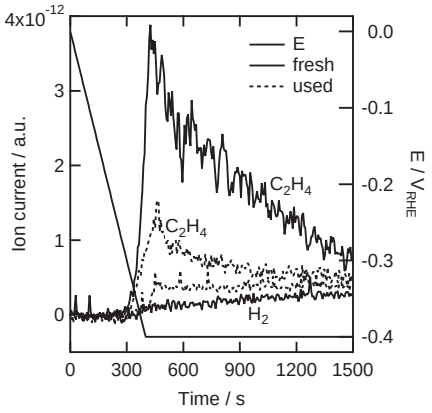

Figure 5.6 The formation of ethylene and hydrogen over time in a CO saturated NaOH solution, while scanning the Cu(100) electrode to -0.4 V and holding it at this potential. The data shown with solid lines is measured on a freshly polished electrode, the data with the dashed lines is measured on an electrode that has been cycled to negative potentials several times.

posite trend: there is no hydrogen formation in the first scan, only a minor hydrogen formation in the second scan, and the hydrogen formation in the fourth scan is significantly larger compared with the third scan. This is also reflected in the current, which increases from scan 1 to scan 4. These results clearly show that the deactivation is strongly potential dependent. A possible explanation for these observations is reconstruction of the electrode surface. On Cu(100) in acidic media a hydrogen induced reconstruction has been reported with a concomitant increase in the hydrogen evolution reaction rate.[164] Therefore, our observed increase in hydrogen formation and decrease in hydrocarbon formation could possibly be explained by such a reconstruction, but clearly, the details of this deactivation phenomenon remain to be understood. We also note that, according to Hori,[107] the deposition of metal impurities from the electrolyte is the most common reason for deactivation. Given the partial reversibility of the deactivation phenomenon shown in Fig. 5.7 we consider this explanation less likely, although we do not exclude that such effects may take place in our

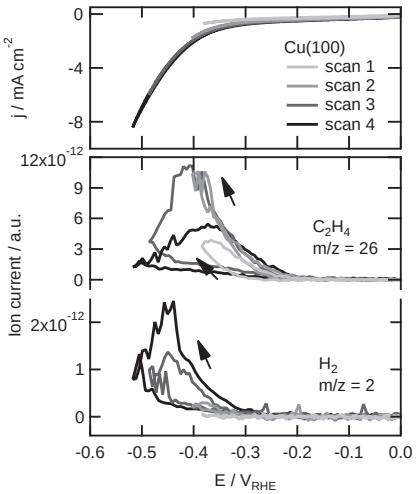

Figure 5.7 Consecutive scans of CO reduction with increasing cathodic potentials. Top: Cyclic voltammograms for the reduction of a saturated CO solution (∼ 1 mM) on Cu(100) in NaOH (pH 13). Bottom: associated mass fragments of volatile products measured with OLEMS.

experiments on a longer time scale. One may also note that on Cu(111) the formation of methane and ethylene is enhanced on the positive-going back scan (see Fig. 5.2) suggesting a potential-driven activation of the (111) surface, in contrast to the potential-driven deactivation of ethylene formation on Cu(100).

Fig. 5.8 shows the results for CO reduction performed on a polycrystalline copper electrode. On this electrode, on which the various facets of the fcc crystal planes should be present, ethylene is formed at -0.5 V in pH 7 and -0.3 V in pH 13, similar to Cu(100) shown in Fig. 5.4. Also, the ethylene and especially methane formation below -0.8 V in pH 7 is very similar to that on Cu(100). Since the observed hydrocarbon formation on polycrystalline copper is similar to that on Cu(100), this suggests that the dominant crystal facet on polycrystalline copper is the (100) facet. Such a conclusion has been drawn previously, based on blank voltammetry at copper in alkaline media.[151]

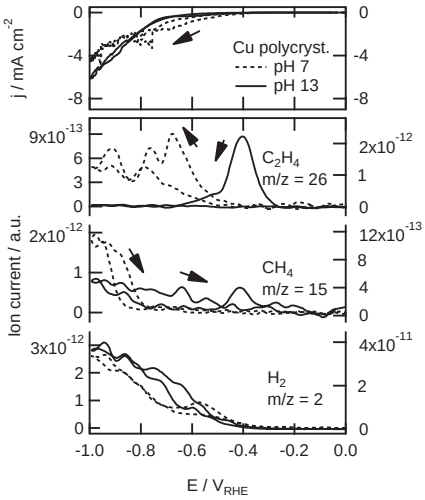

Figure 5.8 Top: Cyclic voltammograms for the reduction of a saturated CO solution (~ 1 mM) on polycrystalline copper in a phosphate buffer (pH 7) and NaOH (pH 13). Bottom: associated mass fragments of volatile products measured with OLEMS. Data for pH 7 is shown shown with a dashed line and plotted against the left axis, data for pH 13 is shown with a solid line and plotted against the right axis.

We note that our experiments at only two different pH values cannot accurately reflect the true pH dependence of the CO reduction. According to the results of Hori *et al.* the formation of methane should take place at the same potential on the RHE scale in both pH 7 and pH 13.[84] However, at pH 13, H_2 evolution is about an order of magnitude faster than at pH 7, presumably due to the absence of specifically adsorbing anions at pH 13,[147] and this may suppress CO reduction. Clearly, the influence of pH and electrolyte composition, such as the presence of strongly adsorbing anions, requires further scrutiny. For a more detailed investigation of the influence of pH and adsorbing anions we refer to Chapter 7. Furthermore, we note that because CO reduction currents are always low and also because hydrogen evolution close to the electrode leads to an effective stirring of the

electrolyte, it is difficult to estimate any mass transport effects in relation to CO reduction.

5.4 Conclusions

Summarizing, our experiments provide strong evidence for the idea that ethylene may be formed through two different mechanisms: a first pathway that has a common intermediate with the formation of methane and that takes place both at (111) and (100) surfaces, and a second pathway in which CO is selectively reduced to C_2H_4 at relatively low overpotentials, presumably through the formation of a surface adsorbed CO dimer.[4,161] The latter pathway takes place preferentially at (100) facets. Moreover, the crystal plane at which this selective reduction to ethylene takes place, seems to be the dominant crystal facet in polycrystalline copper. These insights open up new routes to an affordable (photo-)electrochemical production of fuels from CO_2, especially because the selective ethylene formation pathway from CO has a remarkably low overpotential.

6 | Structure sensitivity of the electrochemical reduction of carbon monoxide on copper single crystals

Abstract

The product selectivity in the electrochemical reduction of carbon dioxide and carbon monoxide strongly depends on the atomic configuration of the copper electrode surface. On Cu(111) methane formation is favored, whereas on Cu(100) ethylene formation is favored, with selective ethylene formation at low overpotentials. To distinguish the reactivity of (100) terraces vs. (100) steps, we have studied carbon monoxide reduction on Cu(322), with the [5(111)x(100)] orientation, and Cu(911), with the [5(100)x(111)] orientation. Only on Cu(911) the selective ethylene formation at low overpotentials is observed, indicating that this reaction pathway occurs on (100) terraces only. We also show that the reduction of ethylene oxide to ethylene is significantly faster on Cu(100) compared with Cu(111), giving further evidence to the importance of the associated intermediate for ethylene formation. On Cu(110), the potential dependence of methane and ethylene formation is similar to Cu(111), and we have observed a primary alcohol amongst the products.

6.1 Introduction

The electrochemical reduction of carbon dioxide to hydrocarbons has been subject of various investigations, since CO_2 is a vast and sustainable carbon feedstock, and the conversion of CO_2 to hydrocarbons could mitigate the increasing CO_2 emissions.[5,98] In 1985 it was discovered by Hori *et al.* that on copper electrodes, carbon dioxide can be electrochemically reduced to hydrocarbons, mainly methane and ethylene.[2] Especially the formation of ethylene, which is widely used in the chemical industry, is unique and only takes place to a significant extent on copper electrodes. Since its discovery this reaction has been studied extensively. On single crystal copper electrodes, the selectivity towards hydrocarbons as well as the ratio of methane over ethylene have been shown to depend on the atomic configuration of the electrode surface.[5,87,88,144] Hori *et al.* have shown that ethylene formation is favored on Cu(100) surfaces, and that the presence of small amounts of (111) and (110) steps in the (100) terraces increases the selectivity to ethylene further.[87] Methane formation, on the other hand, is favored on Cu(111) terraces. Carbon monoxide is a well known intermediate in the reduction of CO_2,[4,5,84] and the reduction of CO_2 and CO have the same dependence on the atomic surface structure.[148]

In Chapter 5 we have shown for CO reduction that ethylene can be formed via two different pathways: (1) on Cu(100), CO is reduced to only ethylene and not methane at relatively low overpotentials, presumably through the formation of a surface adsorbed CO dimer, and (2) both on Cu(100) and Cu(111), at higher overpotentials, CO is reduced to methane and ethylene simultaneously, suggesting a shared intermediate.[144] To investigate whether this selective ethylene formation on Cu(100) at low overpotentials is sensitive towards (100) terraces or (100) step sites, we report here on the electrochemical reduction of CO on two stepped Cu single crystals: Cu(322), with the [5(111)x(100)] orientation, and Cu(911), with the [5(100)x(111)] orientation. We have investigated the reactivity of these surfaces using online electrochemical mass spectrometry (OLEMS).[108] This tip-based sampling technique allows to follow the formation of volatile reaction intermediates and products while changing the potential at the electrode surface.

6.2 Experimental

All experiments were carried out in an electrochemical cell using a three-electrode assembly at room temperature. The cell and glassware were boiled in ultra clean water (Millipore MilliQ gradient A10 system, 18.2 MΩ · cm) before each experiment. A gold wire was used as counter electrode and a reversible hydrogen electrode (RHE) in the same electrolyte was used as reference electrode. All potentials in this paper are referred to this electrode. The potential was controlled using an Ivium A06075 potentiostat.

The single crystal copper electrodes used were bead-type electrodes (icryst) cut and polished with an accuracy down to 0.5°. Prior to each experiment the electrode was electropolished in 66% H_3PO_4 at 3 V vs. a Cu counter electrode for 10 seconds.[154] After polishing, the surface quality was verified regularly using blank voltammetry in 0.1 M NaOH.[165]

The experiments were carried out in 0.1 M K_2HPO_4 + 0.1 M KH_2PO_4 (pH 7) prepared from high purity reagents (Sigma-Aldrich TraceSelect)and ultra clean water. Argon (Air Products, 5.0) bubbling was used to deaerate the electrolyte, before saturation of the electrolyte with carbon monoxide (Linde, 4.7).

Online Electrochemical Mass Spectrometry (OLEMS) was used to detect the gaseous products formed during the reaction. The reaction products at the electrode interface were collected with a small tip positioned close (∼10 µm) to the electrode.[108] The tip is a 0.5 mm diameter porous Teflon cylinder with an average pore size of 10-14 µm in a Kel-F holder. This tip is connected to a mass spectrometer with a PEEK capillary. The tip configurations were cleaned in a solution of 0.2 M $K_2Cr_2O_7$ in 2 M H_2SO_4 and rinsed with ultra pure water before use. A SEM voltage of 2400 V was used, except for hydrogen (m/z = 2) where a SEM voltage of 1200 V was used. The products were measured while changing the potential of the electrode from 0.0 to -1.0 V and back with 1 mV s^{-1}. Because the equilibration of the pressure in the system after introduction of the tip in the electrolyte takes a very long time, all mass fragments show a small decay during the measurement. We corrected for this background by fitting a double exponential function to the data in the potential regions were no change in activity is observed and subtracted this fit from the data. All mass fragments shown in this paper have been background corrected in this way.

6.3 Results and discussion

6.3.1 CO reduction on stepped surfaces

Fig. 6.1 compares the reduction of carbon monoxide on Cu(322) to that on Cu(111) in a phosphate buffer of pH 7. The potential is changed from 0 to -1 V and back with 1 mV per second. The recorded currents are shown in the middle panel, and the volatile products measured during this potential scan are shown in the bottom panel. At -0.4 V the current increases due to the formation of hydrogen. Overall, the current is mainly determined by hydrogen evolution and does not give any specific information about the CO reduction. The hydrogen evolution leads to the formation of gas bubbles trapped between the tip and the single crystal electrode and this explains the somewhat noisy character of the observed mass signals. At -0.9 V the formation of methane and ethylene is detected, represented by m/z = 15 and 26 respectively. Their formation increases when scanning to -1 V, and continue being formed till -0.7 V in the positive going scan. The similar potential dependence for methane and ethylene is comparable to the results obtained for CO reduction on Cu(111). This indicates that methane and ethylene are being formed on the (111) terraces of the Cu(322) surfaces, and that the (100) steps have no particular reactivity for CO. When comparing the ratio of C_2H_4/CH_4 formation, we observe a higher ratio on Cu(322). This shift in selectivity towards C_2H_4 on stepped (111) surfaces has also been observed by Hori *et al.*[87]

Fig. 6.2 shows the results of the same experiment performed on a Cu(911) electrode, as compared with Cu(100). On this electrode, the selective formation of ethylene is observed between -0.5 and -0.8 V, whereas methane is not observed at these potentials. At more negative potentials methane and ethylene are formed simultaneously. These results are very similar to CO reduction on Cu(100), indicating that also on a stepped (100) surface the reduction of CO to ethylene occurs via two different pathways. Moreover, only (100) terraces appear to be active towards the selective ethylene formation at low overpotentials. If (100) step sites would be the active sites in this process, we expect to observe selective ethylene formation at lower potentials also on Cu(322), but from Fig. 6.1 it is clear that this is not the case. The ratio of C_2H_4/CH_4 has significantly decreased on Cu(911) compared with Cu(100). Hori *et al.* have observed a higher selectivity towards

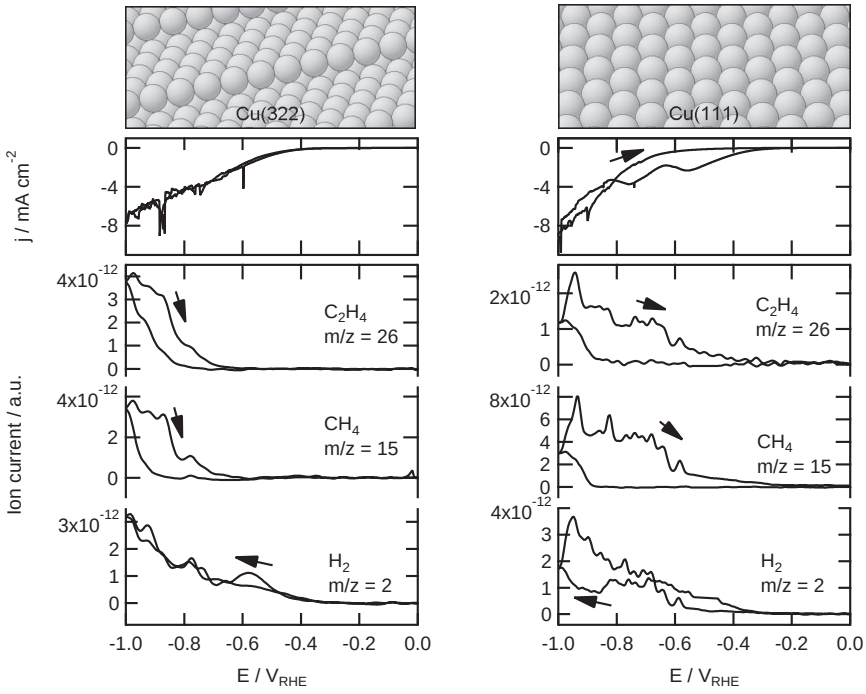

(a) Cu(322) (b) Cu(111)

Figure 6.1 The reduction of a CO saturated (~ 1 mM) phosphate buffer (pH 7) on Cu(322) (a) and Cu(111) (b). The top panels show the crystal facets, the middle panels the corresponding cyclic voltammograms, and the bottom panels the associated mass fragments of volatile products measured with OLEMS.

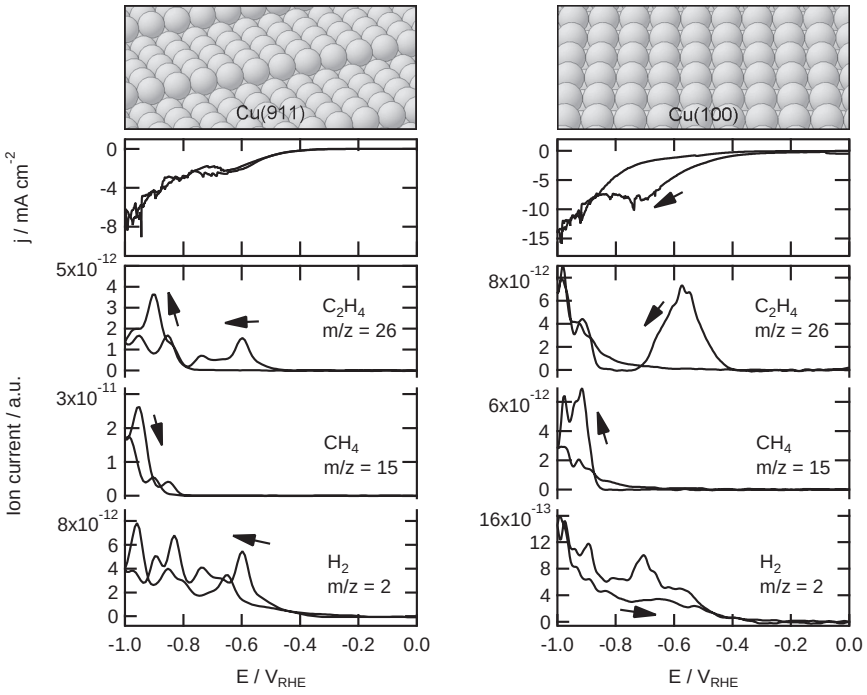

(a) Cu(911) (b) Cu(100)

Figure 6.2 The reduction of a CO saturated (~ 1 mM) phosphate buffer (pH 7) on Cu(911) (a) and Cu(100) (b). The top panels show the crystal facets, the middle panels the corresponding cyclic voltammograms, and the bottom panels the associated mass fragments of volatile products measured with OLEMS.

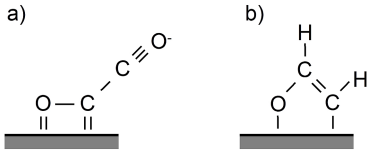

Figure 6.3 Key intermediates in the formation of ethylene: a) the CO dimer and b) the oxametallacycle.

C_2H_4 formation upon the introduction of steps into Cu(100).[87] This selectivity change towards ethylene formation strongly depends on the terrace width: according to Hori *et al.*, it shows an optimum at Cu(711), which has 4 atom wide (100) terraces and a (111) step, but at 2 atom wide terraces the methane formation is higher and the C_2H_4/CH_4 ratio lower compared with Cu(100). The presence of these narrow (100) terraces on our surface could explain the high methane formation observed on Cu(911) in Fig. 6.2, but this clearly would require a more detailed characterization of the surface structure. It should also be noticed that our measurements probe the selectivity during potentiodynamic cyclic voltammetry experiments, whereas Hori's experiments were based on long-term electrolysis experiments at a single potential.

Our work confirms the results of Hori *et al.* who showed that ethylene formation is favored on (100) facets. Gattrell *et al.* proposed in their review on CO_2 reduction on copper electrodes that the square orientation of the atoms on the (100) terrace stabilizes the CO dimer, since it allows for the coordination of the oxygen to the surface.[4] Recent DFT calculations performed in our research group confirm the stabilization of the CO dimer by Cu(100) although in a different orientation than proposed by Gattrell *et al.*, the geometry of this dimer is shown in Fig. 6.3a.[166] These DFT results show that the CO dimer is adsorbed on two opposing bridge sites, binding through one O atom and one C atom to four Cu atoms.

It has been observed that many electrocatalytic reactions that involve the breaking or making of C-O, N-O, N-N and C-C bonds, such as ammonia oxidation, dimethylether oxidation, and nitrite reduction, prefer the (100) site geometry.[167] It is assumed that in such a geometry the repulsion be-

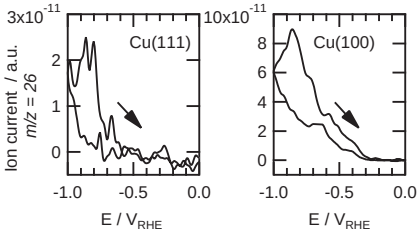

Figure 6.4 The reduction of ethylene oxide to ethylene on Cu(111) (left) and Cu(100) (right).

tween two fragments occupying two opposing bridge sites is minimal because sharing of metal atoms can be avoided. It seems that this also applies for the reduction of CO, so that the square arrangement of the atoms stabilizes the reaction step/intermediates in which the C-C bond is formed.

Steps in (100) facets are usually unbeneficial for the aforementioned bond breaking/making reactions.[167] However, according to Hori *et al.*, the formation of ethylene is enhanced with the presence of (111) and (110) steps in the (100) surface, with an optimum at Cu(711), which has 4 atom wide (100) terraces and a (111) step.[87] Terraces smaller than 4 atoms probably lower the possible assemblies of surface sites where the CO dimer can be formed, thereby limiting the C-C bond formation.

6.3.2 Ethylene oxide reduction

In Chapter 3 we have shown that the only C_2 species that can be reduced to ethylene on (polycrystalline) copper electrodes, is ethylene oxide.[161] Therefore, we have proposed an oxametallacycle (Fig. 6.3b) as intermediate in the formation of ethylene. The aforementioned DFT calculations on Cu(100) also suggest an oxametallacycle as an intermediate in the lowest energy pathway from CO to ethylene.[166] To investigate whether the formation of this oxametallacycle is surface structure dependent, we have performed the reduction of ethylene oxide on Cu(111) and Cu(100). From Fig. 6.4 it can be seen that there is a clear potential difference in the formation of ethylene on Cu(111) and Cu(100). Ethylene is formed at -0.3 V on Cu(100), whereas it is formed at -0.6 V on Cu(111). And although our OLEMS data do not give di-

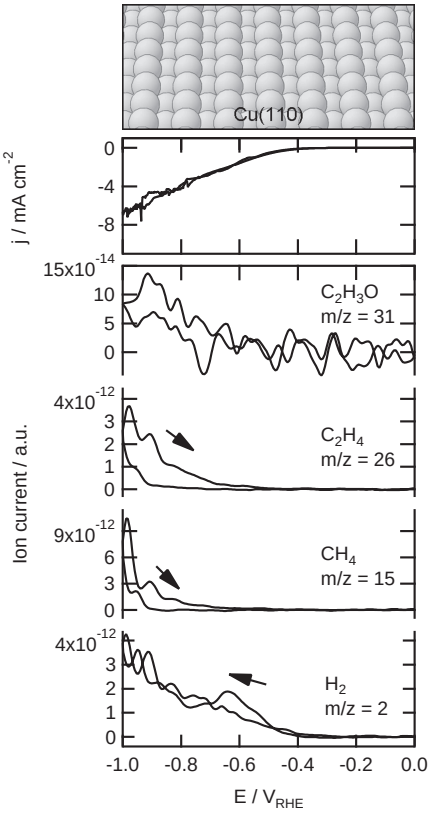

Figure 6.5 Top: the Cu(110) crystal facet. Middle: cyclic voltammogram for the reduction of a CO saturated (∼ 1 mM) phosphate buffer (pH 7) on Cu(110). Bottom: associated mass fragments of volatile products measured with OLEMS.

rect quantitative information about the amounts of product formed, we can still conclude that there is more ethylene formed on Cu(100) compared with Cu(111). Therefore, the stabilization of the oxametallacycle on Cu(100) is in agreement with our model why ethylene formation is enhanced on this surface.

6.3.3 CO reduction on Cu(110)

To investigate the reactivity of (110) sites, we have also investigated the reduction of CO on Cu(110), the results of which are shown in Fig. 6.5. The formation of both methane and ethylene starts at ~ -0.9 V and continues being formed till -0.6 V in the positive going scan, similar to the results obtained for Cu(111). Since (110) could also be written as [2(111)×(111)] and therefore only exhibits (111) sites, this could explain the similar potential dependence as observed on Cu(111). Methane and ethylene exhibit the same potential dependence, suggesting a common reaction intermediate like observed on Cu(322) and Cu(111). Hori *et al.* observed that on surfaces with (110) terraces, relatively high amounts of acetaldehyde, ethanol, propanol and other C_2 and C_3 species are formed.[87] We have detected traces of the mass fragment m/z = 31 below -0.7 V, shown in Fig. 6.5. This fragment is characteristic for primary alcohols. We have not observed this fragment for CO reduction on Cu(100) or Cu(111).

6.4 Conclusions

In this chapter we have shown that the selective reduction of CO to ethylene on copper electrodes at low overpotentials occurs on Cu(100) terraces, whereas (100) step sites are not involved in this reaction. We also have shown that the reduction of ethylene oxide to ethylene is significantly faster on Cu(100) compared with Cu(111), giving further evidence to the importance of the associated intermediate for ethylene formation. The reduction of CO on Cu(110) exhibits a similar potential dependence to Cu(111), and more alcohols are observed.

7 | The influence of pH on the reduction of CO and CO_2 to hydrocarbons on copper electrodes

Abstract

The pH is an important parameter in the reaction mechanism of the electrochemical reduction of carbon dioxide and carbon monoxide to methane and ethylene on copper electrodes. We have investigated the influence of the pH on this reaction using Cu(111) and Cu(100) single crystal electrodes. The results support our recently proposed reaction mechanism, in which two different reaction pathways to ethylene can be distinguished: a first, pH-dependent pathway that has a common intermediate with the formation of methane that occurs mainly on Cu(111), and a second, pH-independent pathway *via* a carbon monoxide dimer. The latter pathway occurs on Cu(100) only.

7.1 Introduction

The still increasing global CO_2 emissions are causing widespread concerns about the possible consequences. Mimicking photosynthesis, by reducing carbon dioxide to hydrocarbons, could be an important step forward in the reduction of carbon dioxide emissions. In this respect, an important discovery was done by Hori in the 1980s, who showed that CO_2 can be electrochemically reduced to hydrocarbons on copper electrodes.[2] Only copper electrodes have been found to catalyze this reaction to a significant extent, and the main carbon products are methane and ethylene.[3] This process could be a solution to store (surplus) sustainable electrical energy as chemical energy, that could be directly used in the current fuel (*e.g.* natural gas) infrastructure.

Since its discovery, ample research has been performed to understand the molecular mechanism of this reaction,[4,5,83,84,86,161,168] and to relate the product selectivity to the electrode surface structure.[4,5,87,88,144,166,169] A better understanding of this reaction on the molecular level could lead to an improved product efficiency and selectivity.

One important parameter in this reaction is the pH. Hori has shown that the formation of methane depends on pH, whereas the formation of ethylene is independent of pH.[84] This observation has played an important role in the various proposed molecular mechanisms.[4,84,161] Therefore, we investigate in this Chapter the influence of pH on the reduction of CO and CO_2 on Cu(100) and Cu(111). We used these electrodes because we have shown in Chapter 5 that there are two different reaction pathways from CO to ethylene:[144,170] a first pathway that has a common intermediate with the formation of methane and that takes place both at Cu(111) and Cu(100) surfaces, and a second pathway in which CO is selectively reduced to C_2H_4 at relatively low overpotentials, presumably through the formation of a surface adsorbed CO dimer. The latter pathway takes place preferentially at (100) facets, and we expect this reaction pathway to be independent of pH. We have studied the pH dependence both in phosphate buffers and in electrolytes with non-specifically adsorbing anions, using online electrochemical mass spectrometry (OLEMS).[108] This technique allows us to follow the formation of products while changing the potential at the electrode. In this way, we can measure the onset potentials for the different products as a

function of pH, and investigate the pH dependence for the different products formed.

7.2 Experimental

All experiments were carried out in an electrochemical cell using a three-electrode assembly at room temperature. The cell and glassware were boiled in ultra clean water (Millipore MilliQ gradient A10 system, 18.2 MΩ · cm) before each experiment. A gold wire was used as counter electrode and a reversible hydrogen electrode (RHE) in the same electrolyte was used as reference electrode. All potentials in this paper are referred to this electrode. The potential was controlled using an Ivium A06075 potentiostat.

The single crystal copper electrodes used were bead-type electrodes (icryst) cut and polished with an accuracy down to 0.5°. Prior to each experiment the electrode was electropolished in 66% H_3PO_4 at 3 V vs. a Cu counter electrode for 10 seconds.[154] After polishing, the surface quality was verified regularly using blank voltammetry in 0.1 M NaOH.[165]

The experiments were carried out in 0.2 M phosphate buffers, 0.2 M $NaClO_4$ solutions or 0.1 M $HClO_4$, H_3PO_4 or NaOH, all prepared from high purity reagents (Sigma-Aldrich TraceSelect, Merck Suprapur) and ultra clean water. Argon (Air Products, 5.0) bubbling was used to deaerate the electrolyte, before saturation of the electrolyte with carbon monoxide (Linde, 4.7) or carbon dioxide (Linde, 4.5).

Online electrochemical mass spectrometry (OLEMS) was used to detect the gaseous products formed during the reaction.[108] The reaction products at the electrode interface were collected with a small tip positioned close (∼50 µm) to the electrode. The tip is a 0.5 mm diameter porous Teflon cylinder with an average pore size of 10-14 µm in a Kel-F holder. This tip is connected to a mass spectrometer with a PEEK capillary. The tip configurations were cleaned in a solution of 0.2 M $K_2Cr_2O_7$ in 2 M H_2SO_4 and rinsed with ultra pure water before use. A SEM voltage of 2400 V was used, except for hydrogen ($m/z = 2$) where a SEM voltage of 1200 V was used. The products were measured while changing the potential of the electrode from 0.0 V to -1.0 V or -1.5 V with 1 mV s^{-1}. Because the equilibration of the pressure in the system after introduction of the tip in the electrolyte takes a very long time, all mass fragments show a small decay during the measurement. We corrected for this background by fitting a double exponential

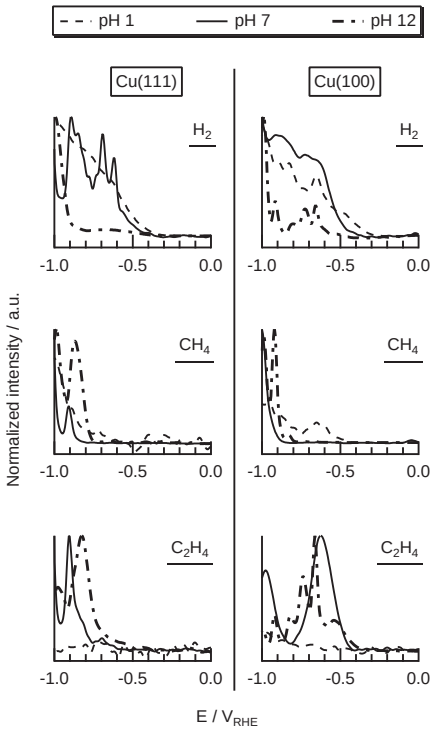

Figure 7.1 The reduction of CO in 0.1 M phosphoric acid (pH 1) and 0.2 M phosphate buffers (pH 7 and 12) on Cu(111) (left) and Cu(100) (right). With OLEMS, the formation of H_2 (m/z=2, top), CH_4 (m/z=15, middle), and C_2H_4 (m/z=26, bottom) were followed.

function to the data in the potential regions were no change in activity is observed and subtracted this fit from the data. All mass fragments shown in this paper have been background corrected in this way. In order to compare and present the various mass fragments in one graph, all mass fragments have been normalized, which is done by dividing each signal by its highest value.

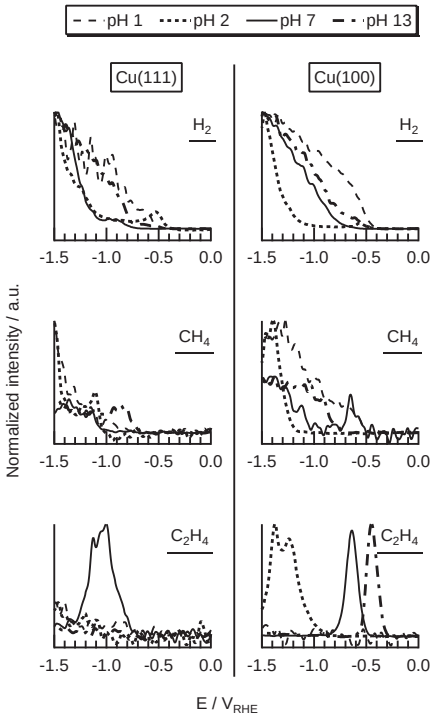

Figure 7.2 The reduction of CO in 0.1 M $HClO_4$ (pH 1), 0.2 M $NaClO_4$ (pH 2 and 7) and 0.1 M NaOH (pH 13) on Cu(111) (left) and Cu(100) (right). With OLEMS, the formation of H_2 (m/z=2, top), CH_4 (m/z=15, middle), and C_2H_4 (m/z=26, bottom) were followed.

7.3 Results

Fig. 7.1 shows the gaseous products of CO reduction in 0.1 M phosphoric acid (pH 1) and 0.2 M phosphate buffers (pH 7 and 12) on Cu(111) and Cu(100), measured with OLEMS. The three detected products are hydrogen (m/z = 2), methane (represented by m/z = 15) and ethylene (represented by m/z = 26). By comparing these three different products, it is clear that they have a different potential dependence. Both on Cu(111) and Cu(100), hydrogen formation always starts around -0.35 V, increasing with more neg-

Table 7.1 Onset potentials (on the RHE scale) for the reduction of CO

		$NaClO_4$		Phosphate buffers	
pH	Product	Cu(111)	Cu(100)	Cu(111)	Cu(100)
1	CH_4	-0.90	-0.50	-0.70	-0.45
	C_2H_4	n/a	n/a	n/a	n/a
2	CH_4	-1.0	-1.0		
	C_2H_4	n/a	-0.8		
7	CH_4	-1.1	-0.90	-0.85	-0.90
	C_2H_4	-0.75	-0.5	-0.65	-0.45
13/12	CH_4	-0.65	-0.75	-0.75	-0.75
	C_2H_4	n/a	-0.30	-0.55	-0.40

ative potentials. Interestingly, at pH 12, the hydrogen formation is limited till -0.9 V, after which it rapidly increases. The formation of methane shows some differences between Cu(111) and Cu(100) at the various pH values. At pH 1, the formation of methane is earlier on Cu(100), starting at -0.45 V. At pH 7, the formation of methane is similar on Cu(111) and Cu(100), starting at around -0.85 V. At pH 12, the formation of methane is quite similar on Cu(111) and Cu(100), starting a little earlier on Cu(111). The biggest differences are observed for the ethylene formation. At pH 1, there is only a very small fraction of ethylene observed on Cu(100). At pH 7 and 12, the formation of ethylene is much earlier on Cu(100) compared to Cu(111), and starts at around -0.4 V.

Similar experiments were performed in electrolytes with non-specifically adsorbing anions, the results of which are shown in Fig. 7.2. We have used 0.1 M $HClO_4$ (pH 1), 0.01 M $HClO_4$ + 0.19 M $NaClO_4$ (pH 2), 0.2 M $NaClO_4$ (pH 7) and 0.1 M NaOH (pH 13). Since at some pH values products were only observed below -1.0 V, we have scanned the potential till -1.5 V. The onset of the hydrogen formation in these electrolytes is similar compared the the phosphate-based electrolytes. Again, the formation of methane is earlier on Cu(100) at pH 1. Also, ethylene is not observed at pH 1. Ethylene is mainly observed on Cu(100), and the onset potential clearly shifts with pH, from -0.80 V at pH 2 to -0.30 V at pH 13. Overall, the observed potential dependence is similar in Figs. 7.1 and 7.2.

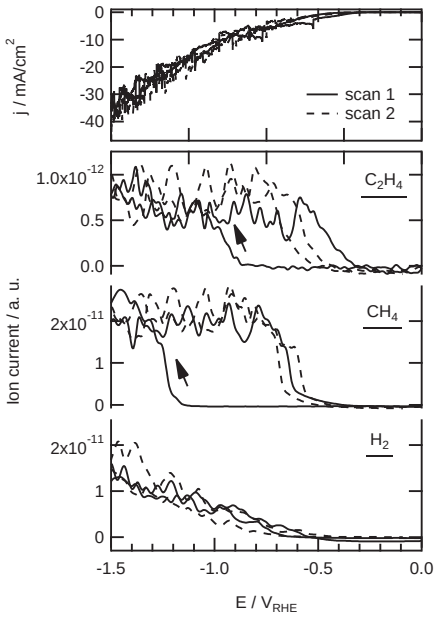

Figure 7.3 The reduction of CO in a 0.2 M phosphate buffer with pH 2 on Cu(111). The top panel shows the current density, the bottom panel the associated mass fragments for the formation of H_2 (*m/z*=2), CH_4 (*m/z*=15), and C_2H_4 (*m/z*=26) measured with OLEMS.

The onset potentials for the measurements shown in Figs. 7.1 and 7.2 are summarized in Table 7.1. From this table it can be seen again that the formation of methane starts, independent of pH, on average around -0.9 V, with Cu(100) at pH 1 as a notable exception. The formation of ethylene on Cu(100) clearly depends on pH, and shifts to less negative potentials with increasing pH.

In Table 7.1, no values are given for the measurement in a phosphate buffer at pH 2. The reason for that is shown in Fig. 7.3. In the first reduction cycle, the onset potential both for methane and ethylene is at -1.15 V. In the reverse scan, the hydrocarbon formation continues till 0.6 V(methane) or -0.4 V (ethylene). In the second scan, the onset potential for both methane

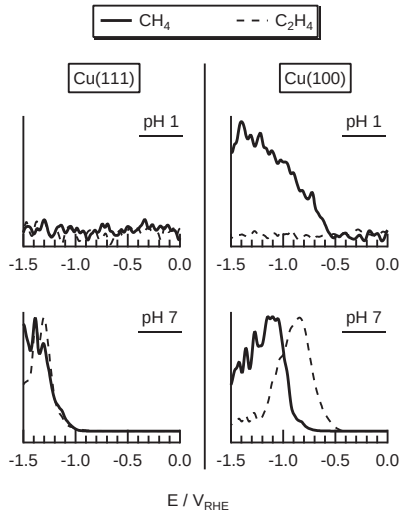

Figure 7.4 The reduction of CO_2 in 0.2 M phosphate buffers with pH 1 and 7 on Cu(111) (left) and Cu(100) (right). With OLEMS, the formation of CH_4 (*m/z*=15, green), and C_2H_4 (*m/z*=26, blue) were followed.

Table 7.2 Onset potentials (on the RHE scale) for the reduction of CO_2 in phosphate

pH	Product	Cu(111)	Cu(100)
1	CH_4	n/a	-0.55
	C_2H_4	n/a	n/a
7	CH_4	-0.95	-0.70
	C_2H_4	-0.95	-0.40

and ethylene is around -0.5 V. Fig. 7.3 shows the results for Cu(111) only, but the same phenomena was observed on Cu(100) (data not shown). This strong shift in onset potential was only observed for a phosphate buffer of pH 2.

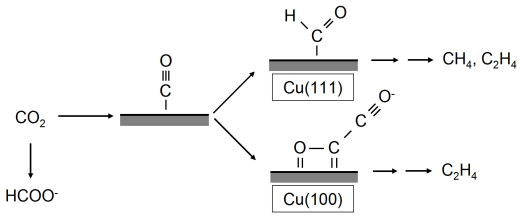

Figure 7.5 Proposed reaction mechanism for the reduction of CO_2 on Cu single crystal electrodes.[144,166]

Next to the reduction of CO, we have also investigated the reduction of CO_2. We have only studied the pH dependence of CO_2 reduction in phosphate buffers, since CO_2 itself strongly influences the pH of the unbuffered electrolytes. We could not use the phosphate buffer of pH 12, since CO_2 is completely converted to CO_3^{2-} at that pH. Therefore, we have only measured the reduction of CO_2 at pH 1 and 7, the results of which are shown in Fig. 7.4 and summarized in Table 7.2. At pH 1, methane formation starts already at -0.55 V on Cu(100), similar to the reduction of CO at pH 1 on Cu(100). On Cu(111), no reduction products of CO_2 were observed at pH 1. At pH 7, on Cu(100) ethylene formation is at lower potentials than methane formation, whereas on Cu(111) methane and ethylene have a similar potential dependence.

7.4 Discussion

7.4.1 Comparison with proposed reaction mechanism

In this section we will discuss our results for CO and CO_2 reduction at various pH values in relation to our proposed reaction mechanism presented in Chapters 3 and 5 and Ref. 166, and depicted schematically in Fig. 7.5. In Chapter 3 we have introduced a new mechanism for the electrochemical reduction of carbon dioxide and carbon monoxide on copper electrodes. We have shown that it is very likely that CHO_{ads} is the key intermediate towards the breaking of the C-O bond and, therefore, the formation of methane. This is in agreement with the observation of Hori *et al.* that the formation of methane, starting from carbon monoxide, depends on pH on the NHE scale

(independent of pH on the RHE scale).[84] For the formation of ethylene we suggested that the first step, starting from carbon monoxide, is the formation of a CO dimer, followed by the formation of an enediol(ate), or the formation of an oxametallacycle. The formation of the (negatively charged) CO dimer explains the pH-independence of reduction of CO to ethylene, as observed by Hori *et al.*[84] In Chapter 5 we have described the reduction of CO on Cu(111) and Cu(100), and we have shown that there are two different reaction pathways from CO to ethylene: a first pathway that has a common intermediate (CHO) with the formation of methane and that takes place both at Cu(111) and Cu(100) surfaces, and a second pathway in which CO is selectively reduced to C_2H_4 at relatively low overpotentials, presumably through the formation of the surface adsorbed CO dimer. The latter pathway takes place preferentially at (100) facets, as shown in Chapter 6 and supported by recent DFT calculations,[166] and this reaction pathway is independent of pH on the NHE scale (and therefore dependent of pH on the RHE scale).

From Table 7.1 we conclude that, on most surfaces, the onset potential of methane both on Cu(111) and Cu(100) is around -0.8 – -0.9 V, independent of pH. The formation of ethylene on Cu(100) shifts from -0.80 V at pH 2 to -0.30 V at pH 13 (Fig. 7.2). On Cu(111) this potential shift is much weaker, and the onset potentials for ethylene are closer to the potentials where methane formation starts. Please note that all our potentials are on the RHE scale. Since the potential of the RHE shifts with pH, a constant onset potential versus RHE at different pH values indicates a pH dependence, whereas a shift in onset potentials indicates a pH independence. Therefore, from the results presented in Figs. 7.1 and 7.2 it can be concluded that the onset potential for ethylene, in particular on Cu(100), does not depend on the pH on the NHE scale, although the observed potential-shift for the formation of ethylene is smaller than the expected 59 mV per pH unit on the RHE scale. For methane the onset potential is much more constant and, therefore, its rate-determining step involves proton transfer. Both the pH-dependent methane formation, and the pH-independent ethylene formation are in agreement with the results of Hori *et al.*[84] These results are also in agreement with our proposed reaction mechanism: the observed pH independence for the formation of ethylene on Cu(100) supports the formation of the CO-dimer on this crystal facet. Also the observation that

on Cu(111) the onset potentials for the formation of ethylene are closer to the (constant) onset potentials of methane supports a pH-dependent pathway where methane and ethylene have a common intermediate (presumably CHO).[171]

Similar conclusions can be drawn from the reduction of CO_2, presented in Fig. 7.4. At pH 7 on Cu(111), methane and ethylene are formed at the same potential. On Cu(100) at pH 7, the formation of ethylene is at a lower potential compared to methane. The reduction of CO_2 to CO and further will always be accompanied with the reduction of water, causing a local increase of pH at the electrode. This opens up a reaction pathway for the formed CO to ethylene via the CO dimer. This pathway is only available on Cu(100), and therefore we only observe a difference in onset potential for methane and ethylene on Cu(100).

7.4.2 Hydrocarbon formation at pH 1

The formation of methane and ethylene at pH 1 shows some interesting differences with the measurements at higher pH values, both for the reduction of CO and CO_2. First, there is hardly any ethylene formed at this pH, also on Cu(100). This indicates that at very low pH values the protonation of CO is favored over the formation of a CO dimer, since no ethylene is observed on Cu(100). Also the further protonation of CHO to methane is favored over the formation of the C-C bond, since also on Cu(111) hardly any ethylene is observed.

Second, it is interesting that methane formation on Cu(100) at pH 1 occurs at the lowest overpotentials, both for CO and CO_2 reduction. The formation of methane at pH 1 on Cu(100) at low overpotentials is interesting because in the literature, Cu(111) has been associated with methane formation.[87,144] In both electrolytes, at pH 1 and pH 12/13, the formation of methane starts significantly earlier on Cu(111) and Cu(100) compared to the measurements at pH 2 and 7. This shift to lower overpotentials for the formation of methane both at very low and high pH is mirrored by the formation of hydrogen. This can be best seen in Fig. 7.2, where the formation of hydrogen is higher at lower overpotentials both at pH 1 and pH 13. This high hydrogen formation at low overpotentials is most pronounced on Cu(100) at pH 1, both in phosphate and perchlorate (Figs. 7.1 and 7.2), and it is also on Cu(100) that the formation of methane has the lowest overpo-

tential at pH 1. From Fig. 7.4 we see that methane formation also occurs at lower overpotentials during CO_2 reduction on Cu(100) at pH 1. On the other hand, no methane is observed on Cu(111) during CO_2 reduction at pH 1. At present, these observations are not straightforward explained by our mechanism.

We note that also on Cu(100) at pH 7 in Fig. 7.2 we observe a small peak in m/z = 15 starting at -0.5 V already. But since this peak is in exactly the same potential region as the detection of relatively huge amounts of m/z = 26, we attribute this peak in the m/z = 15 signal to a fragment of ethylene. The relative abundances of m/z = 15 and 26 in the mass spectrum of ethylene differ by a factor of 100. In Fig. 7.2 the measured ratio is even higher, m/z = 26 is around 150 times larger than m/z = 15. Therefore, we have indicated an onset potential of -0.90 V for the formation of methane on Cu(100) in Table 7.1, and not -0.50 V.

7.4.3 CO reduction in a phosphate buffer at pH 2

We have only observed the strong potential shift between the first and second reduction cycle during the reduction of CO in a phosphate buffer of pH 2, as shown in Fig. 7.3. We may consider two different possible explanations: (1) a reconstruction of the surface and (2) a change in the pH of the electrolyte. We have investigated a possible reconstruction by performing cyclic voltammetry (CV) before and after CO reduction. Although we did observe some changes in the CV after the reduction, pointing towards a more polycrystalline surface, the most interesting observation was that when we used the same electrode again after the CV, without any modification, we observed the same shift in onset potential between the first and second reduction cycle. This indicates that the potential shift is not related to a change in surface morphology. The other explanation, a shift in the pH of the electrolyte, is also unlikely. The pH of the electrolyte is at the pK_a of the $H_3PO_4/H_2PO_4^-$ couple (K_a is the acid dissociation constant), but also the buffers at pH 7 and 12 are at the pK_a of the corresponding acid and conjugate base. Therefore, this does not explain why this potential shift is only observed at pH 2. We have also performed the reduction of CO_2 in the same electrolyte (0.1 M H_3PO_3 + 0.1 M KH_2PO_4, data not shown), but did not observe the potential shift. At present we do not have an explanation for the potential shift observed during the reduction of CO in a phosphate

buffer at pH 2. Since the potential shift is not observed in 0.01 M $HClO_4$ it could be an anion effect, but clearly this requires further scrutiny.

7.4.4 Adsorbing vs. non-adsorbing anions

Since phosphate is a strongly adsorbing anion, we have also performed the reduction of CO in electrolytes with perchlorate, a non-specifically adsorbing anion. However, the trends in onset potentials are the same in Fig. 7.1 and 7.2, and we do not observe a significant difference. Hori *et al.* have compared various anions in the electrolyte used for CO_2 reduction.[5] They have shown that in the presence of phosphate, much more hydrogen and less hydrocarbons are formed compared to *i.a.* perchlorate, sulphate and bicarbonate. This was attributed to the buffering capacity of the phosphate, which cancels the local increase in pH at the electrode surface due to the generated OH^-. Although our OLEMS cannot show absolute quantities, the relative ion currents of hydrogen, methane and ethylene in Fig. 7.1 and 7.2 support the results of Hori *et al.*; we also observe more methane and in particular more ethylene in perchlorate and hydroxide electrolytes. However, the effect is smaller than expected from literature. This could be explained by the the fact that the cations are also different in both systems. We have used potassium phosphate buffers, and sodium perchlorate and hydroxide solutions. The cation has been shown to influence the selectivity and efficiency of the CO_2 reduction.[5,172] Bigger cations increase the selectivity towards CO and hydrocarbons. Therefore, in our results the anion effect is probably partly compensated by the cation effect.

7.5 Conclusions

The observed general pH-dependence of the onset potentials for methane formation confirms the results of Hori *et al.*, showing that the formation of methane is dependent on pH. The onset potentials for ethylene formation on Cu(100) do not depend on pH, which is in agreement with our proposed reaction mechanism via the formation of a pH-independent CO dimer on this crystal facet. On Cu(111), the onset potentials for the formation of ethylene are closer to the (constant) onset potentials of methane formation. This indicates a second, pH-dependent reaction pathway to ethylene with a common intermediate (CHO) towards methane and ethylene, which is also

in agreement with our previous work. At very low and high pH, we have observed that, in particular on Cu(100), the formation of methane shifts to lower overpotentials, which is mirrored by the hydrogen formation. This indicates a relation between hydrogen evolution and methane formation, which at present is not explained by our reaction mechanism. Our reaction mechanism also does not explain why methane is not observed during the reduction of CO_2 on Cu(111) at pH 1. Also at pH 1, no ethylene formation was observed, indicating that the protonation of CO is favored over the formation of the C-C bond at low pH. In a phosphate buffer of pH 2, we have observed a shift in onset potential for methane and ethylene formation between the first and second reduction cycle during the reduction of CO. This potential shift is not related to a change in pH or surface morphology.

Bibliography

[1] P. Friedlingstein, R. A. Houghton, G. Marland, J. Hackler, T. A. Boden, T. J. Conway, J. G. Canadell, M. R. Raupach, P. Ciais and C. Le Quere, *Nature Geosci.*, 2010, **3**, 811–812.

[2] Y. Hori, K. Kikuchi and S. Suzuki, *Chem. Lett.*, 1985, 1695–1698.

[3] Y. Hori, H. Wakebe, T. Tsukamoto and O. Koga, *Electrochim. Acta*, 1994, **39**, 1833–1839.

[4] M. Gattrell, N. Gupta and A. Co, *J. Electroanal. Chem.*, 2006, **594**, 1–19.

[5] Y. Hori, in *Modern Aspects of Electrochemistry*, ed. C. G. Vayenas, R. E. White and M. E. Gamboa-Aldeco, Springer, New York, 2008, vol. 42, pp. 89–189.

[6] W. Wang, S. Wang, X. Ma and J. Gong, *Chem. Soc. Rev.*, 2011, **40**, 3703–3727.

[7] C. Graves, S. D. Ebbesen, M. Mogensen and K. S. Lackner, *Renew. Sust. Energ. Rev.*, 2011, **15**, 1–23.

[8] D. T. Whipple and P. J. A. Kenis, *J. Phys. Chem. Lett.*, 2010, **1**, 3451–3458.

[9] G. Centi and S. Perathoner, *Catal. Today*, 2009, **148**, 191 – 205.

[10] X. Xiaoding and J. A. Moulijn, *Energy Fuels*, 1996, **10**, 305–325.

[11] G. Schneider, Y. Lindqvist and C. I. Branden, *Annu. Rev. Biophys. Biomol. Struct.*, 1992, **21**, 119–143.

[12] D. L. Nelson and M. M. Cox, *Lehninger principles of biochemistry*, W.H. Freeman, 5th edn., 2008, pp. 773–801.

[13] Y. Liu and D. Liu, *Int. J. Hydrogen Energy*, 1999, **24**, 351–354.

[14] M. Ginés, A. Marchi and C. Apesteguía, *Appl. Catal., A*, 1997, **154**, 155–171.

[15] Y. Yang, J. Evans, J. A. Rodriguez, M. G. White and P. Liu, *Phys. Chem. Chem. Phys.*, 2010, **12**, 9909–9917.

[16] G.-C. Wang and J. Nakamura, *J. Phys. Chem. Lett.*, 2010, **1**, 3053–3057.

[17] S.-I. Fujita, M. Usui and N. Takezawa, *J. Catal.*, 1992, **134**, 220–225.

[18] C. S. Chen, J. H. Wu and T. W. Lai, *J. Phys. Chem. C*, 2010, **114**, 15021–15028.

[19] A. A. Gokhale, J. A. Dumesic and M. Mavrikakis, *J. Am. Chem. Soc.*, 2008, **130**, 1402–1414.

[20] P. Liu and J. A. Rodriguez, *J. Chem. Phys.*, 2007, **126**, 164705.

[21] A. Goguet, F. C. Meunier, D. Tibiletti, J. P. Breen and R. Burch, *J. Phys. Chem. B*, 2004, **108**, 20240–20246.

[22] W. Wang and J. Gong, *Front. Chem. Sci. Eng*, 2011, **5**, 2–10.

[23] S.-I. Fujita, M. Nakamura, T. Doi and N. Takezawa, *Appl. Catal., A*, 1993, **104**, 87–100.

[24] A. Lapidus, N. Gaidai, N. Nekrasov, L. Tishkova, Y. Agafonov and T. Myshenkova, *Petrol. Chem.*, 2007, **47**, 75–82.

[25] M. Marwood, R. Doepper and A. Renken, *Appl. Catal., A*, 1997, **151**, 223–246.

[26] E. Vesselli, M. Rizzi, L. De Rogatis, X. Ding, A. Baraldi, G. Comelli, L. Savio, L. Vattuone, M. Rocca, P. Fornasiero, A. Baldereschi and M. Peressi, *J. Phys. Chem. Lett.*, 2010, **1**, 402–406.

[27] C. Huang and J. Richardson, *J. Catal.*, 1978, **51**, 1–8.

[28] J. Sehested, S. Dahl, J. Jacobsen and J. R. Rostrup-Nielsen, *J. Phys. Chem. B*, 2005, **109**, 2432–2438.

[29] H. Nakatsuji and Z.-M. Hu, *Int. J. Quantum Chem.*, 2000, **77**, 341–349.

[30] Q.-L. Tang, Q.-J. Hong and Z.-P. Liu, *J. Catal.*, 2009, **263**, 114–122.

[31] M. Bowker, R. A. Hadden, H. Houghton, J. N. K. Hyland and K. C. Waugh, *J. Catal.*, 1988, **109**, 263 – 273.

[32] J. Yoshihara, S. C. Parker, A. Schafer and C. T. Campbell, *Catal. Lett.*, 1995, **31**, 313–324.

[33] H.-W. Lim, M.-J. Park, S.-H. Kang, H.-J. Chae, J. W. Bae and K.-W. Jun, *Ind. Eng. Chem. Res.*, 2009, **48**, 10448–10455.

[34] Q. Sun, C.-W. Liu, W. Pan, Q.-M. Zhu and J.-F. Deng, *Appl. Catal., A*, 1998, **171**, 301–308.

[35] P. Rasmussen, M. Kazuta and I. Chorkendorff, *Surf. Sci.*, 1994, **318**, 267–280.

[36] L. C. Grabow and M. Mavrikakis, *ACS Catal.*, 2011, **1**, 365–384.

[37] Y. Nitta, O. Suwata, Y. Ikeda, Y. Okamoto and T. Imanaka, *Catal. Lett.*, 1994, **26**, 345–354.

[38] J. Szanyi and D. W. Goodman, *Catal. Lett.*, 1991, **10**, 383–390.

[39] J. Yoshihara and C. T. Campbell, *J. Catal.*, 1996, **161**, 776–782.

[40] J. Nakamura, Y. Choi and T. Fujitani, *Top. Catal.*, 2003, **22**, 277–285.

[41] M. Behrens, F. Studt, I. Kasatkin, S. Kühl, M. Hävecker, F. Abild-Pedersen, S. Zander, F. Girgsdies, P. Kurr, B.-L. Kniep, M. Tovar, R. W. Fischer, J. K. Nørskov and R. Schlögl, *Science*, 2012, **336**, 893–897.

[42] R. W. Dorner, D. R. Hardy, F. W. Williams and H. D. Willauer, *Energy Environ. Sci.*, 2010, **3**, 884–890.

[43] M. Fujiwara, R. Kieffer, H. Ando and Y. Souma, *Appl. Catal., A*, 1995, **121**, 113–124.

[44] K. Fujimoto and T. Shikada, *Appl. Catal.*, 1987, **31**, 13–23.

[45] P. Sai Prasad, J. Bae, K.-W. Jun and K.-W. Lee, *Catal. Surv. Asia*, 2008, **12**, 170–183.

[46] H. Schulz, *Appl. Catal., A*, 1999, **186**, 3–12.

[47] R. A. van Santen, I. M. Ciobîcă, E. van Steen and M. M. Ghouri, in *Advances in Catalysis*, ed. B. C. Gates and H. Knözinger, Elsevier, Amsterdam, 2011, vol. 54, pp. 127–187.

[48] S. Enthaler, J. von Langermann and T. Schmidt, *Energy Environ. Sci.*, 2010, **3**, 1207–1217.

[49] X. Yu and P. G. Pickup, *J. Power Sources*, 2008, **182**, 124–132.

[50] W. Leitner, *Angew. Chem., Int. Ed.*, 1995, **34**, 2207–2221.

[51] P. G. Jessop, F. Joó and C.-C. Tai, *Coord. Chem. Rev.*, 2004, **248**, 2425–2442.

[52] Y. Gao, J. K. Kuncheria, H. A. Jenkins, R. J. Puddephatt and G. P. A. Yap, *J. Chem. Soc., Dalton Trans.*, 2000, 3212–3217.

[53] J. C. Tsai and K. M. Nicholas, *J. Am. Chem. Soc.*, 1992, **114**, 5117–5124.

[54] F. Hutschka, A. Dedieu, M. Eichberger, R. Fornika and W. Leitner, *J. Am. Chem. Soc.*, 1997, **119**, 4432–4443.

[55] Y. Musashi and S. Sakaki, *J. Am. Chem. Soc.*, 2002, **124**, 7588–7603.

[56] C. Yin, Z. Xu, S.-Y. Yang, S. M. Ng, K. Y. Wong, Z. Lin and C. P. Lau, *Organometallics*, 2001, **20**, 1216–1222.

[57] K.-I. Tominaga, Y. Sasaki, M. Saito, K. Hagihara and T. Watanabe, *J. Mol. Catal.*, 1994, **89**, 51–55.

[58] M. T. Koper, *J. Electroanal. Chem.*, 2011, **660**, 254–260.

[59] E. E. Benson, C. P. Kubiak, A. J. Sathrum and J. M. Smieja, *Chem. Soc. Rev.*, 2009, **38**, 89–99.

[60] J.-M. Savéant, *Chem. Rev.*, 2008, **108**, 2348–2378.

[61] *Electochemical and electrocatalytic reactions of carbon dioxide*, ed. B. P. Sullivan, K. Krist and H. E. Guard, Elsevier, Amsterdam, 1993.

[62] A. Gennaro, A. A. Isse, J.-M. Savéant, M.-G. Severin and E. Vianello, *J. Am. Chem. Soc.*, 1996, **118**, 7190–7196.

[63] D. L. Dubois, in *Electrochemical Reactions of Carbon Dioxide*, Wiley-VCH Verlag GmbH & Co. KGaA, 2007, pp. 202–225.

[64] S. Sakaki, *J. Am. Chem. Soc.*, 1992, **114**, 2055–2062.

[65] M. Beley, J. P. Collin, R. Ruppert and J. P. Sauvage, *J. Am. Chem. Soc.*, 1986, **108**, 7461–7467.

[66] M. Hammouche, D. Lexa, M. Momenteau and J.-M. Savéant, *J. Am. Chem. Soc.*, 1991, **113**, 8455–8466.

[67] J. R. Pugh, M. R. M. Bruce, B. P. Sullivan and T. J. Meyer, *Inorg. Chem.*, 1991, **30**, 86–91.

[68] H. Nagao, T. Mizukawa and K. Tanaka, *Inorg. Chem.*, 1994, **33**, 3415–3420.

[69] B. E. Cole, P. S. Lakkaraju, D. M. Rampulla, A. J. Morris, E. Abelev and A. B. Bocarsly, *J. Am. Chem. Soc.*, 2010, **132**, 11539–11551.

[70] A. J. Morris, R. T. McGibbon and A. B. Bocarsly, *ChemSusChem*, 2011, **4**, 191–196.

[71] J. A. Keith and E. A. Carter, *J. Am. Chem. Soc.*, 2012, **134**, 7580–7583.

[72] E. Duñach, D. Franco and S. Olivero, *Eur. J. Org. Chem.*, 2003, **2003**, 1605–1622.

[73] C. Amatore and A. Jutand, *J. Am. Chem. Soc.*, 1991, **113**, 2819–2825.

[74] J. Grimshaw, *Electrochemical Reactions and Mechanisms in Organic Chemistry*, Elsevier Science B.V., Amsterdam, 2000, pp. 147–150.

[75] M. M. Baizer, *Tetrahedron*, 1984, **40**, 935 – 969.

[76] Y. Hiejima, M. Hayashi, A. Uda, S. Oya, H. Kondo, H. Senboku and K. Takahashi, *Phys. Chem. Chem. Phys.*, 2010, **12**, 1953–1957.

[77] A. A. Peterson and J. K. Nørskov, *J. Phys. Chem. Lett.*, 2012, **3**, 251–258.

[78] F. A. Armstrong and J. Hirst, *Proc. Natl. Acad. Sci. USA*, 2011, **108**, 14049–14054.

[79] J.-H. Jeoung and H. Dobbek, *Science*, 2007, **318**, 1461–1464.

[80] Y. Hori, M. Murata and R. Takahashi, *J. Chem. Soc. Faraday Trans. 1*, 1989, **85**, 2309–2326.

[81] K. W. Frese, in *Electochemical and electrocatalytic reactions of carbon dioxide*, ed. B. P. Sullivan, K. Krist and H. E. Guard, Elsevier, Amsterdam, 1993, pp. 145–216.

[82] D. P. Summers, S. Leach and K. W. F. Jr., *J. Electroanal. Chem.*, 1986, **205**, 219–232.

[83] K. P. Kuhl, E. R. Cave, D. N. Abram and T. F. Jaramillo, *Energy Environ. Sci.*, 2012, –.

[84] Y. Hori, R. Takahashi, Y. Yoshinami and A. Murata, *J. Phys. Chem. B*, 1997, **101**, 7075–7081.

[85] Y. Hori, A. Murata, R. Takahashi and S. Suzuki, *J. Am. Chem. Soc.*, 1987, **109**, 5022–5023.

[86] A. A. Peterson, F. Abild-Pedersen, F. Studt, J. Rossmeisl and J. K. Nørskov, *Energy Environ. Sci.*, 2010, **3**, 1311–1315.

[87] Y. Hori, I. Takahashi, O. Koga and N. Hoshi, *J. Mol. Catal. A: Chem.*, 2003, **199**, 39–47.

[88] W. J. Durand, A. A. Peterson, F. Studt, F. Abild-Pedersen and J. K. Nørskov, *Surf. Sci.*, 2011, **605**, 1354–1359.

[89] J. Karl W. Frese, *J. Electrochem. Soc.*, 1991, **138**, 3338–3344.

[90] C. W. Li and M. W. Kanan, *J. Am. Chem. Soc.*, 2012, **134**, 7231–7234.

[91] C. Amatore and J. M. Savéant, *J. Am. Chem. Soc.*, 1981, **103**, 5021–5023.

[92] V. S. Bagotzky and N. V. Osetrova, *Russ. J. Electrochem.*, 1995, **31**, 409–425.

[93] N. S. Lewis and G. A. Shreve, in *Electochemical and electrocatalytic reactions of carbon dioxide*, ed. B. P. Sullivan, K. Krist and H. E. Guard, Elsevier, Amsterdam, 1993, pp. 263–289.

[94] A. J. Morris, G. J. Meyer and E. Fujita, *Acc. Chem. Res.*, 2009, **42**, 1983–1994.

[95] B. Kumar, M. Llorente, J. Froehlich, T. Dang, A. Sathrum and C. P. Kubiak, *Annu. Rev. Phys. Chem.*, 2012, **63**, 541–569.

[96] W. M. Sears and S. R. Morrison, *J. Phys. Chem.*, 1985, **89**, 3295–3298.

[97] A. F. Sammells and R. L. Cook, in *Electochemical and electrocatalytic reactions of carbon dioxide*, ed. B. P. Sullivan, K. Krist and H. E. Guard, Elsevier, Amsterdam, 1993, pp. 217–262.

[98] M. Gattrell, N. Gupta and A. Co, *Energy Convers. Manage.*, 2007, **48**, 1255–1265.

[99] M. Gattrell, N. Gupta and A. Co, *J. Electroanal. Chem.*, 2006, **594**, 1–19.

[100] D. DeWulf, T. Jin and A. Bard, *J. Electrochem. Soc.*, 1989, **136**, 1686–1691.

[101] S. Wasmus, E. Cattaneo and W. Vielstich, *Electrochim. Acta*, 1990, **35**, 771–775.

[102] P. Friebe, P. Bogdanoff, N. Alonso-Vante and H. Tributsch, *J. Catal.*, 1997, **168**, 374–385.

[103] G. M. Brisard, A. P. M. Camargo, F. C. Nart and T. Iwasita, *Electrochem. Commun.*, 2001, **3**, 603–607.

[104] P. Dubé and G. Brisard, *J. Electroanal. Chem.*, 2005, **582**, 230–240.

[105] H. Siegenthaler and K. Jüttner, *J. Electroanal. Chem.*, 1984, **163**, 327–343.

[106] B. Cruickshank, D. D. Sneddon and A. A. Gewirth, *Surf. Sci. Lett.*, 1993, **281**, 308–314.

[107] Y. Hori, H. Konishi, T. Futamura, A. Murata, O. Koga, H. Sakurai and K. Oguma, *Electrochim. Acta*, 2005, **50**, 5354–5369.

[108] A. H. Wonders, T. H. M. Housmans, V. Rosca and M. T. M. Koper, *J. Appl. Electrochem.*, 2006, **36**, 1215–1221.

[109] Y. Kwon and M. T. M. Koper, *Anal. Chem.*, 2010, **82**, 5420–5424.

[110] S. Kaneco, H. Katsumata, T. Suzuki and K. Ohta, *Energy Fuels*, 2006, **20**, 409–414.

[111] Y. Hori, A. Murata and Y. Yoshinami, *J. Chem. Soc. Faraday Trans.*, 1991, **87**, 125–128.

[112] S. Cannizzaro, *Liebigs Ann.*, 1853, **88**, 129–130.

[113] R. C. Elderfield, *J. Chem. Educ.*, 1930, **7**, 594–596.

[114] R. L. Cook, R. C. MacDuff and A. F. Sammells, *J. Electrochem. Soc.*, 1989, **136**, 1982–1984.

[115] J. A. Gladysz and W. Tam, *J. Am. Chem. Soc.*, 1978, **100**, 2545–2547.

[116] I. M. Ciobîcă and R. A. van Santen, *J. Phys. Chem. B*, 2003, **107**, 3808–3812.

[117] O. R. Inderwildi, S. J. Jenkins and D. A. King, *J. Phys. Chem. C*, 2008, **112**, 1305–1307.

[118] S. Shetty, A. P. J. Jansen and R. A. van Santen, *J. Am. Chem. Soc.*, 2009, **131**, 12874–12875.

[119] S. Shetty and R. A. van Santen, *Phys. Chem. Chem. Phys.*, 2010, **12**, 6330–6332.

[120] A. Koverga, D. Wallace and M. T. M. Koper, *in preperation*.

[121] S. Clarke and J. Harrison, *J. Electroanal. Chem. Interfac. Electrochem.*, 1972, **36**, 109–115.

[122] S. Omanović and M. Metikoš-Huković, *J. Appl. Electrochem.*, 1997, **27**, 35–41.

[123] L. Formaro and G. Castelli, *J. Electroanal. Chem. Interfac. Electrochem.*, 1970, **28**, 363–374.

[124] S. Trasatti and L. Formaro, *J. Electroanal. Chem. Interfac. Electrochem.*, 1968, **17**, 343–364.

[125] M. A. Henderson, Y. Zhou and J. M. White, *J. Am. Chem. Soc.*, 1989, **111**, 1185–1193.

[126] T. Shimada, K. Sakata, T. Homma, H. Nakai and T. Osaka, *Electrochim. Acta*, 2005, **51**, 906–915.

[127] A. F. Lee, D. E. Gawthrope, N. J. Hart and K. Wilson, *Surf. Sci.*, 2004, **548**, 200–208.

[128] R. Alcalá, M. Mavrikakis and J. A. Dumesic, *J. Catal.*, 2003, **218**, 178–190.

[129] F. Kadirgan, B. Beden and C. Lamy, *J. Electroanal. Chem. Interfac. Electrochem.*, 1982, **136**, 119–138.

[130] J. T. Jankowiak and M. A. Barteau, *J. Catal.*, 2005, **236**, 379–386.

[131] S. Linic and M. A. Barteau, *J. Am. Chem. Soc.*, 2003, **125**, 4034–4035.

[132] W. A. Brown and D. A. King, *J. Phys. Chem. B*, 2000, **104**, 2578–2595.

[133] R. Burch, S. T. Daniells and P. Hu, *J. Chem. Phys.*, 2004, **121**, 2737–2745.

[134] A. C. A. de Vooys, M. T. M. Koper, R. A. van Santen and J. A. R. van Veen, *Electrochim. Acta*, 2001, **46**, 923–930.

[135] A. C. A. de Vooys, M. T. M. Koper, R. A. van Santen and J. A. R. van Veen, *J. Catal.*, 2001, **202**, 387–394.

[136] C. C. Lee, Y. Hu and M. W. Ribbe, *Science*, 2010, **329**, 642.

[137] J. E. McMurry and M. P. Fleming, *J. Am. Chem. Soc.*, 1974, **96**, 4708–4709.

[138] M. Ephritikhine, *Chem. Commun.*, 1998, 2549–2554.

[139] S. D. Senanayake, G. I. N. Waterhouse, H. Idriss and T. E. Madey, *Langmuir*, 2005, **21**, 11141–11145.

[140] P. L. Arnold, Z. R. Turner, R. M. Bellabarba and R. P. Tooze, *Chem. Sci.*, 2011, **2**, 77–79.

[141] M. Montoya and J. Mellado, *J. Electroanal. Chem.*, 1994, **371**, 215–221.

[142] D. Nematollahi and M. Rafiee, *J. Electroanal. Chem.*, 2004, **566**, 31–37.

[143] S.-E. Bae and A. A. Gewirth, *Faraday Discuss.*, 2008, **140**, 113–123.

[144] K. J. P. Schouten, Z. Qin, E. Pérez Gallent and M. T. M. Koper, *J. Am. Chem. Soc.*, 2012, **134**, 9864–9867.

[145] S.-E. Bae, K. L. Stewart and A. A. Gewirth, *J. Am. Chem. Soc.*, 2007, **129**, 10171–10180.

[146] P. Broekmann, M. Wilms, M. Kruft, C. Stuhlmann and K. Wandelt, *J. Electroanal. Chem.*, 1999, **467**, 307–324.

[147] G. Brisard, N. Bertrand, P. N. Ross and M. N. Marković, *J. Electroanal. Chem.*, 2000, **480**, 219–224.

[148] Y. Hori, H. Wakebe, T. Tsukamoto and O. Koga, *Surf. Sci.*, 1995, **335**, 258–263.

[149] O. Koga, S. Teruya, K. Matsuda, M. Minami, N. Hoshi and Y. Hori, *Electrochim. Acta*, 2005, **50**, 2475–2485.

[150] C. Schlaup and S. Horch, *Surf. Sci.*, 2013, **608**, 44–54.

[151] J. M. M. Droog and B. Schlenter, *J. Electroanal. Chem. Interfac. Electrochem.*, 1980, **112**, 387–390.

[152] V. D. Jović and B. M. Jović, *J. Serb. Chem. Soc.*, 2002, **67**, 531–546.

[153] V. D. Jović and B. M. Jović, *J. Electroanal. Chem.*, 2003, **541**, 13–21.

[154] O. M. Magnussen, L. Zitzler, B. Gleich, M. R. Vogt and R. J. Behm, *Electrochim. Acta*, 2001, **46**, 3725–3733.

[155] S. Härtinger, B. Pettinger and K. Doblhofer, *J. Electroanal. Chem.*, 1995, **397**, 335–338.

[156] V. Maurice, H.-H. Strehblow and P. Marcus, *Surf. Sci.*, 2000, **458**, 185–194.

[157] A. Lukomska and J. Sobkowski, *J. Electroanal. Chem.*, 2004, **567**, 95–102.

[158] J. Kunze, V. Maurice, L. H. Klein, H.-H. Strehblow and P. Marcus, *Electrochim. Acta*, 2003, **48**, 1157–1167.

[159] F. Jensen, F. Besenbacher, E. Lægsgaard and I. Stensgaard, *Surf. Sci.*, 1991, **259**, L774–L780.

[160] J. Kunze, V. Maurice, L. H. Klein, H.-H. Strehblow and P. Marcus, *J. Electroanal. Chem.*, 2003, **554-555**, 113–125.

[161] K. J. P. Schouten, Y. Kwon, C. J. M. van der Ham, Z. Qin and M. T. M. Koper, *Chem. Sci.*, 2011, **2**, 1902–1909.

[162] Y. Gao, H. Tsuji, H. Hattori and H. Kita, *J. Electroanal. Chem.*, 1994, **372**, 195–200.

[163] H. Baltruschat, *J. Am. Soc. Mass Spectrom.*, 2004, **15**, 1693–1706.

[164] H. Matsushima, A. Taranovskyy, C. Haak, Y. Gründer and O. M. Magnussen, *J. Am. Chem. Soc.*, 2009, **131**, 10362–10363.

[165] K. J. P. Schouten, E. Pérez Gallent and M. T. M. Koper, *J. Electroanal. Chem.*, 2013, **699**, 6–9.

[166] F. Calle-Vallejo and M. T. M. Koper, *Angew. Chem. Int. Ed.*, 2013, **52**, 7282–7285.

[167] M. T. M. Koper, *Nanoscale*, 2011, **3**, 2054–2073.

[168] X. Nie, M. R. Esopi, M. J. Janik and A. Asthagiri, *Angew. Chem. Int. Ed.*, 2013, n/a–n/a.

[169] W. Tang, A. A. Peterson, A. S. Varela, Z. P. Jovanov, L. Bech, W. J. Durand, S. Dahl, J. K. Nørskov and I. Chorkendorff, *Phys. Chem. Chem. Phys.*, 2012, **14**, 76–81.

[170] K. J. P. Schouten, E. Pérez Gallent and M. T. M. Koper, *ACS Catal.*, 2013, **3**, 1292–1295.

[171] J. H. Montoya, A. A. Peterson and J. K. Nørskov, *ChemCatChem*, 2013, **5**, 737–742.

[172] M. R. Thorson, K. I. Siil and P. J. A. Kenis, *J. Electrochem. Soc.*, 2013, **160**, F69–F74.

Summary

Hydrocarbon-based fuels are worldwide the most important energy sources and energy carriers. The combustion of these hydrocarbons yields, apart from the desired energy, carbon dioxide (CO_2). This has lead to significant increases of atmospheric CO_2 levels, which is causing a widespread concern about its possible consequences. On the other hand, from a more positive perspective, CO_2 is a vast and sustainable carbon feedstock, that could partly replace the widespread use of petroleum-based hydrocarbons as chemical building blocks. Therefore, converting carbon dioxide into hydrocarbons would not only limit the emission of carbon dioxide, but also supply us with a sustainable carbon feedstock, provided the conversion is performed using sustainable energy, and without much additional CO_2 production.

Already in the 1980s it has been discovered in Japan that it is possible to reduce CO_2 to methane and ethylene using copper electrodes. The formation of methane and especially ethylene is surprising, and only takes place to a significant extent on copper electrodes. In spite of the extensive literature, the molecular mechanism is still unclear, in particular in relation to the carbon-carbon coupling step leading to the formation of ethylene. Understanding this C-C bond formation is important as it could open up routes to the production of high-energy fuels by the (photo-)electrochemical reduction of CO_2. The research presented in this thesis is focused on the understanding of the molecular mechanism of the electrochemical reduction of carbon dioxide using copper electrodes. We have aimed to identify intermediates that determine the selectivity of the reaction to either methane or ethylene.

In Chapter 2 we have aimed to obtain more insights in the key intermediates that determine the selectivity of CO_2 reduction to various products, by comparing the electrochemical reduction of CO_2 to the metal-catalyzed hydrogenation and reduction of CO_2 both homogeneously in solution and heterogeneously in the gas phase. Based on this comparison we have distinguished four main pathways: (1) methane is formed via carboxyl (COOH) and carbon monoxide (CO), (2) methanol is formed via formate (HCOO) and formaldehyde, (3) ethylene is formed via the coupling of CO, leading to surface enolates, and (4) CO_2 is inserted into existing carbon chains, close to the way CO_2 is fixed in nature.

In Chapter 3, we have identified key intermediates that determine if CO_2 is reduced to methane or ethylene by reducing C_1 and C_2 species containing oxygen, to investigate whether or not they can be reduced to either methane or ethylene on copper electrodes. For the the C_1 pathway to methane we have shown that it is very likely that CHO_{ads} is the key intermediate towards the breaking of the C-O bond and, therefore, the formation of methane. For the C_2 pathway to ethylene we have suggested that the first step is the formation of a CO dimer, followed by the formation of a surface-bonded enediol or enediolate, or the formation of an oxametallacycle. Both the enediol(ate) and the oxametallacycle would explain the selectivity of the C_2 pathway towards ethylene.

The formation and stabilization of these intermediates also depends on the atomic configuration of the electrode surface. We have used copper single crystals in order to study this structure dependence. The use of Cu single crystal electrodes requires a method to carefully characterize the surface structure. Therefore, we have developed a characterization method using blank voltammetry in alkaline media, which is presented in Chapter 4. The adsorption of OH^- on copper electrodes in alkaline media appeared to be surface structure dependent, which allows for identification and characterization of the various single crystal facets.

In Chapter 5 we have compared the reduction of carbon monoxide (CO), a well known intermediate of CO_2 reduction on copper electrodes, on the single crystal surfaces Cu(111) and Cu(100). We have observed two different reaction mechanisms for ethylene formation: a first pathway that has a common intermediate with the formation of methane and that takes place preferentially at (111) facets or steps, and a second pathway at (100) facets in

which CO is selectively reduced to ethylene at relatively low overpotentials. We have also shown in this chapter that the reduction of CO on polycrystalline copper is similar to the CO reduction on Cu(100), suggesting that the (100) facets seems to be the dominant crystal facet in polycrystalline copper. This could open up new routes to an affordable (photo-)electrochemical production of hydrocarbons from CO_2.

Since the (100) orientation turned out to be very important for selective ethylene formation we have studied stepped Cu single crystals to compare the reactivity of a surface with (100) terraces to a surface with (100) steps, the results of which are presented in Chapter 6. The selective ethylene formation at low overpotentials was only observed on (100) terraces.

The pH is another important parameter in the reaction mechanism. In Chapter 7 we have investigated the influence of the pH by reducing carbon dioxide and carbon monoxide on Cu(111) and Cu(100) electrodes. The results supported our proposed reaction mechanism, in which two different reaction pathways to ethylene can be distinguished: a first, pH-dependent pathway that has a common intermediate (formyl) with the formation of methane that occurs mainly on Cu(111), and a second, pH-independent pathway via a carbon monoxide dimer. The latter pathway occurs on Cu(100) only.

Samenvatting

Op dit moment zijn koolwaterstoffen, zoals aardolie en aardgas, wereldwijd de belangrijkste energiebronnen en energiedragers. De verbranding van deze koolwaterstoffen levert, naast de gewenste energie, ook koolstofdioxide (CO_2) op. Dit CO_2 wordt ervan verdacht een van de grootste oorzaken van de huidige opwarming van de aarde te zijn. Dit proefschrift beschrijft het onderzoek naar de omzetting van CO_2 naar koolwaterstoffen, het omgekeerde dus van de verbrandingsreactie. Als hiervoor duurzame energie gebruikt zou worden, zou dit een belangrijke stap zijn in het verminderen van de CO_2 uitstoot en het genereren van duurzame koolwaterstoffen als energiedragers.

Al in de jaren tachtig is in Japan een proces ontdekt waarin CO_2 kan worden gereduceerd naar methaan en ethyleen aan een koperelektrode. Methaan is de belangrijkste component van aardgas, en ethyleen is, naast dat het ook een brandstof is, een belangrijke grondstof voor de chemische industrie. Met dit proces zou duurzaam opgewekte elektrische energie kunnen worden gebruikt om CO_2 om te zetten naar deze belangrijke koolwaterstoffen. Daarom is er al veel onderzoek verricht naar dit systeem. Hierbij is onder andere gevonden dat dit proces alleen aan koper elektrodes plaats vindt, en niet of nauwelijks aan elektrodes van andere materialen. Het oppervlak van de koperelektrode heeft dus bijzondere eigenschappen, die er voor zorgen dat deze reactie, die aan elektrodes van andere metalen niet of heel langzaam verloopt, wel mogelijk is. Deze eigenschappen maken dat koper de katalysator is in dit proces. Een katalysator is een stof die de snelheid van een chemische reactie versneld, zonder daarbij zelf verbruikt te worden. Als we deze katalytische eigenschappen van koper beter begrijpen, zou dit mogelijkheden kunnen opleveren om het proces van CO_2 reductie verder te

optimaliseren. Hiervoor is het onder andere nodig dat we precies, op moleculair niveau, begrijpen wat er plaats vind aan het koperoppervlak. Als we namelijk weten via welke reactiestappen en intermediairen het CO_2 wordt omgezet naar methaan en ethyleen, zouden we de opbrengst misschien kunnen verhogen, of selectief methaan of ethyleen kunnen maken. De focus van het onderzoek dat gepresenteerd wordt in dit proefschrift is het identificeren van deze reactiestappen en intermediairen die gevormd worden bij de omzetting van CO_2 naar methaan en ethyleen.

In hoofdstuk 2 hebben we de reactiestappen vergeleken die bekend zijn van andere processen en reacties waarbij CO_2 wordt omgezet naar koolwaterstoffen. Voorbeelden hiervan zijn de fotosynthese, de manier waarop CO_2 in de natuur door planten wordt omgezet in koolstofketens, en verschillende industriële processen waarin CO_2 kan worden gebruikt om koolwaterstoffen te maken. Na al de verschillende tussen- en eind producten in deze reacties vergeleken te hebben, hebben we geconcludeerd dat er vier algemene routes zijn waarin CO_2 wordt gereduceerd: (1) methaan wordt gevormd via carboxyl (COOH) en koolstofmonoxide (CO), (2) methanol wordt gevormd via formaat (HCOO) en formaldehyde, (3) ethyleen wordt gevormd via de koppeling van koolstofmonoxide, en (4) voor langere koolstofketens wordt CO_2 gekoppeld aan bestaande koolstofketens, wat lijkt op de manier zoals dit in fotosynthese gebeurd.

In hoofdstuk 3 hebben we alle organische verbindingen die één (C_1) of twee (C_2) koolstofatomen en een of meer zuurstofatomen bevatten gereduceerd aan een koper elektrode, met als doel om uit te vinden of de reductie van deze stoffen gemeenschappelijke (tussen)producten en/of intermediaren hebben met de reductie van CO_2 naar methaan en ethyleen. De hiervoor gebruikte techniek is OLEMS, wat staat voor online elektrochemische massaspectrometrie. Hiermee kunnen we de gasvormige producten die gevormd worden aan de koper elektrode detecteren met een massaspectrometer, terwijl de elektrische potentiaal van de electrode wordt aangepast. Hierdoor kunnen we de reactie als functie van de potentiaal bestuderen. Op basis van de resultaten hebben we geconcludeerd dat voor de C_1 route naar methaan de vorming van formyl (HCO) belangrijk is. Voor de C_2 route naar ethyleen wordt er eerst aan het koperoppervlak een dimeer gevormd van koolstofmonoxide, waarna een enolaat of een oxametallacycle wordt gevormd. Laatstgenoemde intermediairen kunnen verklaren waarom selectief

ethyleen als C_2 product wordt gevormd.

Omdat uit de wetenschappelijke literatuur al bekend was dat de vorming van methaan en ethyleen ook afhangt van de structuur van het oppervlak, hebben we de invloed van eenkristallijne koperelektrodes op de reductie van CO_2 bestudeerd. In deze eenkristallen zitten de atomen in een rooster gerangschikt. Door het eenkristal onder verschillende hoeken door te snijden, kunnen verschillende oppervlaktestructuren worden verkregen. In hoofdstuk 4 wordt een elektrochemische methode gepresenteerd om deze verschillende structuren te kunnen onderscheiden. Dit is nodig om zodoende de oppervlakte structuur te kunnen relateren aan de CO_2 reductie. Hiervoor wordt gebruik gemaakt van cyclische voltammetrie in basische oplossingen. Bij cyclische voltammetrie wordt de stroom gemeten als functie van een constant veranderende potentiaal. De OH^- ionen in de basische oplossing adsorberen bij verschillende potentialen aan het koperoppervlak, afhankelijk van de oppervlaktestructuur, wat resulteert in een verandering in de stroom bij deze potentialen. Dit geeft een karakteristiek voltammogram voor elke eenkristallijne koperelektrode.

In hoofdstuk 5 wordt de reductie van koolstofmonoxide vergeleken op twee van deze koper eenkristallen, nl. Cu(111) en Cu(100). In Cu(111) zitten de atomen zo dicht mogelijk op elkaar gepakt, wat een hexagonaal patroon oplevert. In Cu(100) zitten de atomen in een vierkant patroon, en hebben de atomen wat meer ruimte. Koolstofmonoxide reductie levert dezelfde producten op als koolstofdioxide reductie, en is daarom een belangrijk intermediair in de CO_2 reductie. Door met behulp van de OLEMS techniek de reductie van koolstofmonoxide aan de twee genoemde koper eenkristallen te bestuderen, zijn we erachter gekomen dat er twee verschillende routes zijn die tot de vorming van ethyleen leiden: een route die zowel op Cu(111) als op Cu(100) mogelijk is en samengaat met de vorming van methaan, en een route waarbij selectief alleen ethyleen gevormd op Cu(100). De benodigde elektrische potentiaal voor de tweede route is aanmerkelijke lager dan die van de eerste route.

Omdat de (100) structuur erg belangrijk bleek voor de vorming van ethyleen, zijn we in het onderzoek gepresenteerd in hoofdstuk 6 dieper op deze (100) structuur ingegaan. Hiervoor hebben we gestapte koper eenkristallen gebruikt, om zodoende te kunnen aantonen of grotere gebieden met de (100) structuur, zogenaamde (100) terrassen, of (100) stappen de selectie-

ve vorming van ethyleen katalyseren. Uit dit onderzoek is gebleken dat dit alleen voor (100) terrassen geldt.

In hoofdstuk 7 hebben we de invloed van de pH (de zuurgraad) op de reductie van koolstofdioxide en koolstofmonoxide op Cu(111) en Cu(100) beschreven. De resultaten komen overeen met het voorgestelde mechanisme, waarin twee reactieroutes naar ethyleen kunnen worden onderscheiden: een eerst route die afhankelijk is van de pH en een gemeenschappelijk intermediair (formyl) heeft met de vorming van methaan. Deze route is voornamelijk beschikbaar op Cu(111). De tweede route naar ethyleen hangt niet af van de pH, en komt alleen voor op Cu(100). Dit wijst op de vorming van een dimeer van koolstofmonoxide als belangrijkste stap in de vorming van ethyleen op Cu(100).

List of publications

This thesis is based on the following publications:

Chapter 2
K. J. P. Schouten and M. T. M. Koper
Key intermediates in the hydrogenation and electrochemical reduction of CO_2
in *Photoelectrochemical Water Splitting: Materials, Processes and Architectures*
ed. H.-J. Lewerenz and L. Peter, The Royal Society of Chemistry, *in press*

Chapter 3
K. J. P. Schouten, Y. Kwon, C. J. M. van der Ham, Z. Qin and M. T. M. Koper
A new mechanism for the selectivity to C_1 and C_2 species in the electrochemical reduction of carbon dioxide on copper electrodes
Chem. Sci., 2011, **2**, 1902 - 1909.

Chapter 4
K. J. P. Schouten, E. Pérez Gallent and M. T. M. Koper
The electrochemical characterization of copper single crystal electrodes in alkaline media
J. Electroanal. Chem., 2013, **699**, 6 - 9.

Chapter 5
K. J. P. Schouten, Z. Qin, E. Pérez Gallent and M. T. M. Koper
Two pathways for the formation of ethylene in CO reduction on single crystal copper electrodes
J. Am. Chem. Soc., 2012, **134**, 9864 - 9867.

Chapter 6
K. J. P. Schouten, E. Pérez Gallent and M. T. M. Koper
Structure sensitivity of the electrochemical reduction of carbon monoxide on copper single crystals
ACS Catal., 2013, **3**, 1292 - 1295

Chapter 7
K. J. P. Schouten, E. Pérez Gallent and M. T. M. Koper
The influence of pH on the reduction of CO and CO_2 to hydrocarbons on copper electrodes
J. Electroanal. Chem., *submitted*

Other publications:

R. Reske, M. Duca, M. Oezaslan, K. J. P. Schouten, M. T. M. Koper, and P. Strasser
Controlling catalytic selectivities during CO_2 electroreduction on thin Cu metal overlayers
J. Phys. Chem. Lett., 2013, **4**, 2410 - 2413

A. M. Gómez-Marín, K. J. P. Schouten, M. T. M. Koper and J. M. Feliu
Interaction of hydrogen peroxide with a Pt(111) electrode
Electrochem. Commun., 2012, **22**, 153 - 156

Y. Kwon, S. E. F. Kleijn, K. J. P. Schouten and M. T. M. Koper
Cellobiose hydrolysis and decomposition by electrochemical generation of acid and hydroxyl radicals
ChemSusChem, 2012, **5**, 1935 - 1943

Y. Kwon, K. J. P. Schouten and M. T. M. Koper
Mechanism of the catalytic oxidation of glycerol on polycrystalline gold and platinum electrodes
ChemCatChem, 2011, **3**, 1176 - 1185

J. Yang, M. Duca, K. J. P. Schouten and M. T. M. Koper
Formation of volatile products during nitrate reduction on a Sn-modified Pt electrode in acid solution
J. Electroanal. Chem., 2011, **662**, 87 - 92

K. J. P. Schouten, M. J. T. C. van der Niet and M. T. M. Koper
Impedance spectroscopy of H and OH adsorption on stepped single-crystal platinum electrodes in alkaline and acidic media
Phys. Chem. Chem. Phys., 2010, **12**, 15217 - 15224

I. M. N. Groot, K. J. P. Schouten, A. W. Kleyn, and L. B. F. Juurlink
Dynamics of hydrogen dissociation on stepped platinum
J. Chem. Phys., 2008, **129**, 224707

Curriculum Vitae

Klaas Jan Schouten werd geboren in Gouda op 12 februari 1986 en groeide op in Moordrecht. Na het volgen van het atheneum aan het Driestar College te Gouda begon hij in 2004 aan de studie scheikunde aan de Universiteit Leiden. Tijdens zijn bachelor heeft hij meegewerkt met Irene Groot en Ludo Juurlink aan het onderzoek naar de dissociatie van waterstof op gestapte platinaoppervlakken met behulp van een moleculaire bundel in ultrahoogvacuüm. Vervolgens, tijdens zijn master, heeft hij met Ludo Juurlink een ultrahoogvacuüm apparaat gebouwd en daarmee de desorptie van waterstof van gestapte platina oppervlakken met verschillende stapdichtheden bestudeerd. In een tweede project heeft hij met Janneke van der Niet en Marc Koper de adsorptie van H^+ en OH^- aan gestapte platinaoppervlakken in zuur en alkalisch milieu vergeleken met behulp van elektrochemische impedantie spectroscopie. Hij behaalde zijn master titel *cum laude* in 2009 binnen de afstudeerrichting fysische en theoretische chemie. Hierna begon hij aan zijn promotieonderzoek onder leiding van Marc Koper, waar dit proefschrift het resultaat van is. Gedurende dit onderzoek heeft hij verschillende bachelor en master studenten begeleid. De resultaten van het onderzoek heeft hij op verschillende nationale en internationale conferenties en symposia gepresenteerd.